JOURNAL of CHARACTERIZATION

https://jcharacterization.com
https://jcharacterization.org

Journal of Characterization
Cilt 1, Özel Sayı, pp. 1-7, December 2021

ISSN: 2757-9166
Research Article

Borlanmış Co-Mg Alaşımlarının Mikroyapısal ve Mekanik Özelliklerinin İncelenmesi

İsmail Yıldız[1*], İbrahim Güneş[2]

[1*] Afyon Kocatepe Üniversitesi, İscehisar Meslek Yüksekokulu, Makine ve Metal Teknolojileri Bölümü, 03750, Afyonkarahisar/Türkiye (ORCID: 0000-0002-9207-591X), iyildiz@aku.edu.tr
[2]Giresun Üniversitesi, Mühendislik Fakültesi, İnşaat Mühendisliği Bölümü, 28200, Giresun/Türkiye (ORCID 0000-0001-7595-0121), ibrahim.gunes@giresun.edu.tr

(İlk Geliş Tarihi 23.12.2021 ve Kabul Tarihi 30.12.2021)

(**DOI: 10.29228/JCHAR.55612**)

ATIF: Yıldız, I., Güneş, I., Borlanmış Co-Mg Alaşımlarının Mikroyapısal ve Mekanik Özelliklerinin İncelenmesi . *Journal of Characterization*, (1), Özel Sayı, pp 1-7, 2021.

Öz

Yapılan çalışmada, Co-Mg alaşımına (%95 Co ve %5 Mg kompozisyon) borlama yöntemi ile kaplama yapılmıştır. Co ve Mg metal tozları faz diyagramındaki yüzdelik dilimlere göre kompozisyon karışım oranları belirlenmiştir. Belirlenen oranlarla kapalı kaplar içerisine konulan toz karışımlar 24 saat süre ile döner karıştırıcıda karışmıştır. Homojen karışım daha sonra geometrik şekle sahip olması için kalıplara dökülerek preslenmiştir. Preslenmiş numuneler kontrollü atmosferik fırın içerisine konularak 530 °C sıcaklıkta sinterlenmiştir. Bu işlem sonrasında numuneler borlama işlemi yapılması için silindirik olarak tasarlanmış kutular içerisinde alt ve üst taraflarına Ekabor II tozu dökülüp hava almaması için şamot çamuru ile kapatılarak 900 °C sıcaklık ve 1.5–4.5 saat değişen sürelerde borlama işlemi yapılmıştır. Borlanmış numunelere en son XRD ve SEM analizlerin yanı sıra mikrosertlik testleri yapılmıştır. XRD analiz sonucunda CoB, Co_2B ve Co fazları ortaya çıkmıştır. SEM analiz sonrasında ise bor tabakaları oluşmuş ve tabaka kalınlık ölçümleri sonucunda en yüksek değer 4.5 saat süre sonrasında 120 µm olarak bulunmuştur. Mikrosertlik ölçümü sonrasında ise en yüksek değer 1930 $HV_{0,05}$ olarak ölçülmüştür.

Anahtar Kelimeler: Co-Mg alaşım, borlama, mikrosertlik, XRD, SEM

Investigation of Microstructural and Mechanical Properties of Boronized Co-Mg Alloys

Abstract

In the study, the Co-Mg alloy (95% Co and 5% Mg composition) was coated by boriding method. Composition mixing ratios were determined according to percentiles in the phase diagram of Co and Mg metal powders. Powder mixtures placed in closed containers at the determined rates were mixed in a rotary mixer for 24 hours. The homogeneous mixture was then poured into molds and pressed to form a geometric shape. Pressed samples were placed in a controlled atmospheric furnace and sintered at 530 °C. After this process, the pieces were borided at a temperature of 900 °C and for 1.5–4.5 hours by pouring Ekabor II powder on the top and bottom of the cylindrical designed boxes for boriding, and covered with chamotte mud to prevent air leakage. Performed the latest XRD and SEM analyses as well as microhardness tests were performed on the borided samples. As a result of XRD analysis, CoB, Co_2B, and Co phases emerged. After SEM analysis, boron layers formed, and the highest value was found as 120 µm after 4.5 hours due

to layer thickness measurements. After the microhardness measurement, the highest value measured was 19 30 $HV_{0.05}$.

Keywords: Co-Mg alloy, boriding, microhardness, XRD, SEM

1. Giriş

Malzemelerin yüzey direncini artırma yöntemlerden olan elektrokimyasal yöntemler arasında borlama yer almaktadır [1-5]. Aşınmanın yanı sıra korozyon, yorulma ve oksidasyon direnci gibi önemli özelliklere sahip olması nedeniyle diğer yöntemlere göre avantajlar vardır [6,7]. Borlama yönteminin uygun sıcaklıklar ve sürelerde yapılmasıyla kaplanan malzemelerin mekanik özellikleri iyi hale gelmektedir. Kaplama ortamında oksitleyici durumların olmaması için çok iyi vakum yapılması gerekmektedir [8].

Co bazlı alaşımlar kullanıldıkları ortamlarda önemli özelliklere sahip olmaları nedeniyle en çok tercih edilen alaşımları arasındadır [9,10]. Bu özellikler arasında, yüksek yorulma dayanımı, aşınma ve korozyon direnci gibi özellikler gelmektedir. Bu alaşımlara uygulanan farklı kaplama yöntemleri ile mevcut özelliklerinde daha da iyileşmeler olmaktadır [11]. Kaplama yöntemleri arasında yer alan borlama, bor atomlarının ana malzeme olarak metal ya da alaşım yüzeyine difüzyon etmesi yoluyla yüzeylerde borür tabakasının oluşması sonrasında elde edilmektedir. Burada önemli olan uygulanan borlama sıcaklığı, malzemelerin kimyasal bileşimi, bor materyali ve borlama sonrasında FeB, Fe_2B ve CoB, Co_2B gibi metalik fazlar oluşmaktadır [12,13].

Gerçekleşen çalışmada sonucunda, Co-Mg alaşımlarına borlama yönteminin etkileri incelenmiştir. Sinterleme sonrasında elde edilen numunelere kutu borlama yöntemi ile borlama işlemi yapılmıştır. Bu işlem sonucunda oluşan bor tabakaları SEM ve XRD analiz ile belirlenmiş, vickers sertlik testleri yapılarak sertlikleri ölçülmüş ve yüzeylerde oluşan yapılar tespit edilmiştir.

2. Materyal ve Metot

Yapılan çalışmada, % 99,5 saflığa sahip Co ve Mg metal tozları ile Co-Mg alaşımları (%95 Co-%5 Mg kompozisyon) oluşturulmuştur. Mikron boyutundaki bu tozlar homojen bir şekilde karıştırılmaları için döner bir karıştırıcıda 24 saat süre ile kapalı kutu içerisinde karıştırılmıştır. Karışan tozlar dairesel şekle sahip olmak için özel olarak hazırlanmış metal kalıplara dökülerek şekillendirilmiştir. Bu işlem yaklaşık olarak 25 N kuvvet sonucunda yapılmıştır. Ortaya çıkan numunelere 530 °C sıcaklıkta 2 saat süreyle ısıl işlem uygulanmıştır.

Isıl işlem sonrasında dairesel numuneler kapalı kutu içerisinde borlama yöntemi ile borlanmıştır. Bu yöntem, kontrollü atmosferik fırın ortamında kapalı kutular içerisine konulan numunelerin alt ve üst kısımlarına Ekabor II toz dökülerek yapılmıştır (Şekil 1). Bu işlem için literatürde 800-1100 °C arası sıcaklıklarda borlama çalışmaları yapılmış [14,15], bu çalışmada ise 900 °C sıcaklık ve1,5-4,5 saat süre aralıklarda ısıl işlem uygulanmıştır. Isıl işlem sonrası fırından çıkarılan numuneler hava ile soğumasından sonra metalografik analiz olarak XRD ve SEM, vickers mikrosertlik testi yapılmıştır.

XRD analiz çalışmasında, alfa ışını, 0,02 °/dk tarama hızı ve 2 Theta tarama açısı uygulanmıştır. Numunelerin yoğunlukları d=m/v formülüne göre hesaplanmıştır. Burada m, numune kütlesi; v, numune hacmidir. Borlama sonucu yüzeylerde oluşan borür tabakarın sertlik ölçümleri SHIMADZU HMV–2 model sertlik cihazı ile yüzeyden merkeze doğru 50 gr. yük altında vickers yöntemiyle yüzeyden içeriye doğru 5 farklı ölçüm yapılarak ortalama sonuç elde edilmiştir.

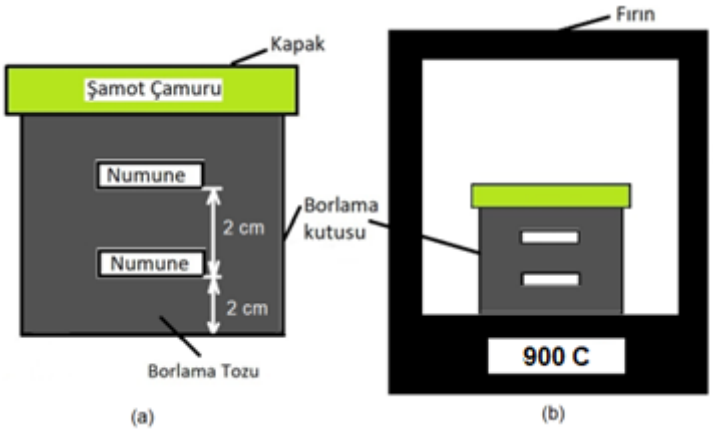

Şekil 1. Kapalı fırın ortamında borlama işleminin yapılışı (a: Numunelerin kutu içerisine yerleştirilmesi, b: Numunenin borlanması).

3. Bulgular

Co-Mg tozlarına sırasıyla presleme, sinterleme, yoğunluk, borlama ve metalografik analiz ile sertlik ölçümleri yapılmıştır. 530 °C sıcaklıkta 2 saat süre ile yapılan sinterleme sonrasında yoğunluk ölçümü ile Co-Mg alaşımında yoğunluk 7,21 gr/cm^3 olarak ortaya çıkmıştır. Borlama işlemi 900 °C sıcaklık ve 1.5–4.5 saat sürelerde yapılmıştır (Şekil 2).

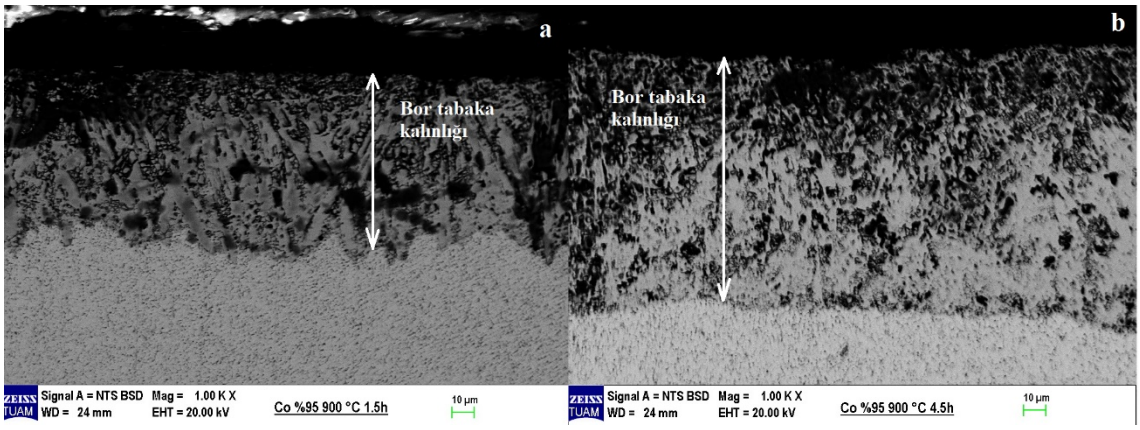

Şekil 2. Borlanmış % 95 Co ile % 5 Mg alaşımının mikroyapı görüntüleri (a: 900 °C 1,5 saat, b: 900 °C 4,5 saat)

Borlama sonrasında numunelere metalografik analiz olarak XRD ve SEM analiz yapılmıştır. XRD analiz sonucunda CoB, Co_2B ve Co faz yapıları ortaya çıkmıştır (Şekil 3). Sıcaklık ve süre artışına bağlı olarak CoB, Co_2B faz değerleri 2000 ve 2500 değerlerinde bulunmuştur. Johnston vd., Campos-Silva vd. yaptıkları borlama çalışmalarını [16,17], 950 ve 1000 °C'de gerçekleştirmiş, oluşan bor tabakaları için XRD sonucunda CoB ve Co_2B faz yapılarını 1500 yoğunluk değerine yakın olarak elde etmişlerdir. SEM analiz çalışması sonrası en iyi mikroyapı ve bor katmanı Şekil 2(b)'de de görüleceği üzere 900 °C sıcaklık 4.5 saat süre sonrasında ortaya çıkmış ve yapılan bor tabaka kalınlığı ölçüm sonucunda 120 µm kalınlık ölçülmüştür. Mikrosertlik ölçümü için numune üzerinden kaplama bölgelerinden 5 farklı ölçüm yapılarak 1930 $HV_{0,05}$ değer ölçülmüştür (Şekil 4).

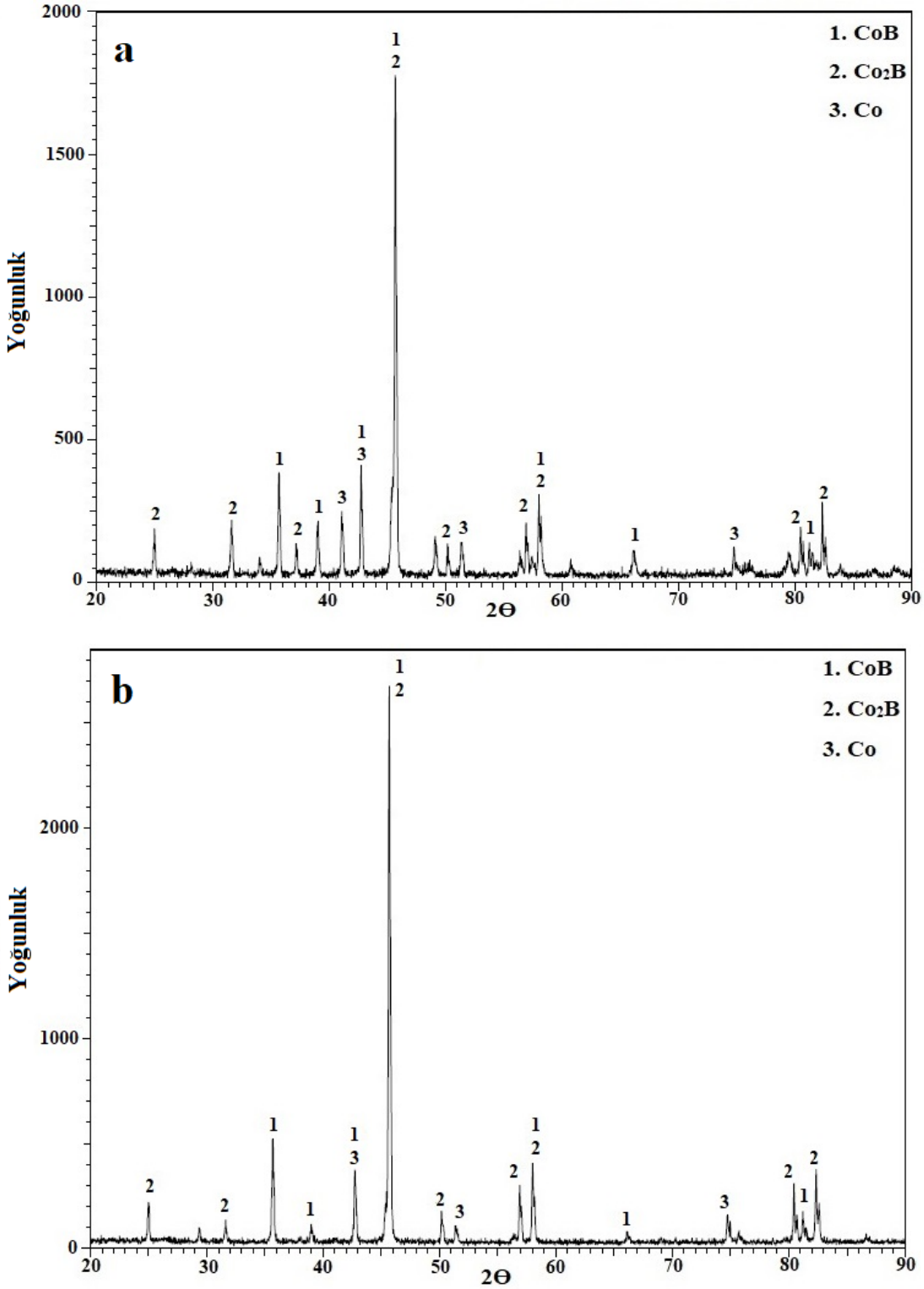

Şekil 3. Borlanmış % 95 Co ile % 5 Mg alaşımının XRD analiz görüntüleri (a: 900 °C 1,5 saat, b: 900 °C 4,5 saat)

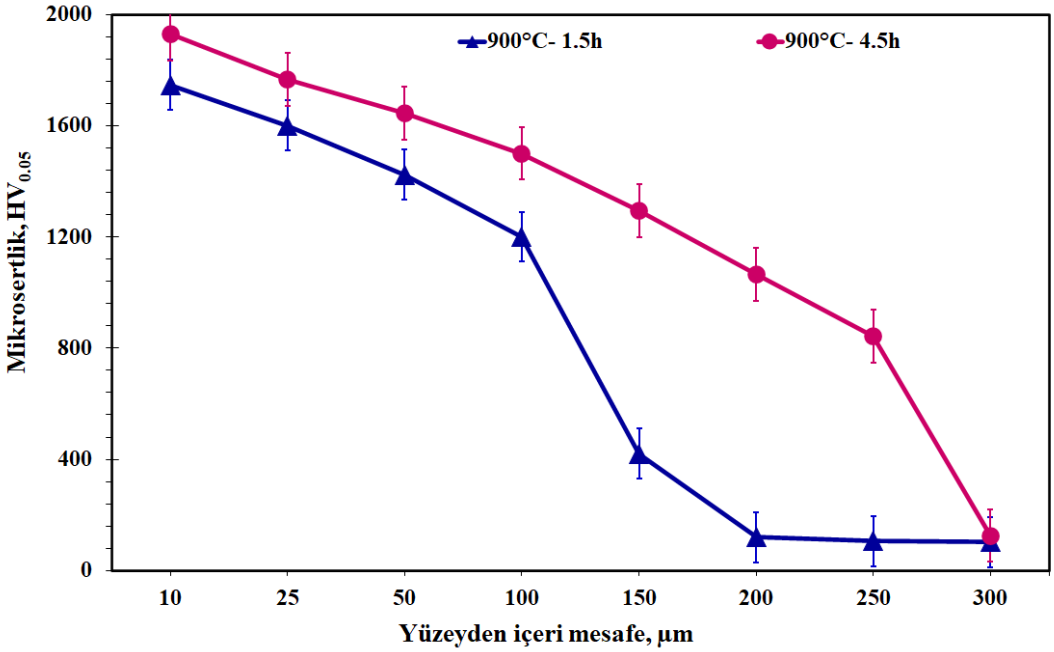

Şekil 4. Borlanmış % 95 Co ile % 5 Mg alaşımına yapılan mikrosertlik analiz sonucu

4. Sonuçlar ve Tartışma

Co-Mg alaşımının borlama sonrasında yapılan test ve analizler sonrasında ortaya çıkan sonuçlar aşağıda verilmiştir:

 Borlama işlemi sonrasında en yüksek bor tabaka kalınlığı 4,5 saat süre sonrasında 120 µm olarak bulunmuştur.
 Co-Mg alaşımların sinterleme sonrası ölçülen yoğunluk değeri 7,21 gr/cm^3 olarak bulunmuştur.
 Sinterleme sonrası yapılan sertlik testi sonucu 135±9 $HV_{0,05}$ değeri ortaya çıkmıştır.
 Metalografik analiz olarak XRD analizi yapılmıştır. Analiz sonucu olarak CoB, Co_2B ve Co faz yapıları elde edilmiştir. Bu yapıların değerleri sıcaklık ve süre artışına bağlı olarak artmıştır. Bu durum borlamanın olduğunu göstermiştir.
 Borlama sonrası yapılan mikrosertlik testi sonucu numunelerde sırasıyla 1820 $HV_{0,05}$ ve 1930 $HV_{0,05}$ sertlik değerleri ölçülmüştür.
 Gerçekleşen borlama yönteminde sıcaklık ve süreye paralel olarak borür tabakaları belirgin hale gelmiş, tabaka kalınlarında artışlar olmuştur. 900 °C, ortaya çıkan sonuçlara göre en iyi borlama sıcaklığı olarak belirlemiştir.

Alaşım içerisinde bulunan Mg, hava ile temasa geçtiğinde çok çabuk bozulabilen bir malzemedir. Yapılan sinterleme ve borlama çalışmalarında yapıda bozulmaların oluşması Mg malzemesinden kaynaklanmıştır. Kapalı vakum ortamına sahip sistem içerisinde hem sinterleme hem de borlamanın yapılması daha uygun olacaktır.

5. Teşekkür

Yapılan çalışma, Afyon Kocatepe Üniversitesi Bilimsel Araştırma Projeleri'nden 17.MYO.05 no'lu Genel Amaçlı proje ile desteklenmiştir. Desteklerinden dolayı çok teşekkür ederim.

Kaynaklar

[1] F. Hongze, L. Zhou, S. Wang, et al. "Formation and kinds of boride on microstructure evolution and mechanical properties in Ti47.5Al2.0Cr2.0NbxB alloys", *Intermetallics*, vol. 141, 107427, 2022.

[2] I. Yıldız, I. Gunes, "Borlanmış % 5 Mg katkılı Ni-Mg alaşımının yüzey özelliklerinin incelenmesi", *Politeknik Dergisi*, vol. 23(1), pp. 97-104, 2020.

[3] C. T. Sezgin, F. Hayat, "The effects of boriding process on tribological properties and corrosive behavior of a novel high manganese steel", *Journal of Materials Processing Technology*, vol. 300, 117421, 2022.

[4] I. Yıldız, I. Gunes, "%3,0 Mg içeren Borlanmış Co-Mg Alaşımının Yüzey Özelliklerinin İncelenmesi", *El-Cezerî Journal of Science and Engineering,* vol: 6 (3), 533-542, 2019.

[5] M.A. Doñu-Ruiz, N. López-Perrusquia, A. Renteria-Salcedo, et al., "Tribocorrosion behavior of boride coating on CoCrMo alloy produced by thermochemical process in 0.35% NaCl solution", *Surface and Coatings Technology*, vol. 425,127698, 2021.

[6] D. Fernández-Valdés, O. Vasquez-De la Rosa, G.A. Rodríguez-Castro, A. et al., "A numerical-experimental study of AISI 316L borided steels under cyclic contact loading", *Surface and Coatings Technology*, vol. 423, 127556, 2021.

[7] I. Gunes, I. Yıldız, "Investigation of Adhesion and Tribological Behavior of Borided AISI 310 Stainless Steel", *Revista Materia*, vol. 21, pp. 61-71, 2016.

[8] I. Gunes, A. G. Celik, "Surface Characterization of Borided S220 Rebar", *Journal of Characterization*, vol. 1(2), 66-70, 2021.

[9] X. Yang, C Li, Zhenhua Ye, X Zhang, et al., "Effects of tribo-film on wear resistance of additive manufactured cobalt-based alloys during the sliding process", *Surface and Coatings Technology*, vol. 427, 127784, 2021.

[10] H. Arabnejad, H. Uddin, K. Panda, et al., "Testing and modeling of particle size effect on erosion of steel and cobalt-based alloys", *Powder Technology*, vol. 394, 1186-1194, 2021.

[11] R. Kamalakannan, K. DineshKumar and K. NarenRaj, "The sliding wear behavior of CrCuFeNi alloyed with various combinations of cobalt", *Materials Today: Proceedings*, In Press, 2021.

[12] I. Gunes, I. Yıldız, "Rate of Growth of Boride Layers on Stainless Steels", *Oxidation Communication*, vol. 38(4/A), 2189-2198, 2015.

[13] Li Li, Peng Liu, Yongzhi Zhou, Huamei Duan, Mujun Long, Dengfu Chen, Mechanical properties and electronic structures of borides in Ni-Co-B alloy system, Materials Letters, vol. 309,131312, 2022.

[14] C. T. Sezgin, F. Hayat, "The effects of boriding process on tribological properties and corrosive behavior of a novel high manganese steel", *Journal of Materials Processing Technology*, vol. 300, 117421, 2022.

[15] I. Campos-Silva, E. J. Hernández-Ramirez, A. Contreras-Hernández, et al. "Pulsed-DC powder-pack boriding: Growth kinetics of boride layers on an AISI 316 L stainless steel and Inconel 718 superalloy", *Surface and Coatings Technology*, vol. 421, 127404, 2021.

[16] J. M. Johnston, M. Jubinsky, S. A. Catledge, "Plasma boriding of a cobalt-chromium alloy as an interlayer for nanostructured diamond growth", *Applied Surface Science*, vol. 328, 133-139, 2015.

[17] I. Campos-Silva, D., Bravo-Bárcenas, H., Cimenoglu, et al., "The boriding process in CoCrMo alloy: Fracture toughness in cobalt boride coatings", *Surface and Coating Technology,* vol. 260, 362-368, 2014.

JOURNAL of CHARACTERIZATION

https://jcharacterization.com
https://jcharacterization.org

Journal of Characterization
Vol 1, Special Issue, pp 8-18, December 2021

ISSN: 2757-9166
Research Article

A novel method to prepare of silane based superhydrophobic thin film

Atilla Evcin[1, a)] and Büşra Dalkılınç[2,b)]

[1]Afyon Kocatepe University, Materials Science and Engineering Department, 03200, Afyonkarahisar, Turkey
[2]Afyon Kocatepe University, Biomedical Engineering Department, 03200, Afyonkarahisar, Turkey
[a)]*Corresponding author: evcin@aku.edu.tr orcid id: 0000-0002-0163-5097*
[b)] *busradalkilincbs@gmail.com orcid id: 0000-0002-0917-9620*

This article is an extended version of the paper published in the TFD36 Abstract book (International Physics Congress 2020).

(Received date: 24.12.2021 and Accepted date: 30.12.2021)

(**DOI: 10.29228/JCHAR.55622**)

REFERENCES: Evcin A., Dalkılınç B., A novel method to prepare of silane based superhydrophobic thin film, *Journal of Characterization*, (1), Special Issue, 8-18, 2021.

Abstract

In this study, an organic-inorganic hybrid material was first prepared by the sol-gel method. 3-aminopropyltriethoxysilane (3-APTES) and tridecafluorooctyltriethoxysilane (Evonik F 8261) were used as precursors. The silane coupling agents were dissolved in a mixture of water, decane and hydrochloric acid for 2 hours. Soda-lime glass substrates were coated with the silane-based coating solution with the aid of a film applicator. The coated films were dried in an oven at 80°C to allow alcohol, organic solvent and excess water to evaporate from the films. After evaporation of the solvents, the samples were characterized by contact angle, FT-IR, SEM, goniometer, light transmittance, haze and gloss meter. Superhydrophobic surface was successfully obtained from 3 APTES/tridecafluorooctyltriethoxysilane hybrid compounds.

Keywords: Thin film, sol-gel method, hybrid materials, superhydrophobic, contact angle.

Silan bazlı süperhidrofobik ince film hazırlamak için yeni bir yöntem

Öz

Bu çalışmada ilk olarak organik-inorganik bir hibrit malzeme sol-jel yöntemi ile hazırlanmıştır. Öncü olarak 3-aminopropyltriethoxysilan (3-APTES) ve tridecafluorooctyltriethoxysilan (Evonik F 8261) kullanıldı. Silan birleştirme ajanları su, dekan ve hidroklorik asit karışımı içerisinde 2 saat çözündürüldü. Soda-kireç cam substratları, bir film aplikatörü yardımı ile silan bazlı kaplama çözeltisi ile kaplandı. Kaplanan filmler, alkol, organik çözücü ve fazla suyun filmlerden buharlaşmasına izin vermek için bir fırında 80°C'de kurutuldu. Çözücülerin buharlaştırılmasından sonra numuneler, temas açısı, FT-IR, SEM, gonyometre, ışık geçirgenliği, haze ve parlaklık ölçer cihazı ile karakterize edildi. Süperhidrofobik yüzey, 3-APTES / tridecafluorooctyltriethoxysilane hibrid bileşiğinden başarıyla elde edildi.

Anahtar Kelimeler: İnce film, sol-jel yöntemi, hibrit malzemeler, süperhidrofobik, temas açısı.

1. Introduction

When coating a surface, layers that do not exceed a few micrometers in thickness are called thin films. Thin films, which are of great interest among recent research studies, are used in the advancement of electronic devices in the maritime industry, the automotive industry, the healthcare industry, the aerospace industry and many more [1]. Differences in production methods and conditions of production methods reveal many different properties in thin films. These features provide thin film materials with superior properties compared to other materials and guide new studies. With the development of technology, many new production techniques have emerged and developed in the production of thin films [2]. Thin film production techniques are divided into various subgroups according to the physical and chemical properties of the material surfaces and their physical state [1]. Electroplating method is the coating process of the metal layer by forming discharge points on the conductive surfaces that act as cathodes in the electrolysis vessel [3]. Electroless plating is a simple way to produce various metals with high impact and improved mechanical properties by deposition of nickel without the use of electric current [4]. The spray pyrolysis coating method consists of the atomization of a liquid solution by blowing air towards the heated surface [5]. Thermochemical coating is a type of coating that forms nitride, carbide or boride layers on the material surface to improve the surface [6]. In the coating process with thermal spraying, the raw material particles to be used in the coating are pushed to the surface to be coated at high speed, while they are heated by the gas in the system and the surface is coated [7]. Chemical vapor deposition (CVD) is the process in which the substrate is exposed to one or more volatile precursors that can react and decompose on the substrate surface to produce the desired thin film residue [8]. The physical vapor deposition method (PVD) can be summarized as the process of bonding the solid raw material to the material to be coated in a controlled manner by turning it into plasma with high energy [9].

Sol-gel technique is one of the thin film production techniques. Sol-gel technology began to be used in the 1800s [10]. Sol-gel process has been an important, widespread and widely popular method for the preparation of thin films due to its advantages. Its applications are wide, offering several advantages over other methods, including good homogeneity, low cost, and high purity [11]. The sol-gel method can be used in the production of almost all single-component or multi-component oxide films. The sol-gel process involves the formation of colloidal suspensions (sol) of solid particles in the liquid phase and then three-dimensional solid inorganic networks (gel) in a continuous liquid phase [12]. Sol-gel method is a coating technique applied to improve the surface properties of glass, ceramic, metal and plastic backings and to gain new properties such as optics, electronics, chemicals and mechanics [13]. In our study, a colloidal suspension (left) was formed using 3-APTES and Evonik F8261 materials and used to form thin films.

Hybrid materials are of great interest as a new class of materials due to their original properties based on the combination of organic and inorganic polymers [14,15]. As a result of the combination of organic and inorganic materials in the same material with the appropriate processing method, new properties emerge in terms of mechanical, electrical, physical or optical properties [14,16]. However, their biocompatibility, biodegradation and chemical structure have also been among the research topics. Hybrid materials have revealed new developments in the creation of various smart and functional materials [17]. The chemistry of the silane surface modification reaction is shown in Figure 1 [18]. In our study, a hybrid material was obtained by combining organic 3-APTES and inorganic Evonik F8261 with strong bonds and coated as a thin film on the glass surface.

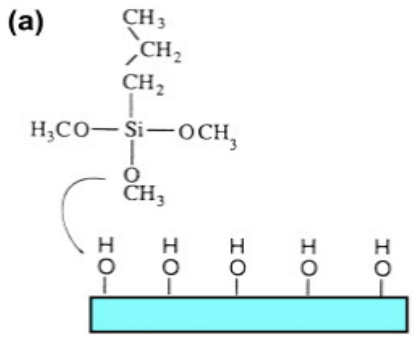

Figure 1. Silane surface modification reaction [18]

The introduction of superhydrophobic surfaces into the scientific world began with the study of the lotus flower, which is known to be constantly clean in muddy and dirty environments. Inspired by the lotus flower, attempts have been made about the water holding and repellent properties of solid surfaces [19]. Examples of these initiatives are self-cleaning artificial and smart surfaces by removing water and pollutants. The protective effects on artificial surfaces are enhanced [20,21].

When contact is established between a liquid and a solid, the angle between the liquid surface and the solid surface is defined as the contact angle [22,23]. Whether a surface is hydrophobic or hydrophilic is measured by the contact angle between the water and the surface [18,19,24]. Figure 2 shows the different situations that the sui le surface can create [25]. Surface wettability can be classified according to the contact angle (θ) value as follows:

If θ<90º the surface is hydrophilic

If θ<10º the surface is superhydrophilic

If θ>90º the surface is hydrophobic

If θ>150º, the surface is superhydrophobic [26,27].

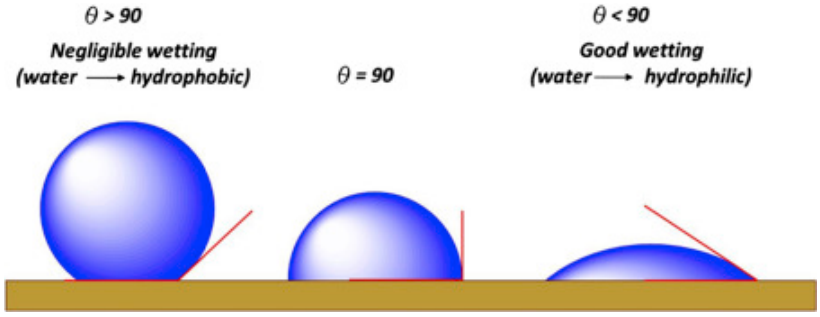

Figure 2. Surface wettability according to contact angle

2. Material and Method

In experimental studies, 3-aminopropyltriethoxysilane (3-APTES) (Merck), tridecafluorooctyltriethoxysilane (Evonik F 8261) (Aldrich-Sigma), Decane (Merck), Hydrochloric acid (1M) and pure water were used as precursors. Materials were used as supplied.

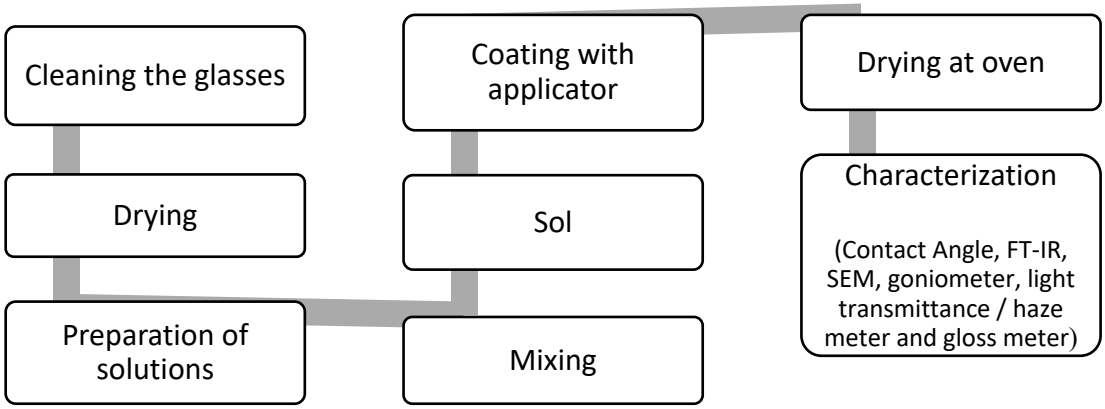

Figure 3. Experiment flow chart

2.1. Preparation of Glass Surfaces

In the whole study, rectangular glass surfaces of 2.5x7.5 cm were used as the surface. To achieve an ideal coating layer, the glass substrates were cleaned with the cleaning procedure described below. For surface pretreatment, the glass surfaces were ultrasonically cleaned with double distilled water for 10 minutes. The chemical cleaning procedure was carried out by soaking the glass substrates in NaOH, Purified water, H3PO4, Purified water for 5 minutes, respectively. All glass surfaces were dried at 80 °C for 2 h before coating. Thus, it was made ready for use.

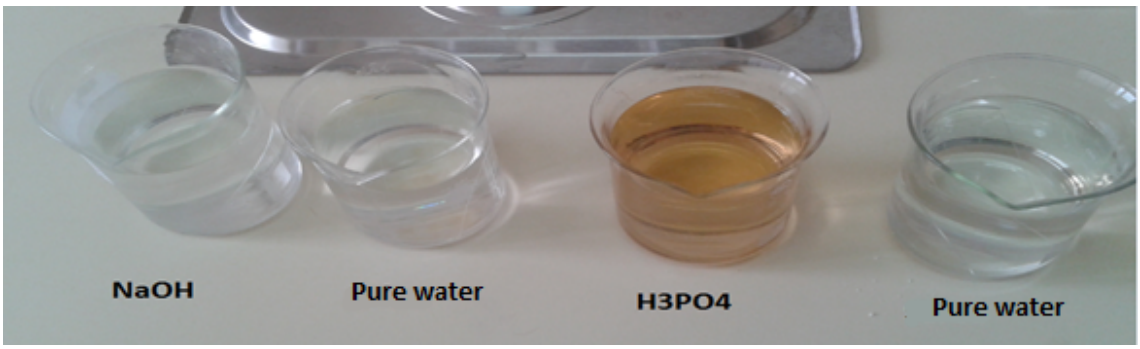

Figure 4. Glass cleaning procedure

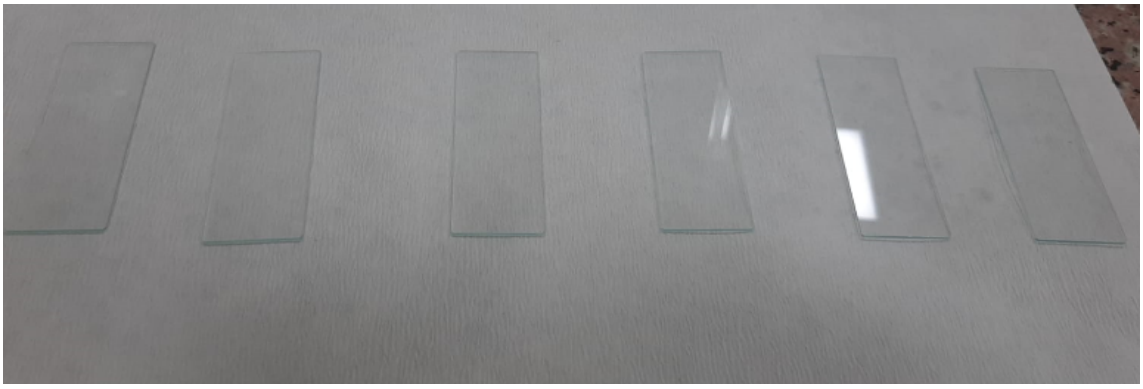

Figure 5. Cleaned glass surfaces

In the experimental study, three different solutions were prepared and coated on six glass samples. It is aimed to impart hydrophobic or superhydrophobic properties to hydrophilic glasses.

Table 1. Composition of prepared solutions

	Recipe-1	Recipe-2	Recipe-3
3-APTES	3,31 g	3,31 g	3,31 g
Decane	10 g	10 g	10 g
Evonik F8261	-	1 mL	2 mL
Pure Water	2 mL	2 mL	2 mL
Hydrochloric Acid (1M)			

2.2. Thin Film Coating on Glass with the Help of Film Applicator

The prepared solution was taken with a pipette and covered with a film-drawing applicator on previously cleaned and prepared glasses. The windows are covered with a single layer. Two glass samples were coated from each solution. The coated samples were left to dry in an oven at 80 °C. Necessary tests were performed on the drying glass samples and information was obtained about the surface properties.

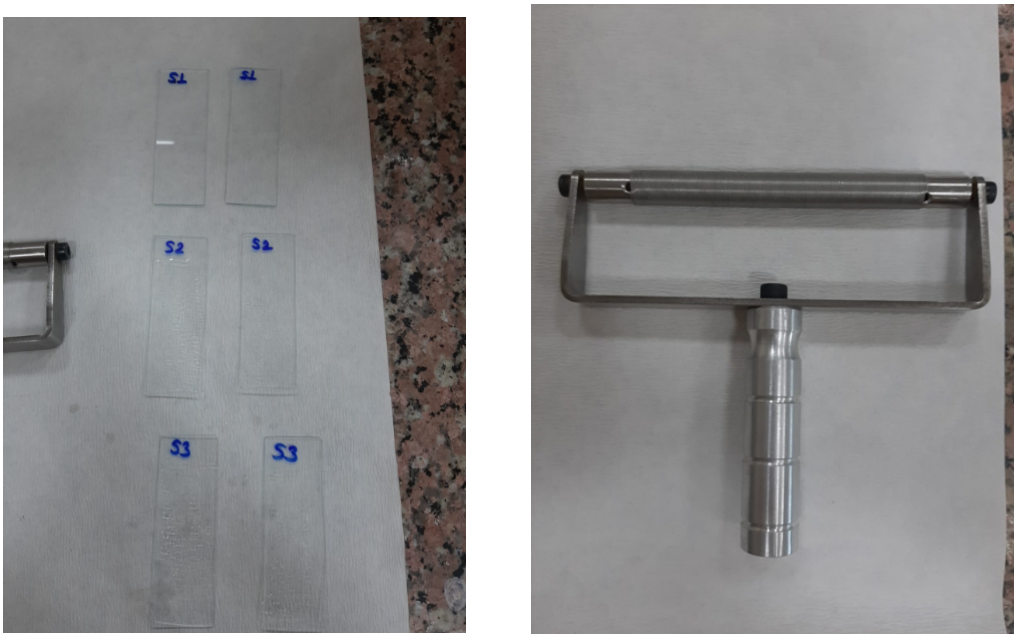

Figure 6. Coated glasses and film applicator

2.3. Tests applied to samples

The prepared solution was taken with a pipette and covered with a film-drawing applicator on previously cleaned and prepared glasses. The windows are covered with a single layer. Two glass samples were coated from each solution. The coated samples were left to dry in an oven at 80 °C. Necessary tests were performed on the drying glass samples and information was obtained about the surface properties.

3. Results and Discussion

3.1. Contact Angle Results

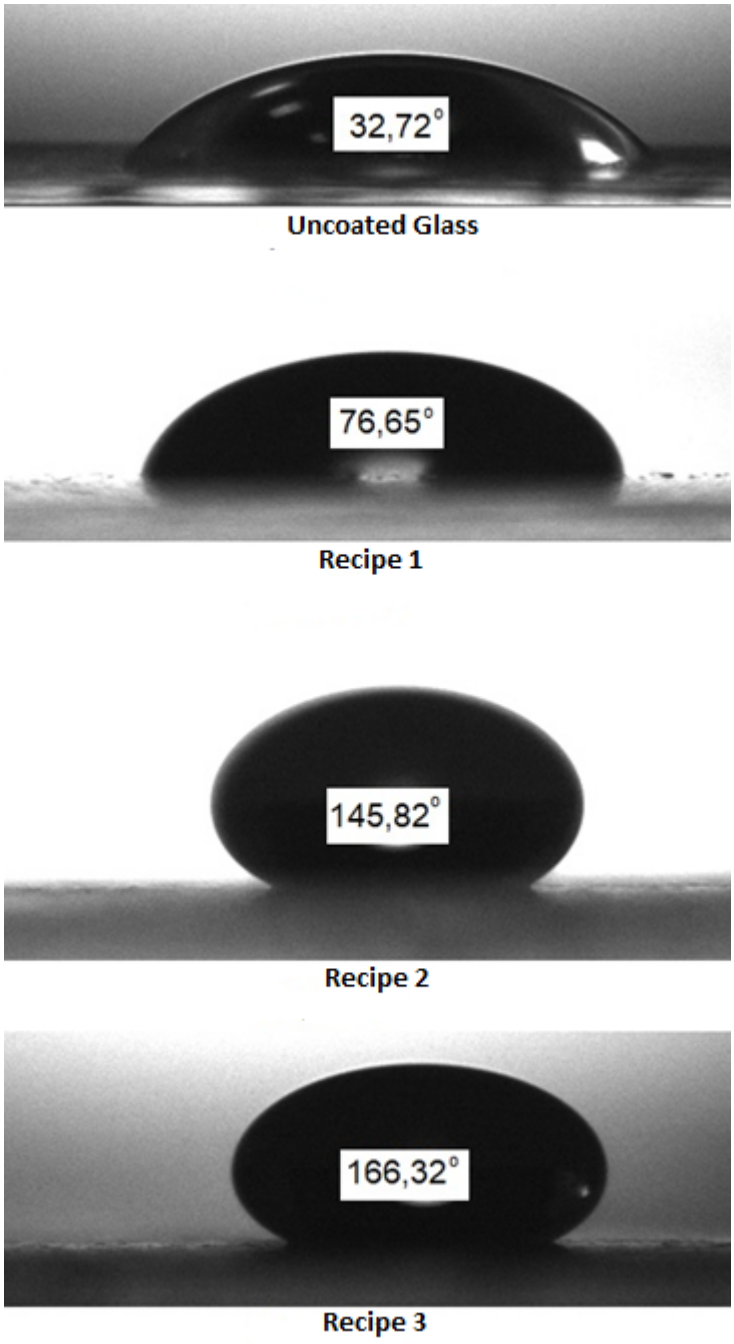

Figure 7. Contact angle of solution coated surface

As seen in Figure 7, the surface contact angle of the uncoated glass with water was 32 °, while the contact angles were found to be 76°, 145 ° and 166 °, respectively, after all three coatings. While the uncoated glass is hydrophilic, a hydrophobic surface was obtained especially in Recipes 2 and 3. Recipe 2 and 3 include tridecafluorooctyltriethoxysilane (Evonik F 8261), one of the fluoroalkyl silane compounds. Increasing the amount of this compound significantly increased the contact angle.

3.2. FT-IR Results

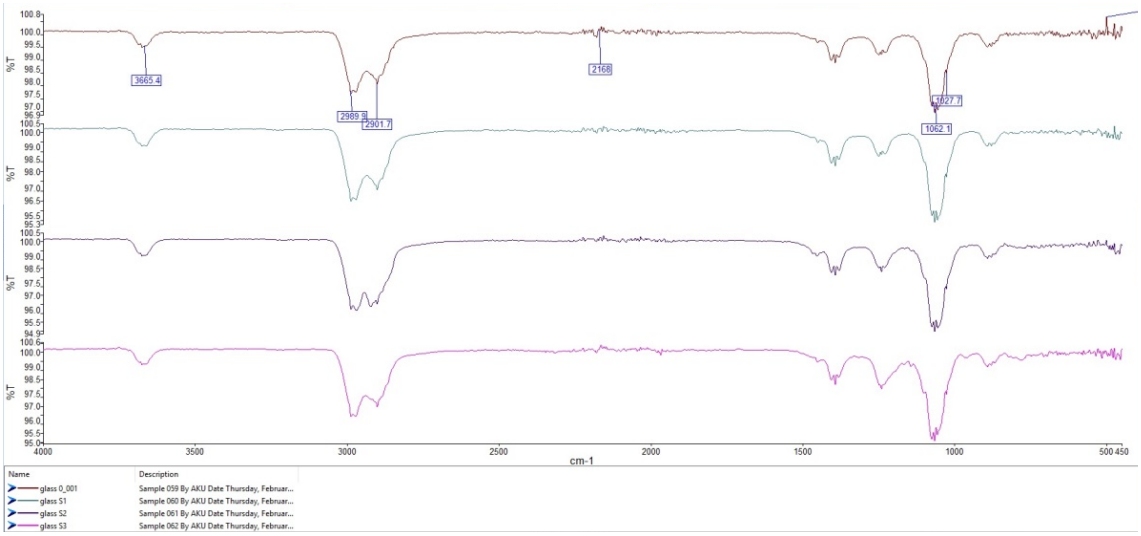

Figure 8. FTIR analysis.

FTIR analysis of coatings is given in Figure 8. The peaks observed at approximately 3665 cm-1 and 2901 cm-1 in hydrophilic glass belong to free or adsorbed water with hydrogen bond interactions. The peak at 1062 cm-1 can be attributed to Si–O–Si mode vibrations. The spectrum is dominated by a broad absorption band between 1250 and 1062 cm-1, which corresponds to the Si-O-C and Si-O-Si vibrations, indicating the presence of the siloxane network as expected. The peak at 1566 cm-1 confirms the presence of primary amines, but the peak around 1655 cm-1 indicates the presence of double-bonded nitrogen as well. The presence of C-F bonds in the form of CF, CF2 or CF3 is also located at 610, 770, 960 and 1,027 cm-1.

3.3. Light Transmittance / Haze Meter and Gloss Meter

The results of the tests performed with the Light Transmittance/Haze meter and Luminosity meter shown in Figure 10 are given in Table 2. As can be seen in Table 2, a slight decrease in light transmittance was recorded with the coating. Haze (blur) increased and brightness decreased.

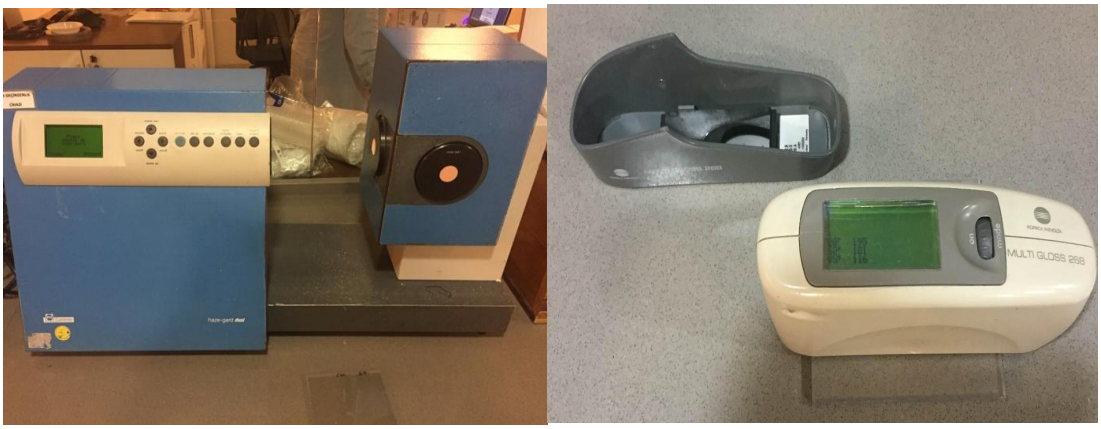

Figure 10. Light transmittance/haze meter and gloss meter used in the experiments

Table 2. Light Transmittance / Haze Meter and Gloss Meter Results

	GLASS	R1	R2	R3
% Transmittance	94	93	92	91
% Haze	0,54	1,14	2,65	4,42
Brightness (60 °)	174	165	156	148

3.4. SEM Results

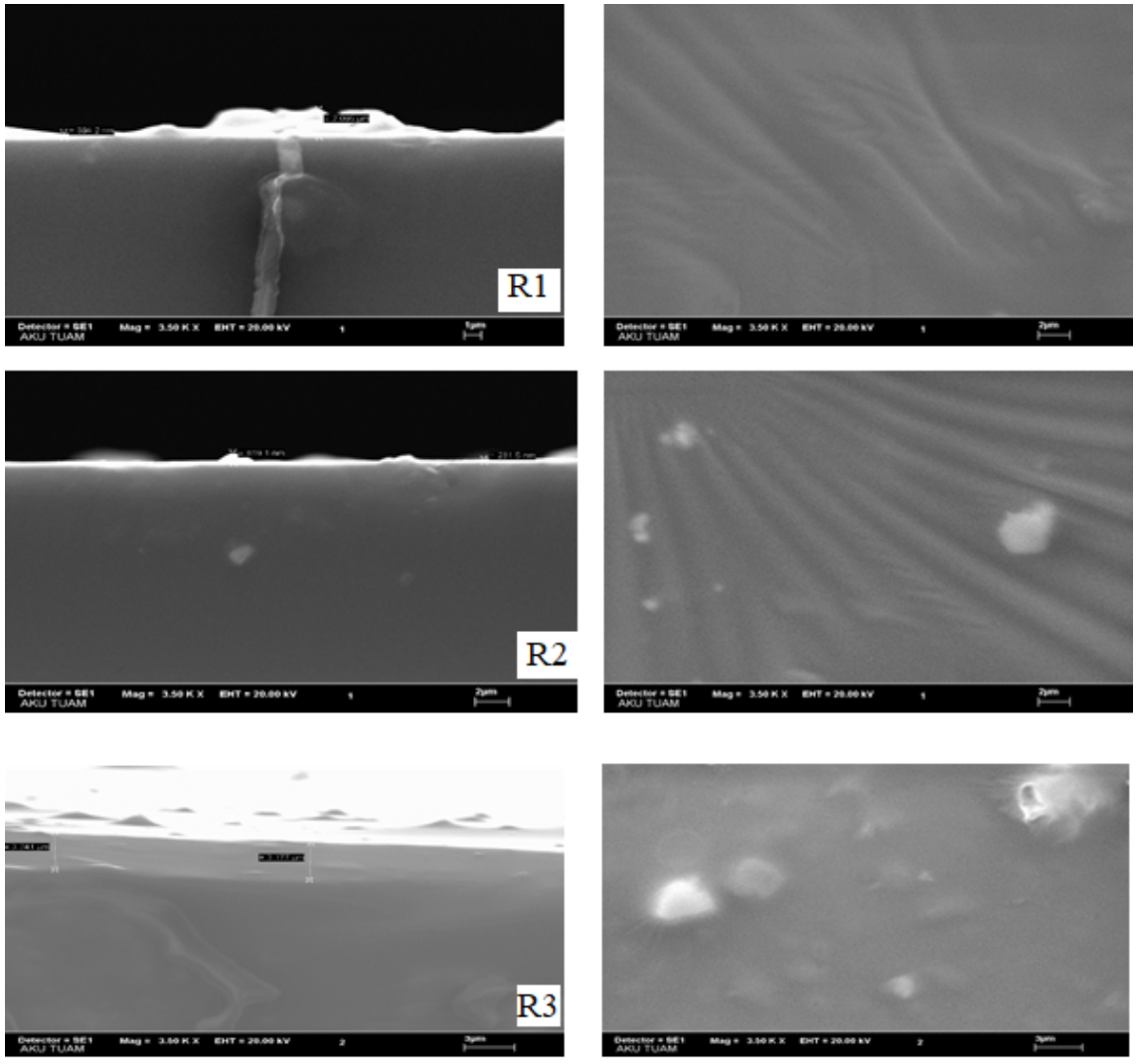

Figure 9. Scanning electron microscopy (SEM) analyzes of prescriptions

As can be seen from the cross-sections of the SEM photographs in Figure 9, the layers coated on the glass are less than 2 micrometers thick. It can be seen from the surface pictures that it is homogeneously dispersed and no cracks occur.

4. Conclusions and Recommendations

In this study, silane-based organic-inorganic hybrid coating was successfully formed on the glass surface by sol-gel method. Amino-based silane and fluoro silane compounds formed a superhydrophobic layer on the glass surface. Maximum contact angle is 166 degree. Thickness of layer is about 2 micrometers and homogenous surface was obtained by sol-gel method.

5. Acknowledge

I would like to thank Afyon Kocatepe University Institute of Science and Scientific Research Projects Coordination Unit (BAPK) for the support of the project numbered 20.FEN.BİL.30.

References

[1] SÖNMEZOĞLU, S., Mehmed, K. O. Ç., & Seçkin, A. K. I. N. (2012). İnce film üretim teknikleri. Erciyes Üniversitesi Fen Bilimleri Enstitüsü Fen Bilimleri Dergisi, 28(5), 389-404.

[2] Gessert, Timothy. (2012). Chapter 1.19: Cadmium Telluride Photovoltaic Thin Film: CdTe. Earth and Planetary Sciences. 1. 10.1016/B978-0-08-087872-0.00122-0.

[3] Zhang, B., Li, B., Gao, S., Li, Y., Cao, R., Cheng, J., ... & Liu, B. (2020). Y-doped TiO2 coating with superior bioactivity and antibacterial property prepared via plasma electrolytic oxidation. Materials & Design, 192, 108758.

[4] Vetrivezhan, P., Ayyanar, C., Arunraj, P. V., Vasanthkumar, P., & Ganesan, D. (2021). Electroless deposition of aluminium alloy LM25 by SiC and Ni-P nano coating. Materials Today: Proceedings.

[5] Weber, S. B., Lein, H. L., Grande, T., & Einarsrud, M. A. (2013). Influence of the precursor solution chemistry on the deposition of thick coatings by spray pyrolysis. Surface and Coatings Technology, 221, 53-58.

[6] Günen, A., Kanca, Y., Karahan, İ. H., Karakaş, M. S., Gök, M. S., Kanca, E., & Çürük, A. (2018). A comparative study on the effects of different thermochemical coating techniques on corrosion resistance of STKM-13A steel. Metallurgical and Materials Transactions A, 49(11), 5833-5847.

[7] Mostaghimi, J., Chandra, S., Ghafouri-Azar, R., & Dolatabadi, A. (2003). Modeling thermal spray coating processes: a powerful tool in design and optimization. Surface and Coatings Technology, 163, 1-11.

[8] Martin, P. M. (2009). Handbook of deposition technologies for films and coatings: science, applications and technology. William Andrew.

[9] Liu, M. J., Zhang, K. J., Zhang, Q., Zhang, M., Yang, G. J., Li, C. X., & Li, C. J. (2019). Thermodynamic conditions for cluster formation in supersaturated boundary layer during plasma spray-physical vapor deposition. Applied Surface Science, 471, 950-959.

[10] Akpan, UG ve Hameed, BH (2010). Katkılı TiO2 fotokatalizörlerinin sol-jel yöntemindeki gelişmeler. Uygulamalı Kataliz A: 375 (1), 1-11.

[11] Chen, D. H., & He, X. R. (2001). Synthesis of nickel ferrite nanoparticles by sol-gel method. Materials Research Bulletin, 36(7-8), 1369-1377.

[12] Wang, Y. T., Zhang, X. T., Xu, J. B., Shen, Y., Wang, C. A., Li, F. W., ... & Shen, R. Q. (2020). Fabrication and characterization of Al–CuO nanocomposites prepared by sol-gel method. Defence Technology.

[13] Qu, L., Rahimi, S., Qian, J., He, L., He, Z., & Yi, S. (2020). Preparation and characterization of hydrophobic coatings on wood surfaces by a sol-gel method and post-aging heat treatment. Polymer Degradation and Stability, 109429.

[14] Zhang, Q., Zhang, X., Cheng, W., Li, Z., & Li, Q. (2020). In situ-synthesis of calcium alginate nano-silver phosphate hybrid material with high flame retardant and antibacterial properties. International Journal of Biological Macromolecules, 165, 1615-1625.

[15] Zhao, X., Li, Z., Guo, Q., Yang, X., & Nie, G. (2021). High performance organic-inorganic hybrid material with multi-color change and high energy storage capacity for intelligent supercapacitor application. Journal of Alloys and Compounds, 855, 157480.

[16] Wang, Y., Fan, H., Wong, P. K., Wu, Y., & Rittmann, B. (2021). Biodegradation of tetracycline using hybrid material (UCPs-TiO2) coupled with biofilms under visible light. Bioresource Technology, 323, 124638.

[17] Rejab M.R., Hamdan M.H., Quanjin M., Siregar J.P., Bachtiar D., Muchlis Y. Historical Development of Hybrid Materials. *Mat. Sci. Mat. Eng.* 2020;4:445–455. doi: 10.1016/j.pmatsci.2015.12.001

[18] Ratner, B. D., Hoffman, A. S., & McArthur, S. L. (2020). Physicochemical surface modification of materials used in medicine. In Biomaterials science (pp. 487-505). Academic Press.

[19] Xia, Z., Xiao, Y., Yang, Z., Li, L., Wang, S., Liu, X., & Tian, Y. (2019). Droplet impact on the super-hydrophobic surface with micro-pillar arrays fabricated by hybrid laser ablation and silanization process. Materials, 12(5), 765.

[20] Raibeck, L., Reap, J., & Bras, B. (2009). Investigating environmental burdens and benefits of biologically inspired self-cleaning surfaces. CIRP Journal of Manufacturing Science and Technology, 1(4), 230-236.

[21] Wang, X., Jing, C., Chen, Y., Wang, X., Zhao, G., Zhang, X., Zhang, Y. (2020). Active corrosion protection of super-hydrophobic corrosion inhibitor intercalated Mg–Al layered double hydroxide coating on AZ31 magnesium alloy. Journal of Magnesium and Alloys, 8(1), 291-300.

[22] Zhenyu, S., Zhanqiang, L., Hao, S., & Xianzhi, Z. (2016). Prediction of contact angle for hydrophobic surface fabricated with micro-machining based on minimum Gibbs free energy. Applied Surface Science, 364, 597-603.

[23] Gallardo-Moreno, A. M., Navarro-Pérez, M. L., Vadillo-Rodríguez, V., Bruque, J. M., & González-Martín, M. L. (2011). Insights into bacterial contact angles: Difficulties in defining hydrophobicity and surface Gibbs energy. Colloids and Surfaces B: Biointerfaces, 88(1), 373-380.

[24] Yi, S. W., Yu, I. K., Kim, W. J., & Choi, S. H. (2021). Cold Plasma Deposition of Polymeric Nanoprotrusion, Nanoparticles, and Nanofilm Structures on a Slide Glass Surface. Processes 2021, 9.

[25] Hebbar, R. S., Isloor, A. M., & Ismail, A. F. (2017). Contact angle measurements. In Membrane characterization. Elsevier.

[26] Xia, Z., Zhao, Y., Yang, Z., Yang, C., Li, L., Wang, S., & Wang, M. (2021). The simulation of droplet impact on the super-hydrophobic surface with micro-pillar arrays fabricated by laser irradiation and silanization processes. Colloids and Surfaces A: Physicochemical and Engineering Aspects, 612, 125966.

[27] Karim, A. M., Rothstein, J. P., & Kavehpour, H. P. (2018). Experimental study of dynamic contact angles on rough hydrophobic surfaces. Journal of colloid and interface science, 513, 658-665.

JOURNAL of CHARACTERIZATION

https://jcharacterization.com
https://jcharacterization.org

Journal of Characterization
Vol 1, Special Issue, pp 18-28, December 2021

ISSN: 2757-9166
Research Article

Effect of solvent type and number of coating layers on the contact angle of hydrophilic TiO2 thin film

Atilla Evcin[1, a)] and Emine Yaşar[2,b)]

[1]Afyon Kocatepe University, Materials Science and Engineering Department, 03200, Afyonkarahisar, Turkey [2]Afyon Kocatepe University, Biomedical Engineering Department, 03200, Afyonkarahisar, Turkey

[a)]*Corresponding author: evcin@aku.edu.tr orcid id: 0000-0002-0163-5097*

[b)] *emineyasar_21@hotmail.com orcid id:0000- 0002-7234-2259*

This article is an extended version of the paper published in the TFD36 Abstract book (International Physics Congress 2020).

(Received date: 24.12.2021 and Accepted date: 30.12.2021)

(**DOI: 10.29228/JCHAR.55618**)

REFERENCES: Evcin A., Yaşar E., Effect of solvent type and number of coating layers on the contact angle of hydrophilic TiO2 thin film. *Journal of Characterization*, (1), Special Issue, 18-28, 2021.

Abstract

In this study, titanium isopropoxide was chosen as a precursor. It was dissolved in isopropanol for 30 minutes. Then non-ionic surfactants (Triton X-100), were used to obtain the separation and mono dispersion in the sol-gel reaction. In this experiment, the dip-coating method was chosen as a coating method. Soda-lime glass substrates were coated with the alkoxide-based coating solution by a dip coater. The coated films were dried at 80 °C in an oven to allow the alcohol, organic solvent, and excess water to evaporate from the films. After evaporation of solvents, coated glasses were characterized by scanning electron microscopy (SEM), goniometer, light Transmittance/Haze meter, and Gloss meter. The hydrophilic surface was successfully obtained from titanium alkoxide-based coating solution.

Keywords: sol-gel method, alkoxide, hydrophilic, thin film

Çözücü tipinin ve kaplama tabakası sayısının hidrofilik TiO_2 ince filmin temas açısına etkisi

Öz

Bu çalışmada, başlangıç kimyasalı olarak titanyum izopropoksit seçildi. İzopropanol içinde 30 dakika çözündürüldü. Daha sonra sol-jel reaksiyonunda ayırma ve mono dispersiyon elde etmek için iyonik olmayan yüzey aktif maddeler (Triton X-100) kullanıldı. Bu deneyde, kaplama yöntemi olarak daldırma kaplama yöntemi seçilmiştir. Soda-kireç cam substratlar, bir daldırma kaplayıcı ile alkoksit bazlı kaplama çözeltisi ile kaplandı. Kaplanmış filmler, alkolün, organik çözücünün ve fazla suyun filmlerden buharlaşmasına izin vermek için bir fırında 80°C'de kurutuldu. Çözücülerin buharlaştırılmasından sonra, kaplanmış camlar taramalı elektron mikroskobu (SEM), gonyometre, ışık Geçirgenliği/Buğu ölçer ve Parlaklık ölçer ile karakterize edildi. Hidrofilik yüzey, titanyum alkoksit bazlı kaplama çözeltisinden başarıyla elde edildi.

Anahtar Kelimeler: sol-jel yöntemi, alkoksit, hidrofilik, ince film

1. Introduction

Recently, with the advancement of technology, materials are needed to show more performance and expectations are increasing. New production methods have been developed in line with these expectations and needs. The sol-gel method is also one of the developed methods.

The sol-gel method is the process of transition of sol composition from a liquid sol phase to a solid gel phase using pre-initiators (metal salts and metal alkoxides), solvents, and catalysts [1]. Sol-gel technology can be applied in many different fields such as glass and ceramic industry [2], chemical sensors, nuclear studies, space technology, production of more useful and more efficient materials for electronic devices.[3]. Coating glass, ceramic, metal, polymeric surfaces with the sol-gel method provides the improvement of many surface properties of the material [4,5]. With the surface modifications made in this way, surface properties of materials such as roughness, surface energy, surface charge, hydrophilicity, compatibility, and usability are improved [6]. The sol-gel method provides advantages such as low application temperature, wide usage area, easy accessibility of the materials to be used.

The sol-gel immersion technique is based on the principle of dipping the desired substrate into the prepared sol-gel solution at a certain speed and removing it at the same speed (Figure 1) [7]. The most used method in thin-film production is sol-gel technology. During sol-gel thin-film formation by immersion, the substrate is drawn vertically from the desired coating solution so that the precursors are concentrated on the substrate surface by a procedure that includes simultaneous drying and gravitational discharge with continuous condensation reactions [8]. The immersion method is a process applied at constant speed, controlled temperature, and atmospheric conditions. Coating thickness depends on substrate withdrawal speed, surface tension of substrate, density, and viscosity of coating solution.[9].

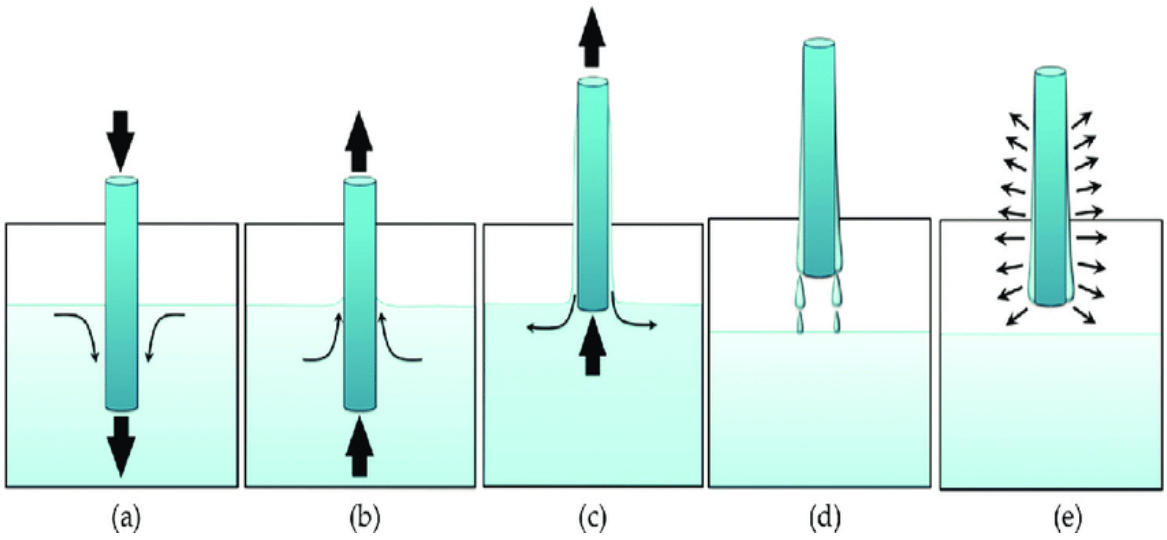

Figure 1. Dip coating steps [6].

The contact angle is one of the common approaches for measuring the wettability of a solid surface, which can be used to determine and indicate the chemical, physical properties of surfaces, and refers to the angle that occurs between a solid/liquid/gas interface at the surface of the solid [10]. The magnitude of the angle also indicates that the interaction between solid and liquid is low [11]. When the contact angle is 0°, the liquid spreads completely over the surface; When it is 180°, it does not spread at all. When the angle is over 90 degrees, the solid surface is hydrophobic; It becomes hydrophilic when the angle is below 90° [12]. The size of this angle between the surfaces depends on the difference between the adhesion and cohesion forces [13].

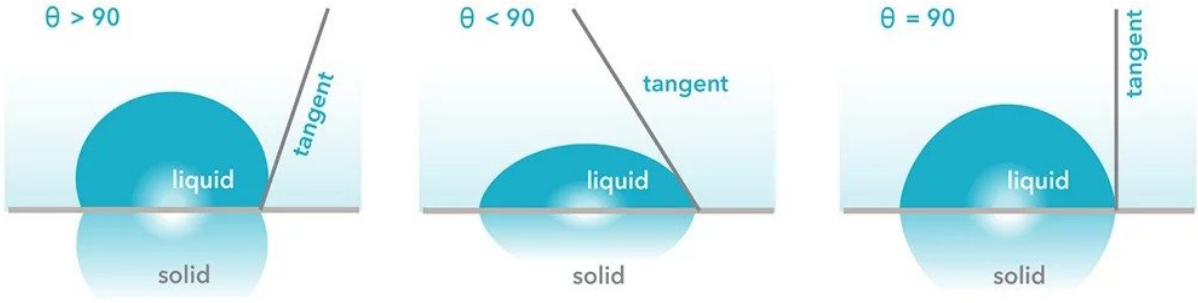

Fig 2. Different contact angles on a surface (int ref 1)

The simplest contact angle is called the constant drop-off or static contact angle. However, there are a number of fixed contact angles that exist for the surface depending on factors such as chemical homogeneity, topography, and roughness.

The wettability of the surfaces depends on the free energy of the surface and the geometric properties of the material surface [14]. In the case of water, surface wettability can be classified as hydrophobic, hydrophilic, superhydrophobic, and superhydrophilic according to the value of the contact angle [15].It has a very important place for controlling the wetting ability [16], adhesion and selective absorption, development of medical equipment, self-cleaning and anti-fogging and similar studies. Some of these applications require liquids to fully wet solid surfaces.

The term "superhydrophilic" was first used by Fujishima et al. 17]. Surfaces with contact angle less than 10 ° with water are superhydrophilic surfaces [18]. On superhydrophilic surfaces, water spreads on a flat surface, not as droplets [19]. Stains and dirt on the surface can be easily washed off with this spreading water layer. Superhydrophilic materials have applications in many fields, including vehicle glass, window glass, microscopes, glasses, solar panel covers, electronic device screens and optical instruments, oil-water separation, self-cleaning surfaces [20,21].

2. Material and Method

Titanium (IV) isopropoxide (TTIP) (Sigma–Aldrich Co.), Triton X-100 (sigma), hydrochloric acid (37% HCl), phosphoric acid (Sigma H3PO4), acetone (Sigma), isopropyl alcohol (Sigma), and deionized water (DI) are used as precursors. All the reagents were used as received. The glass substrates of 1.5 cm 5 cm were used as substrates in all experiments. To get a uniform coating layer, the glass substrates were cleaned by the cleaning procedure described below.

For surface pre-treatment, the glass surfaces were ultrasonically cleaned with double distilled water for 10 min. Chemical cleaning procedure was carried out by soaking the glass substrates in NaOH, DI, H3PO4, and DI for 5 min respectively. All glass substrates were dried at 80 °C for 2 h before coating.

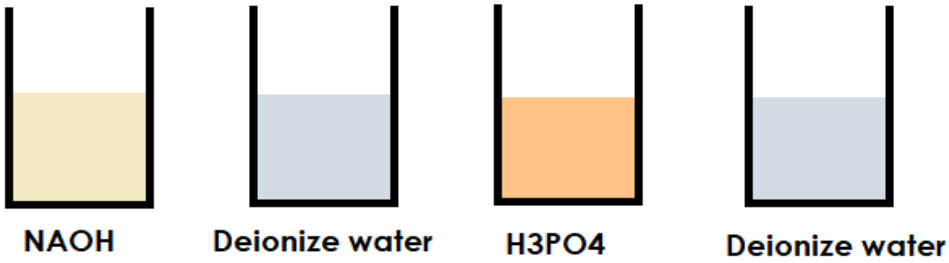

Fig 3. washing substrates

TiO2 solutions were prepared by dissolving TTIP in isopropyl alcohol and DI. Sol was continuously stirred for 1 hour at room temperature and added HCl to adjust the pH of the solution. The prepared sol holds on room condition for 2 days aging process.

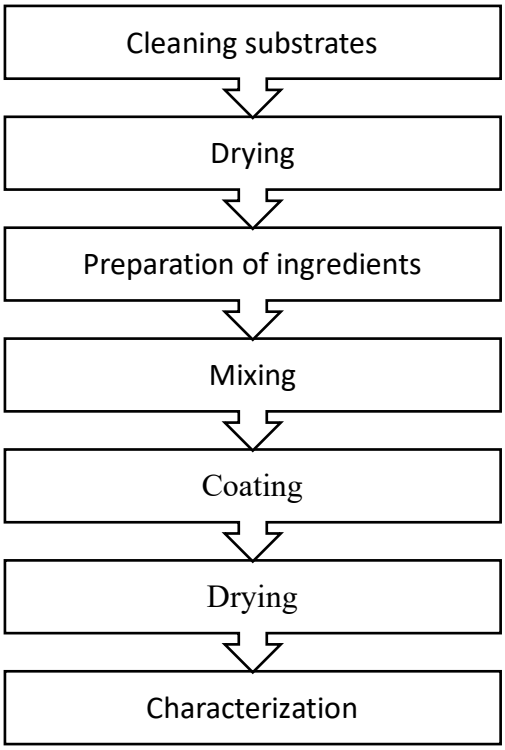

Fig 4. Flowchart of experiment

2.1. Dip Coating

The prepared Ti solution is placed in a Borosilicate Beaker. Glass substrates were deposited by a home-made dip-coater with heating chamber (Fig 5). Films were deposited at 10 mm.s-1 withdrawal speed at room temperatures. Then coated glasses were heated at 60 ° C for 10 minutes in the heating chamber and coated next layer. The dipping process was repeated 5 times. Finally, all coated glasses were applied to heat treatment at 450 °C for 1 hour.

Fig 5. Home-made dip coater.

The contact angle of each sample was obtained by using the Sessile Drop technique at room temperature (25 ±2 ºC) using pure water with "KSV Attension Theta Lite TL 101 Optical Tensiometer" instrument (Fig 6). 2 polar (water and ethylene glycol) and 1 apolar (diiodomethane) liquids were used in contact angle measurements.

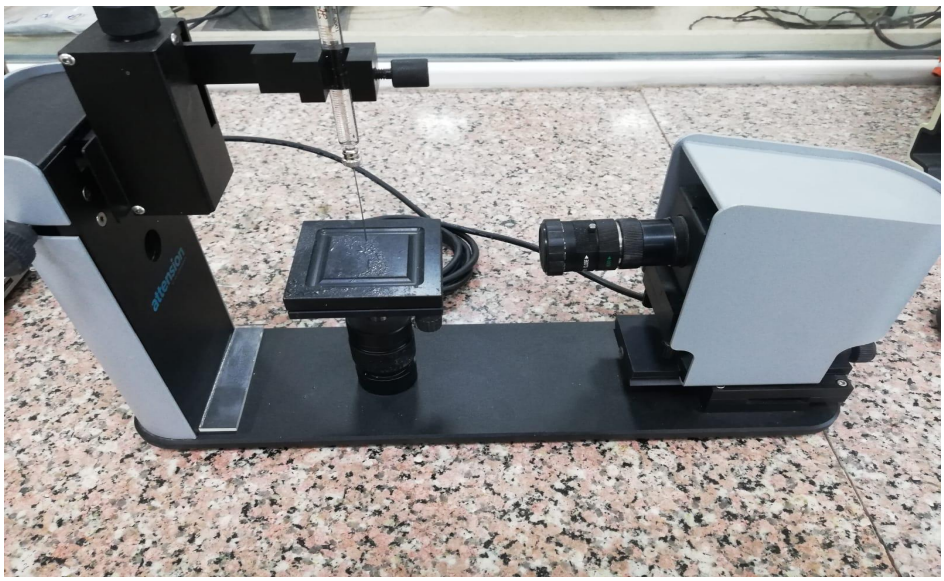

Fig 6. KSV Attension Theta Lite.

Surface and cross-section images of the coating layers were made with the Leo 1430 VP model scanning electron microscope (SEM). A clear view could not be obtained from the cross-section in 1 and 2 layer coatings.

Thin films were characterized by BYK-Gardner haze gard dual Light Transmittance / Haze Meter, and Konica Minolta Multi Gloss 268 Gloss Meter (Fig.7). The Haze-Gard Dual measures Total Transmittance and Haze according to two international standards: ISO 13468 and ASTM D1003. The Gloss meter is a portable and compact gloss meter consisting of three measuring angles (20°, 60° and 85°), each in accordance with DIN 67 530, ISO 2813, ISO 7668 ASTM D 523, BS 3900, BS 6161, and JIS Z 8741 standards.

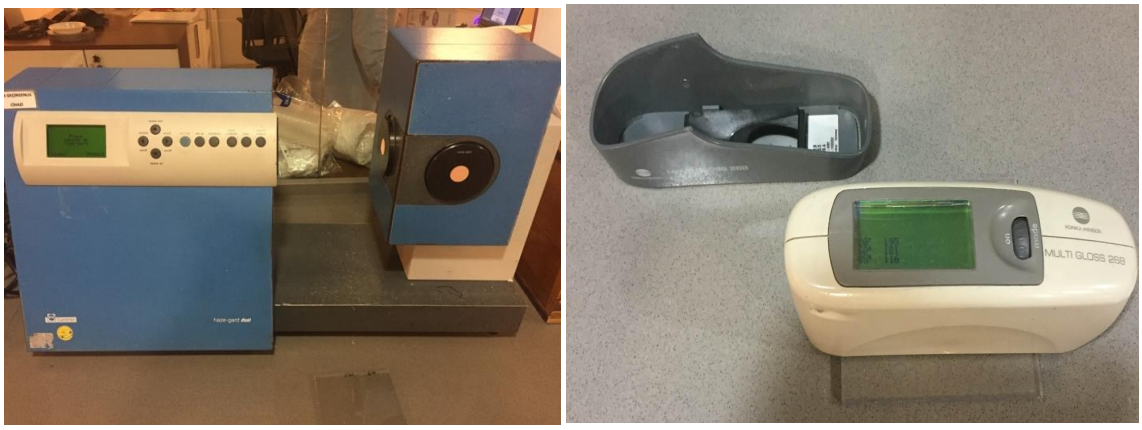

Fig. 7 Light Transmittance /Haze Meter and Gloss Meter

3. Results and Discussion

3.1. Contact angle Measurements

Tablo 1. Contact angle results

	Water	CA (°)	Ethylene glycol	CA (°)	Diiodo methane	CA (°)
1. Layer		50.28		50.97		48.27
2. Layers		54.14		51.39		50.17
3. Layers	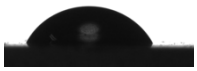	64.62		57.70		50.29
4. Layers	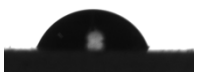	75.43		59.58		53.41
5. Layers	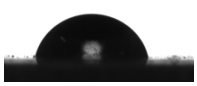	80.59	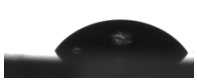	66.22		53.77

It can be seen from Table 1, as the number of layers increased, the contact angle value increased for all liquids. However, the surface showed hydrophilic character in all coating layers. The increase in the number of layers was less effective for apolar liquid than for a polar liquid. The lowest contact angle value is 48.27 degrees in 1 layer for diiodomethane. The highest contact angle value is 80,59 degrees in 5 layers for water.

Micro cracks occurring in the coatings appear in the surface images. film thicknesses are 804.7 nm, 679.6 nm, and 772.1 nm for 3, 4, and 5 coatings, respectively. As expected, the increase in the number of layers resulted in an increase in film thickness.

Table 2. SEM images of layers

	1. Layer	2. Layers	3. Layers	4. Layers	5. Layers
Surface	NA	NA	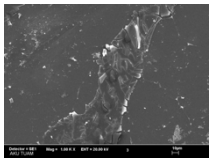	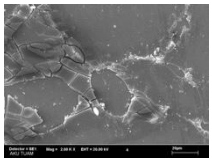	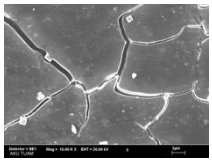
Cross section	NA	NA	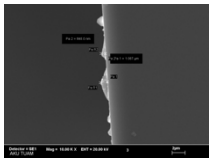	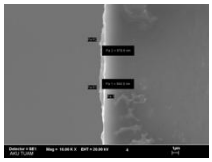	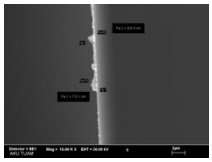

Table 2. Physical properties of layers

Properties	1. Layer	2. Layers	3. Layers	4. Layers	5. Layers
% Transmittance	91	90	90	89	88
% Haze	2,54	3,87	5,46	6,88	9,10
Gloss (60°)	174	156	148	126	108

SEM-EDX data of the coating layer are given in Figure 8.

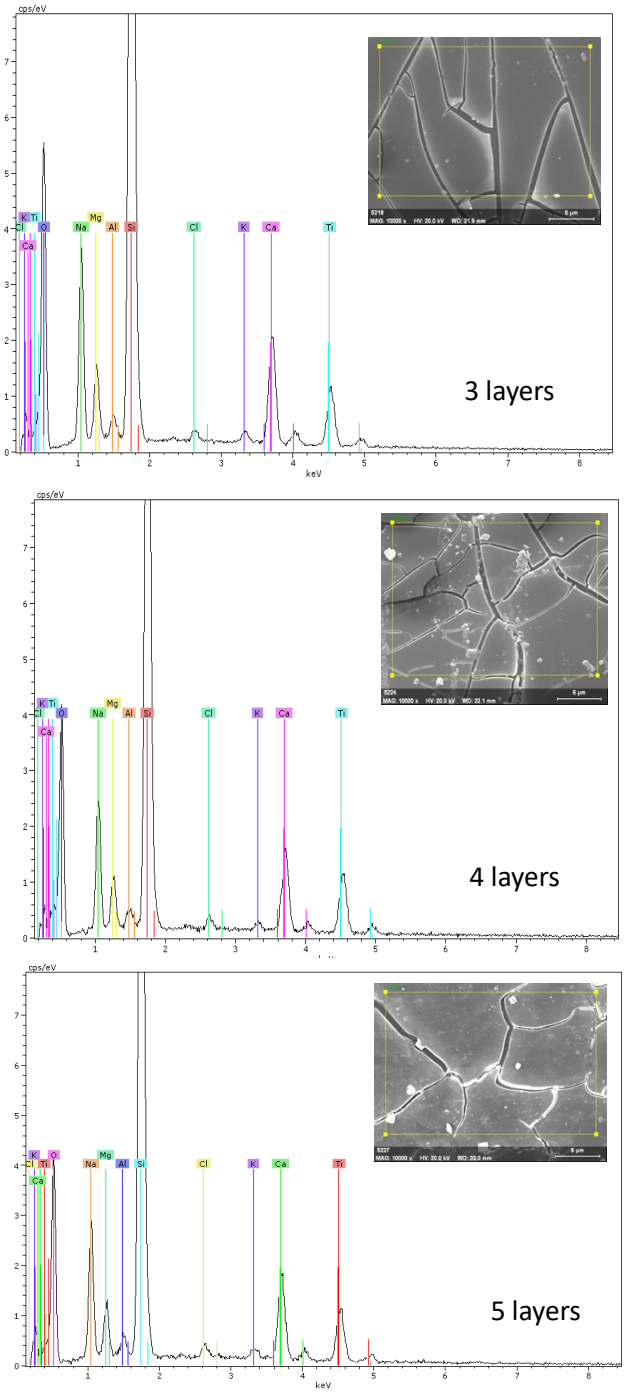

Element	Atom. C [wt.-%]		
	3 layers	4 layers	5 layers
Oxygen	57.03	64.17	65.06
Sodium	7.87	6.29	6.14
Magnesium	2.41	1.76	1.65
Aluminium	0.75	0.42	0.42
Silicon	26.30	21.97	21.18
Chlorine	0.53	0.25	0.19
Potassium	0.45	0.28	0.21
Calcium	2.83	2.60	2.52
Titanium	1.82	2.26	2.63

Fig. 8 SEM-EDX results

From the EDX data in Figure 8, non-titanium elements come from the base glass. The presence of the element titanium indicates that the coating has taken place. As can be seen from Figure 8, with the increase in the number of layers, the percentage by weight of the titanium atom also increases. This is a sign of how sensitive the coating has been made.

Figure 9 shows the elemental map of the coating surface. The distribution of orange-colored titanium and green-colored oxygen atoms can be seen on the surface.

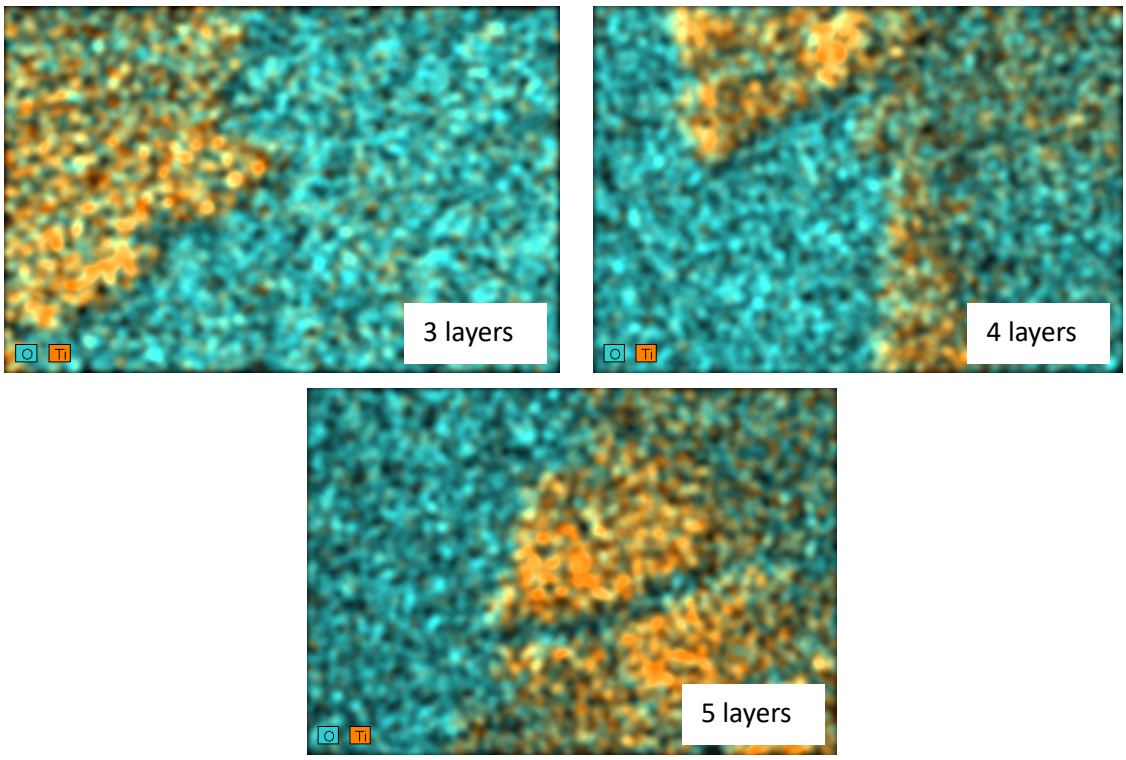

Figure 9 Colorized photograph of selected area of coatings

4. Conclusions and Recommendations

In this study, hydrophilic coating was obtained by sol-gel method. The effects of the solvent type and the number of coating layers on the contact angle in the coating on glass have been revealed.

As the number of coating layers increased, the percentage of light transmittance and gloss value decreased. However, the haze value increased.

All coated samples were hydrophilic. The increase in the number of coating layers caused an increase in the contact angle.

Depending on the solvent type, the contact angle value is in the form of water>ethyleneglycol>diiodomethane from larger to smaller.

5. Acknowledge

I would like to thank Afyon Kocatepe University Institute of Science and Scientific Research Projects Coordination Unit (BAPK) for the support of the project numbered 20.FEN.BİL.32.

References

1.Toygun, Ş., Köneçoğlu, G., & Kalpakli, Y. (2013). General Principles Of Sol-Gel. Sigma: Journal of Engineering & Natural Sciences/Mühendislik ve Fen Bilimleri Dergisi, 31(4).

2.Sangchay, W. (2016). The self-cleaning and photocatalytic properties of TiO2 doped with SnO2 thin films preparation by sol-gel method. Energy Procedia, 89, 170-176.

3.Akpan, U. G., & Hameed, B. H. (2010). The advancements in sol–gel method of doped-TiO2 photocatalysts. Applied Catalysis A: General, 375(1), 1-11.

4.Keszei, S. J., Pekker, P., Fehér, C., Balogh, S., Jakab, M., Nagy, L., & Skoda-Földes, R. (2020). Application of sol-gel methods to obtain silica materials decorated with ferrocenyl-ureidopyrimidine moieties. Preparation of hollow spheres and modification of a carbon electrode. Microporous and Mesoporous Materials, 308.

5. Wang, Y. T., Zhang, X. T., Xu, J. B., Shen, Y., Wang, C. A., Li, F. W., ... & Shen, R. Q. (2020). Fabrication and characterization of Al–CuO nanocomposites prepared by sol-gel method. Defence Technology. 110380.

6. Otitoju, T. A., Ahmad, A. L., & Ooi, B. S. (2017). Superhydrophilic (superwetting) surfaces: A review on fabrication and application. Journal of industrial and engineering chemistry, 47, 19-40

7. Göksu E. (2016). Sol-Jel Yöntemiyle Antibakteriyel İnce Film Kaplanması/Yüksek Lisans Tezi,Afyon Kocatepe Üniversitesi Fen Bilimleri Enstitüsü, Afyonkarahisar

8. Brinker, C. J., Frye, G. C., Hurd, A. J., & Ashley, C. S. (1991). Fundamentals of sol-gel dip coating. Thin solid films, 201(1), 97-108.

9. Kurtulus, C., Kurtulus, R., Surface Modification of Anhydrous Borax with Stearic Acid by Wet Coating Method, *Journal of Characterization,* Vol 1 (1), 1-9, 2021.

10. Adam, N. K. (1964). The chemical structure of solid surfaces as deduced from contact angles

11. Drelich, J., & Chibowski, E. (2010). Superhydrophilic and superwetting surfaces: definition and mechanisms of control. Langmuir, 26(24), 18621-18623.

12. Marmur, A., Della Volpe, C., Siboni, S., Amirfazli, A., & Drelich, J. W. (2017). Contact angles and wettability: towards common and accurate terminology. Surface Innovations, 5(1), 3-8.

13.Song, J. W., & Fan, L. W. (2020). Temperature dependence of the contact angle of water: A review of research progress, theoretical understanding, and implications for boiling heat transfer. Advances in Colloid and Interface Science, 102339.

14. R. N. Wenzel, "Resistance of solid surfaces to wetting by water," Industrial Engineering Chemistry, vol. 28, pp. 988–994, 1936.

15. Yuan, Y., & Lee, T. R. (2013). Contact angle and wetting properties. In Surface science techniques (pp. 3-34). Springer, Berlin, Heidelberg.

16. J. Fang, A. Kelarakis, L. Estevez, Y. Wang, R. Rodriguez ve E. P. Giannelis, "Superhydrophilic and solvent resistant coatings on polypropylene fabrics by a simple deposition process," Journal of Materials Chemistry, vol. 20, pp. 1651–1653, 2010.

17.A. Fujishima, T. N. Rao ve D. A. Tryk, "Titanium dioxide photocatalysis," Journal of Photochemistry and Photobiology C: Photochemistry Reviews, vol. 1, pp. 1–21, 2000.

18.Çiğil, A. B., Kandirmaz, E. A., Birtane, H., & Kahraman, M. V. Yüksek Hidrofilik Polietilen İmin Kaplamaların Hazırlanması Ve Karakterizasyonu. Düzce Üniversitesi Bilim ve Teknoloji Dergisi, 7(3), 973-984.

19.J. Drelich, E. Chibowski, D. D. Mengb ve K. Terpilowskic, "Hydrophilic and superhydrophilic surfaces and materials," Soft Matter, vol. 7, no. 21, pp. 9804-9828, 2011.

20.Zhang, H., Guo, G., Liu, L., Tao, F., Ren, J., & Zheng, L. (2019). Durable, water-cleanable, superhydrophilic coatings for oil/water separation under harsh conditions. Journal of Saudi Chemical Society, 23(8), 1007-1015.

21. Adachi, T., Latthe, S. S., Gosavi, S. W., Roy, N., Suzuki, N., Ikari, H., & Terashima, C. (2018). Photocatalytic, superhydrophilic, self-cleaning TiO2 coating on cheap, light-weight, flexible polycarbonate substrates. Applied Surface Science, 458, 917-923.

İnt ref 1 https://www.nanoscience.com/techniques/tensiometry/

JOURNAL of CHARACTERIZATION

Journal of Characterization
Vol 1, Special Issue, pp. 29-35, December 2021

ISSN: 2757-9166
Research Article

https://jcharacterization.com
https://jcharacterization.org

Effect of Starch Addition on Porosity in Reaction Sintering of Alumina and Magnesia

Melih Özçatal[1*], M. S. Başpınar[2], Hakan Çiftçi[3]

[1*] Afyon Kocatepe University, Faculty of Technology, Department of Metallurgical and Materials Engineering, Afyonkarahisar, Turkey, (ORCID: 0000-0002-0831-9038), mozcatal@aku.edu.tr
[2] Afyon Kocatepe University, Faculty of Technology, Department of Metallurgical and Materials Engineering, Afyonkarahisar, Turkey, (ORCID: 0000-0003-2086-1935), sbaspinar@aku.edu.tr
[3] Afyon Kocatepe University, Faculty of Engineering, Department of Mining Engineering, Afyonkarahisar, Turkey, (ORCID: 0000-0001-7910-7350), hakanciftci86@gmail.com

(Received date: 28.12.2021 and Accepted date: 31.12.2021)

(**DOI: 10.29228/JCHAR.55662**)

REFERENCES: Özçatal, M., Çiftçi, H., Başpınar, M.S, Effect of Starch Addition on Porosity in Reaction Sintering of Alumina and Magnesia. *Journal of Characterization*, (1), Special Issue, 29-35, 2021.

Abstract

Porous magnesium aluminate ceramics were produced with a sintering process of α-Al_2O_3 and MgO. Up to 20% by weight of corn starch were used as a pore-forming agent. Pellets were prepared by powder metallurgy technique and produced by solid-state sintering route. The porosity of the sintered pellets was characterized with and without adding corn starch, respectively. In particular, the effects of corn starch additive on density, porosity, and microstructure were investigated. Almost full density was obtained in the samples without starch addition. The study results showed that corn starch addition increased the porosity of the sintered samples. Maximum porosity of 47.86 % was achieved with the addition of 20 wt. % corn starch of 1400°C sintering temperature.

Keywords: Porous $MgAl_2O_4$, Starch Addition, Microstructure, Sintering

Alümina ve Magnezyanın Reaksiyon Sinterlenmesinde Nişasta İlavesinin Gözeneklilik Üzerindeki Etkisi

Öz

Gözenekli magnezyum alüminat seramikler, α-Al_2O_3 ve MgO'nun sinterlenmesiyle üretilmiştir. Gözenek oluşturucu madde olarak ağırlıkça %20'ye kadar mısır nişastası kullanılmıştır. Peletler, toz metalurjisi tekniği ile hazırlanmış ve katı hal sinterleme yöntemiyle üretilmiştir. Sinterlenmiş peletlerin gözenekliliği, mısır nişastası eklenerek ve eklenmeden karakterize edilmiştir. Özellikle mısır nişastası katkısının yoğunluk, gözeneklilik ve mikro yapı üzerindeki etkileri araştırılmıştır. Nişasta ilavesi yapılmayan numunelerde hemen hemen tam yoğunluk elde edilmiştir. Çalışma sonuçları, mısır nişastası ilavesinin sinterlenmiş numunelerin gözenekliliğini arttırdığını göstermiştir. 1400°C sinterleme sıcaklığında ağırlıkça % 20 mısır nişastası ilavesi ile % 47.86 gözeneklilik elde edilmiştir.

Anahtar Kelimeler: Gözenekli $MgAl_2O_4$, Nişasta İlavesi, Mikroyapı, Sinterleme

1. Introduction

In general, porous ceramics share many common properties such as high porosity, high chemical stability, good thermal shock resistance, and excellent thermal insulation, enabling their use in various applications, including gas and liquid filters, carriers, and insulation [1-4].

Porous magnesium aluminate spinel ($MgAl_2O_4$) is one of the refractory ceramics widely used as gas filters, catalytic supports, and separation membranes because of their high melting point (2135°C), high specific surface area, high thermal shock resistance, relatively low thermal conductivity and thermal expansion coefficient, and good chemical inertness [5-6].

Pore-forming agents are one of the most frequently used methods to produce porous ceramics with controlled microstructure (porosity and pore size) [7-9]. During the heating of the ceramics to the final firing temperature, these pore-forming substances burn, leaving empty pores in the ceramic. Among the various pore-forming agents, those of biological origin, especially starch, have gained a significant position [10-13]. Starch is inexpensive, non-toxic, environmentally friendly, and exhibits defect-free combustion between about 300 and 600°C [14]. Starch can be used as a pore-forming agent. It can be used as an additive in slip casting or as a combined pore-forming and body-forming agent in so-called starch consolidation [15]. In addition to these techniques, this study, it is aimed to form pores by adding corn starch to the anhydrous system.

In our previous work, the dense spinel ceramics with high strengths have been prepared using Al_2TiO_5 as an additive in reaction sintering of α-Al_2O_3 and MgO [16]. Using the results obtained in the previous study, the composition showing a high densification tendency was chosen in this study. Accordingly, it is aimed to close the cracks that may occur due to the voids formed by the corn starch with high densification during sintering.

In this work, corn starch was utilized to prepare porous MA spinel ceramic materials with reactive sintering of α-Al_2O_3 and MgO. The effects of starch ratio and sintering temperatures on the microstructure, density, and porosity were investigated.

2. Materials and Method

In this study, α-Al_2O_3 (>99.7%, 2 μm, Nabaltec), MgO (>98%, Merck), and corn starch (Piyale, Turkey) were used as raw material and Al_2TiO_5 (AT) as an additive material. AT was prepared by solid-state sintering reaction by adding 10 wt. % MgO to the equimolar mixture of α-Al_2O_3 and TiO_2 and sintering at 1450°C for 3 hours [16]. The samples obtained were powdered using a ring mill and used as an additive material in this study. After adding 10 % by weight of AT to equal mole amounts of α-Al_2O_3 and MgO, the powders were mixed in an ethanol medium for 30 minutes in a porcelain mill. Then, it was kept in an oven at 80°C for 24 hours, and the ethanol was removed. Compositions were formed by adding 5, 10, and 20 % corn starch by weight to the dry powder mixture obtained. These compositions were homogenized by mixing for 10 minutes in a dry environment in a porcelain mill. The samples were formed into pellets by weighing 8 grams of powder and pressed under 30 MPa pressure in a steel mold (diameter = 30 mm) using a uniaxial semi-automatic press. Three samples were produced for each composition. The names and compositions of the prepared samples are given in Table 1.

A high-temperature furnace (Protherm) with a $MoSi_2$ heating element was used for sintering. The samples were sintered at 1400 and 1500°C for 1 hour in an air atmosphere. The heating rate of the furnace was 5°C/min, and the cooling rate was 2°C/min. According to Archimedes' principle, bulk density, apparent porosity, and water absorption values were calculated. The Archimedes method tests were verified with three samples. A powder diffractometer with Cu Kα radiation (λ=1.5418 Å) and a secondary graphite monochromator was used for phase analysis (Shimadzu, XRD-6000). X-ray diffraction (XRD) spectra were obtained by scanning from 25° to 70° angles (2θ), at a goniometer speed of 1.25°/min, at an accelerating voltage of 40 kV and a current of 30 mA. The fractured surfaces of the samples were coated with carbon and investigated with a scanning electron microscope (SEM) (LEO-1430VP).

Table 1. Corn starch ratios and sintering temperature of the samples.

Sintering Temperature/ Corn Starch Ratio (wt. %)	***0***	***5***	***10***	***20***
Sintered at 1400°C (1h)	M014	M514	M1014	M2014
Sintered at 1500°C (1h)	M015	M515	M1015	M2015

3. Results and Discussion

The bulk density values of the samples determined by the Archimedes' method are given in Figure 1. Corn starch addition decreased the bulk density as expected. The theoretical density of MA spinel is 3,58 g/cm^3. The bulk density of the M015 sample was measured as 3.336 g/cm^3. The apparent porosity of this sample, which was sintered at 1500°C without adding corn starch, was measured as 0.159 % and the water absorption percentage as 0.047. It can be said that the MA spinel that will form the skeleton approaches almost full density at this composition and sintering temperature. The sample sintered at 1400°C without corn starch addition has a bulk density of 2.464 g/cm^3. At the sintering temperature of 1400°C, these samples did not show full densification and had porosity without adding corn starch. Figure 2 shows the apparent porosity of the sintered samples. Porosity decreased with increasing sintering temperature [17-18]. At the same time, the porosity values increased with the addition of corn starch. With the addition of 20 % corn starch, approximately 50 % porosity was obtained in the samples sintered at 1400°C.

The water absorption % of the samples is given in Figure 3. With the increase of sintering temperature, the water absorption values showed a significant decrease. With the addition of corn starch to the system, the increase in water absorption values became evident. Water absorption values are lower than the apparent porosity. This indicates the presence of both open and closed pores in the system.

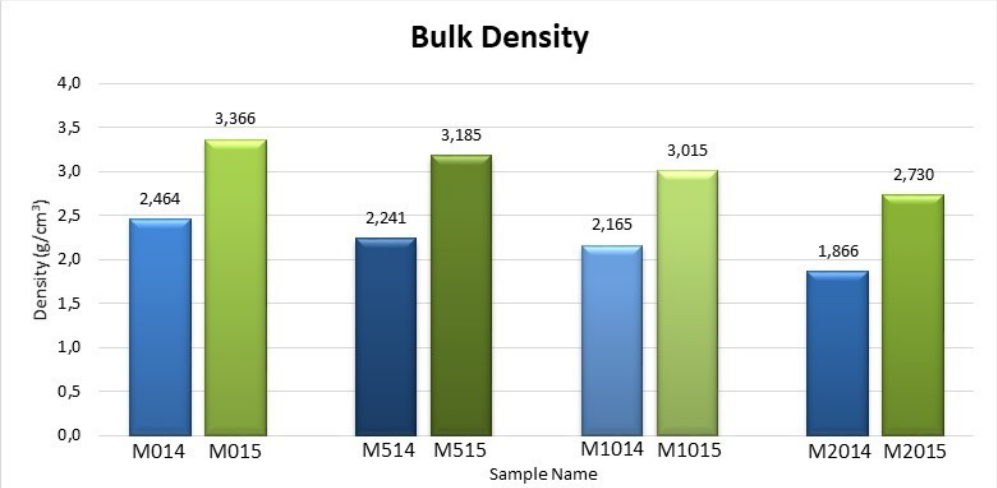

Figure 1. Bulk density of the sintered pellets.

Water absorption values are an indirect indicator of the amount of open pores. If the water absorption values of a material with a specific porosity value are very close to the apparent porosity values, the existing pores in the material are primarily open pores. However, if the difference between these values is large, the material has both open and closed pores. The relationship between water absorption and apparent porosity values can be explained in this way.

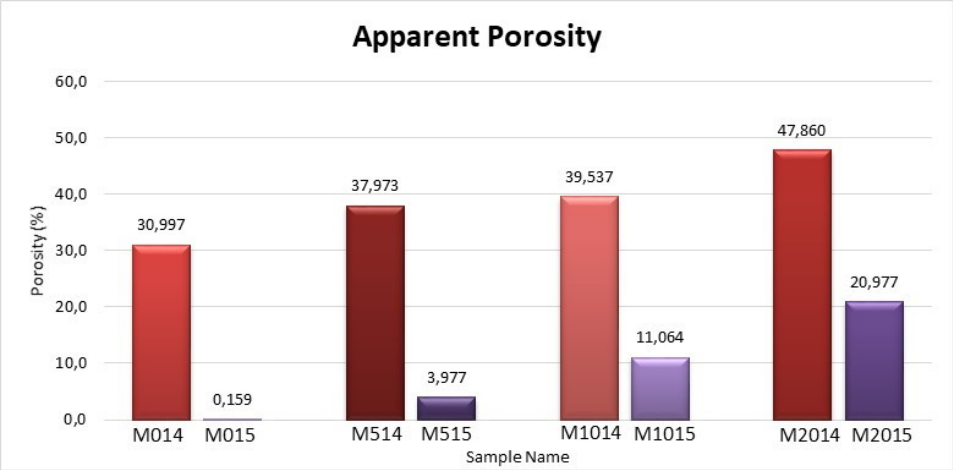

Figure 2. Apparent porosity of the sintered pellets.

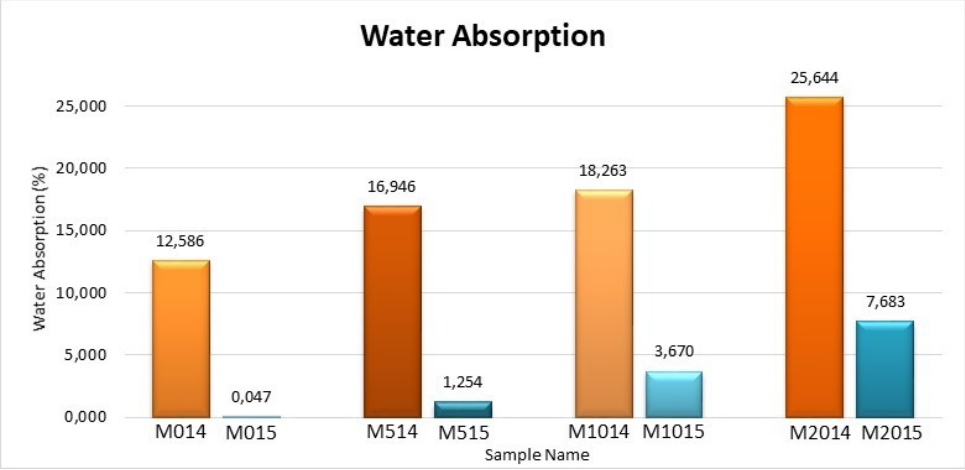

Figure 3. Water absorption of the sintered pellets.

XRD phase analyzes of sintered samples are given in Figure 4. The main phases were determined by performing XRD analyzes on samples without starch additives. The primary phase is MA spinel. A high amount of MA spinel phase was formed at both sintering temperatures. In this case, the starting powders α-α-Al_2O_3 and MgO reacted to form the MA phase. The sintered samples contain a small amount of the Al_2TiO_5 phase. Al_2TiO_5 phase was used as an additive to increase the densification. As the sintering temperature increased, the intensities of the minor peaks decreased.

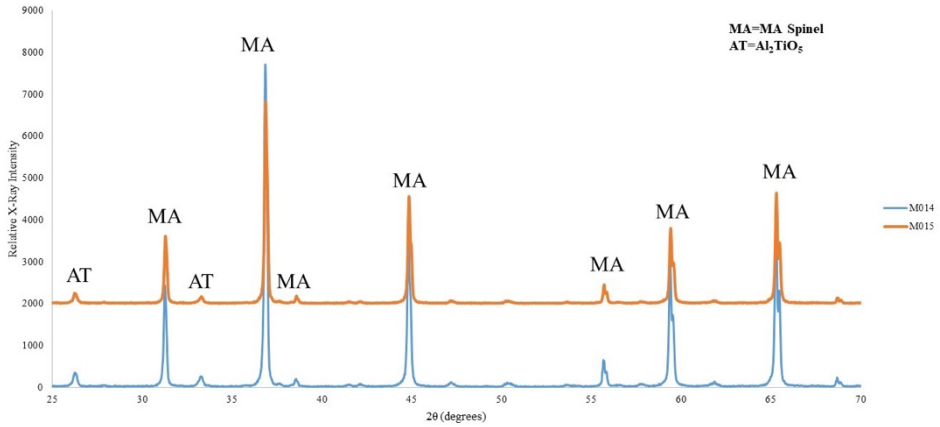

Figure 4. XRD phase analysis of the sintered samples.

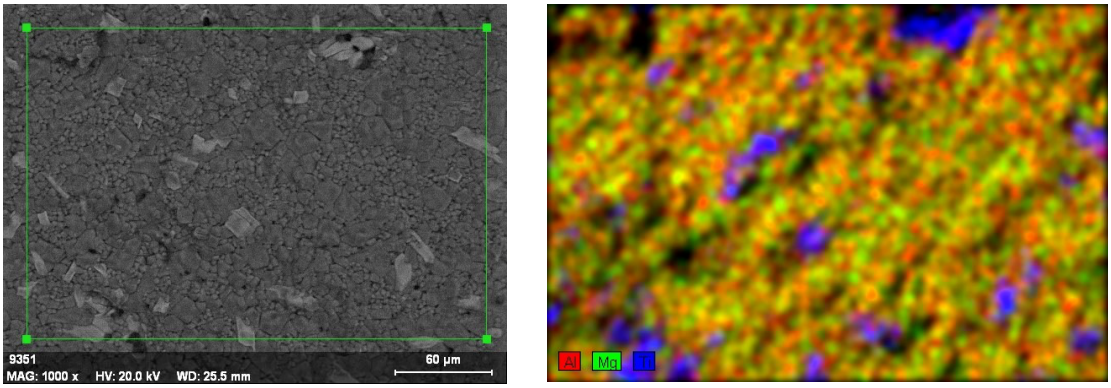

Figure 5. SEM micrographs (M015), BSE micrograph (left), SEM-EDX mapping micrograph (right).

SEM-BSE micrograph of the fractured surface of sample M015 is shown in Figure 5. It is seen that the sample has a dense structure. Unreacted AT grains appear in white, MA grains appear in gray. In addition, although overgrown MA grains are visible, the sample contains few pores. These results are consistent with the bulk density and porosity values obtained with Archimedes'.

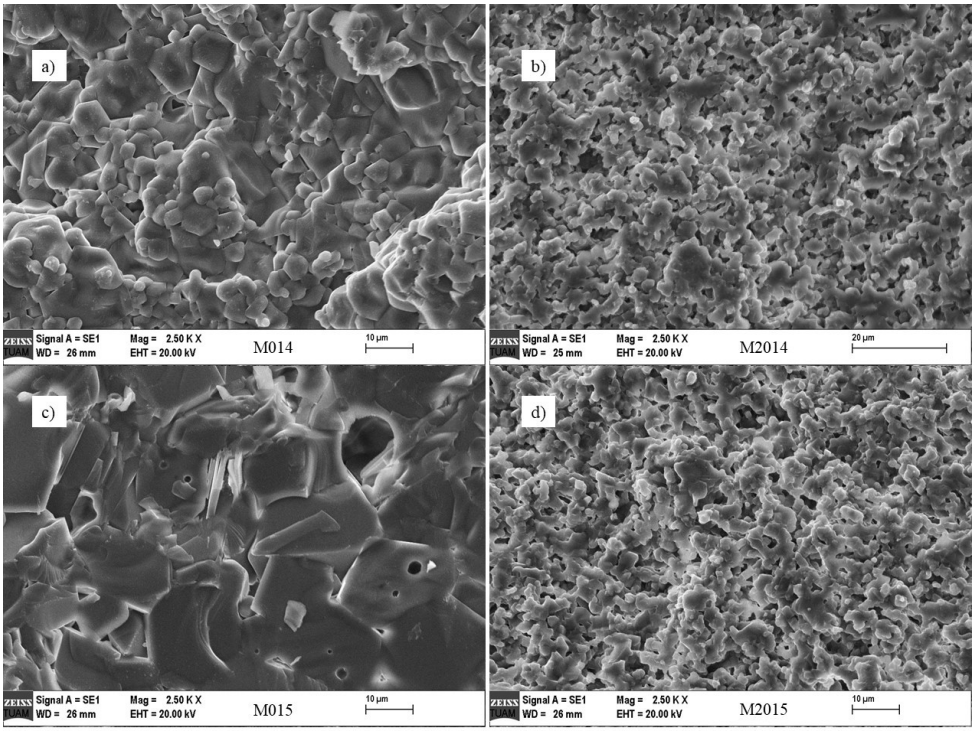

Figure 6. SEM-SE micrographs, a) Sample without starch additive sintered at 1400°C, b) Sample with starch additive sintered at 1400°C, c) Sample without starch additive sintered at 1500°C, d) Sample with starch additive sintered at 1500°C.

SEM-SE micrographs of the fractured surface of the samples are given in Figure 6. Samples sintered without starch additives have very little porosity. Grain growth is observed as the sintering temperature rises from 1400°C to 1500°C. Even overgrown grains are evident. The porosity is seen in the samples in which corn starch is added to the composition. It can be thought that corn starch burns during sintering and forms voids in its positions. According to DTA analysis, during heating, corn starch dehydrates up to about 115°C and loses 11.50 % of its weight. The second weight loss between 275 and 325°C occurs with the combustion of amylopectin groups, and 65.29% of the starch weight is lost. Finally, with the removal of the amylose group between 325-525°C, it loses 22.66% of its weight and completely disappears from the system [19-20].

4. Conclusions and Recommendations

This study carried out MA spinel production with porosity successfully using corn starch. Corn starch acted as a pore former.

As a result of sintering the starting powders by trying a composition that will create a high density, MA spinel with a value close to the theoretical density was produced according to Archimedes' results in the samples without starch. These results were in agreement with the XRD phase analysis.

According to the SEM results, very few pores were detected in the samples without starch. The porosity of the samples increased due to the voids formed due to the removal of starch from the system.

Approximately 50% porosity was obtained in the samples sintered at 1400°C with the addition of 20 % by weight of corn starch.

5. Acknowledge

This study was supported by Afyon Kocatepe University Scientific Research Projects Commission Project No: 18.KARİYER.52.

References

[1] R. K. Nishihora, P. L. Rachadel, M. G. N. Quadri, and D. Hotza, “Manufacturing porous ceramic materials by tape casting—A review,” *Journal of the European Ceramic Society*, vol. 38, no. 4, pp. 988–1001, 2018.

[2] L. Han, J. Wang, F. Li, H. Wang, X. Deng, H. Zhang, and S. Zhang, “Low-temperature preparation of Si3N4 whiskers bonded/reinforced SiC porous ceramics via foam-gelcasting combined with catalytic nitridation,” *Journal of the European Ceramic Society*, vol. 38, no. 4, pp. 1210–1218, 2018.

[3] W. Huo, X. Zhang, Y. Chen, Y. Lu, J. Liu, S. Yan, J.-M. Wu, and J. Yang, “Novel mullite ceramic foams with high porosity and strength using only fly ash hollow spheres as raw material,” *Journal of the European Ceramic Society*, vol. 38, no. 4, pp. 2035–2042, 2018.

[4] Y. Li, X. Yang, D. Liu, J. Chen, D. Zhang, and Z. Wu, “Permeability of the porous Al2O3 ceramic with bimodal pore size distribution,” *Ceramics International*, vol. 45, no. 5, pp. 5952–5957, 2019.

[5] I. Ganesh, “A review on magnesium aluminate (MgAl2O4) spinel: synthesis, processing and applications,” *International Materials Reviews*, vol. 58, no. 2, pp. 63–112, 2013.

[6] H. Chen, F. Liang, W. Fang, H. Chen, X. Du, F. Wang, and L. Zhao, “Fabrication of Microporous Corundum-Spinel Refractory Castables by Foam-Gelcasting Methods,” *Journal of Materials Engineering and Performance*, vol. 24, no. 8, pp. 3049–3055, 2015.

[7] R. W. Rice, Ed., *Ceramic Fabrication Technology*. New York: Marcel Dekker, 2002.

[8] A. R. Studart, U. T. Gonzenbach, E. Tervoort, and L. J. Gauckler, “Processing Routes to Macroporous Ceramics: A Review,” *Journal of the American Ceramic Society*, vol. 89, no. 6, pp. 1771–1789, 2006.

[9] Z. Zivcová, E. Gregorová, and W. Pabst, “Alumina ceramics prepared with new pore-forming agents,” *Processing and Application of Ceramics*, vol. 2, no. 1, pp. 1–8, 2008.

[10] H. Alves, Tarì G, A. Fonseca, and J. Ferreira, “Processing of porous cordierite bodies by starch consolidation,” *Materials Research Bulletin*, vol. 33, no. 10, pp. 1439–1448, 1998.

[11] A. Lemos and J. Ferreira, "Porous bioactive calcium carbonate implants processed by starch consolidation," *Materials Science and Engineering: C*, vol. 11, no. 1, pp. 35–40, 2000.

[12] E. Týnová, W. Pabst, E. Gregorová, and J. Havrda, "Starch Consolidation Casting of Alumina Ceramics - Body Formation and Microstructural Characterization," *Key Engineering Materials*, vol. 206-213, pp. 1969–1972, 2001.

[13] E. Gregorová and W. Pabst, "Porosity and pore size control in starch consolidation casting of oxide ceramics—Achievements and problems," *Journal of the European Ceramic Society*, vol. 27, no. 2-3, pp. 669–672, 2007.

[14] E. Gregorová, W. Pabst, and I. Bohačenko, "Characterization of different starch types for their application in ceramic processing," *Journal of the European Ceramic Society*, vol. 26, no. 8, pp. 1301–1309, 2006.

[15] Z. Živcová, E. Gregorová, W. Pabst, D. S. Smith, A. Michot, and C. Poulier, "Thermal conductivity of porous alumina ceramics prepared using starch as a pore-forming agent," *Journal of the European Ceramic Society*, vol. 29, no. 3, pp. 347–353, 2009.

[16] M. Özçatal and M.S. Başpınar, "An Initial Study, the Effect of MgO Addition on Some Physical Properties of Al2TiO5," *Oct. 5-6, 2017 Paris - France ICIET-17, CABHS-17, CAEME-17, LHFHM-17 & BLEDS-17*, 2017.

[17] C. Kurtuluş and R. Kurtuluş, "Synthesis of Wollastonite from Boron Waste and Glass Scraps by Solid-State Reaction," *Journal Of Characterization*, vol. 1, no. 1, pp. 26–33, 2021.

[18] I. Yıldız, A. Evcin, E. Çelmeli, and I. Gündüz, "Grafen Nanotabaka Katkılı Alümina Esaslı Kompozit Üretimi ve Karakterizasyonu," *Journal Of Characterization*, vol. 2, no. 2, pp. 71–80, 2021.

[19] A. Kalemtas, G. Topates, M. T. A. Aydin, and N. Özey, "Starch consolidation of SiC ceramics: processing and low-temperature sintering in an air atmosphere," *Journal of Asian Ceramic Societies*, vol. 8, no. 1, pp. 106–115, 2020.

[20] G. Topateş, U. Petasch, J. Adler, F. Kara, and H. Mandal, "Production and permeability of porous Si3N4 ceramics produced by starch addition," *Journal of Asian Ceramic Societies*, vol. 1, no. 3, pp. 257–261, 2013.

JOURNAL of CHARACTERIZATION

https://jcharacterization.com
https://jcharacterization.org

Journal of Characterization
Vol 1, Special Issue, 36-41, December 2021

ISSN: 2757-9166
Research Article

Investigation of Surface Properties of Borided Chromium-Cobalt Alloys

İsmail Yıldız

Afyon Kocatepe University, Iscehisar Vocational School, Department of Machinery and Metal Technologies, 03750, Afyonkarahisar/Turkey (ORCID: 0000-0002-9207-591X), iyildiz@aku.edu.tr

(Received date 24.12.2021 and Accepted date 31.12.2021)

(DOI: 10.29228/JCHAR.55671)

ATIF: Yıldız, I., Surface Characterization and Boriding of Chromium and Cobalt Alloys. *Journal of Characterization*, (1), Special Issue, 36-41, 2021.

Abstract

In the study, Co-Cr alloy containing 10% Co was successfully borided by boriding method at 900 °C temperature for 1.5-4.5 hours. After boriding, the properties of boron layers were investigated with XRD, SEM, surface roughness, density and microhardness tester. After boriding on Cr-Co alloys, CrB and Cr_2B emerged as the main dominant phases. After SEM, saw-tooth structures were formed in the boron layers. The thickness of boride layer varied from 32,24 to 143.84 μm depending on the process time. Boride layer has a hardness varied from 1752 to 1865 $HV_{0.05}$ for Cr-Co alloy, whereas the Vickers hardness value of the untreated Cobalt and Chromium were 194 $HV_{0.05}$ respectively.

Keywords: Cr-Co alloy, boride, hardness, density

Borlanmış Krom-Kobalt Alaşımlarının Yüzey Özelliklerinin İncelenmesi

Oz

Çalışmada %10 Co içeren Co-Cr alaşımı 900 °C sıcaklıkta 1.5-4.5 saat borlama yöntemiyle başarılı bir şekilde borlanmıştır. Borlama sonrası bor tabakalarının özellikleri XRD, SEM, yüzey pürüzlülüğü, yoğunluk ve mikrosertlik test cihazı ile incelenmiştir. Cr-Co alaşımlarında borlamadan sonra CrB ve Cr_2B ana baskın fazlar olarak ortaya çıkmıştır. SEM'den sonra bor tabakalarında testere dişi yapıları oluşmuştur. Bor tabakasının kalınlığı işlem süresine bağlı olarak 32,24 ile 143,84 μm arasında değişmektedir. Bor tabakası, Cr-Co alaşımı için 1752 ila 1865 $HV_{0.05}$ arasında değişen bir sertliğe sahipken, borlama öncesinde ise vickers sertlik değeri 194 $HV_{0.05}$ idi.

Anahtar Kelimeler: Cr-Co alaşım, borlama, sertlik, yoğunluk

1. Introduction

Cobalt-chromium (Co-Cr) alloys have been used for a long time, especially in prostheses and dental implants, which are among biomaterials due to their strength [1-3]. In metallic dental materials, studies on these alloys have always been at the forefront, mainly because of the chemical balance and biocompatibility of Co-Cr alloys. Contrary to these alloys, previous studies were focused on low alloy casting, which is less durable and does not have good properties. Therefore, depending on the development of technology, the usage area of Co-Cr alloys has become widespread and has improved its properties [4-7].

Boriding process is a thermochemical surface treatment which increases the hardness of boron atoms by spreading to the surface of Ni, Co and Mg alloys at high temperatures. Pure nickel, pure cobalt, Co-Cr alloys or Co-Cr-Mo alloys are good candidates for boronizing [8-10]. Boronizing improves surface of Co-Cr alloys hardness and wear, heat or corrosion resistance. Furthermore, the main advantage of boronizing is that boronized metals have a high surface hardness even at low friction coefficients. Its only disadvantage is that the borided layer has a fragile structure [11-13]. Boronizing is performed by heating materials with well-cleaned surfaces in solid, liquid or gaseous media between 800 and 1000 °C and from 1 to 12 hours. The most commonly used method is pack boronizing performed in closed containers [14,15].

In literature, there are many studies on resistance and effects of boron layer against the growth of boride layer by some elements (Co Cr, Fe, Al, Ni, Ti) [16-18]. However, since Mg is a highly reactive element, it has not been studied much on magnesium doped alloys. The primary aim of this study is to investigate the impact of chromium in cobalt on boriding process. For this purpose, Co-Cr alloys were borided and investigated some mechanics properties.

2. Material and Method

2.1. Boriding and Characterization

In this study, Cr and Co metal powders with 99% purity used in alloy materials with 90% Cr-10% Co compositions. Cr-Co metal powders were mixed in sealed boxes for 24 hours to obtain Cr-Co alloy materials with these compositions. The mixed powders shaped by pressing in the press under approximately 300 bar pressure. The samples obtained were subjected to heat treatment at 1000 °C for 2 hours in a closed oven environment.

Boriding method was done in closed boxes to prevent the samples from oxidizing under the effect of heat. In this method, Ekabor II powder, which has a boriding feature, is poured on the top and bottom of the Cr-Co alloys to be borided to cover them. After this process, the lid parts of the boxes are tightly closed with chamotte mud to prevent air. Figure 1 shows the boron crucible of Cr-Co alloys.

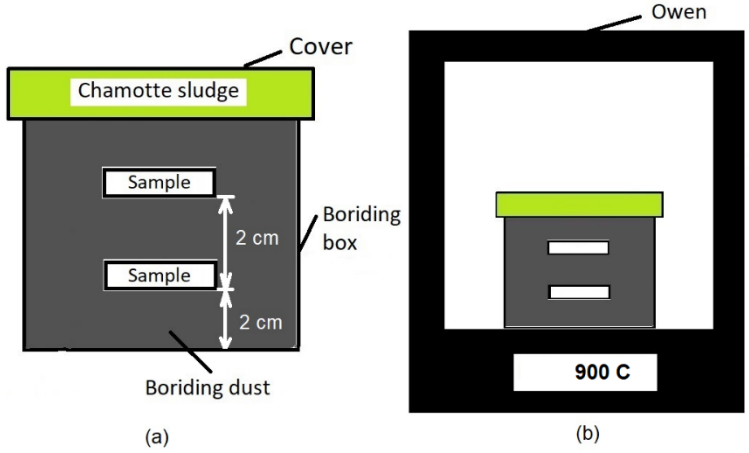

Figure 1. Placement of boring boxes in the furnace

Samples in the box heated at 900 ° C for 1.5 and 4.5 hours. After this step, the samples were taken out of the oven and allowed to cool with air. Microstructures of the borided samples were determined by Nikon MA200 optical microscope after boriding. The phases formed in boron structures were revealed in Shimadzu 6000 XRD. SEM analysis was performed with the LEO 1430 VP model SEM device. Hardness measurements of the borided and non-borided samples were carried out in the Shimadzu HMV-2 Vickers hardness tester under 50 g loading.

3. Results and Discussion

3.1. Characterization of Boride Coatings

Borided microstructure images of Co-Cr alloy after 900 °C temperature and 1.5-4.5 hours are shown in Figure 2a-2b.

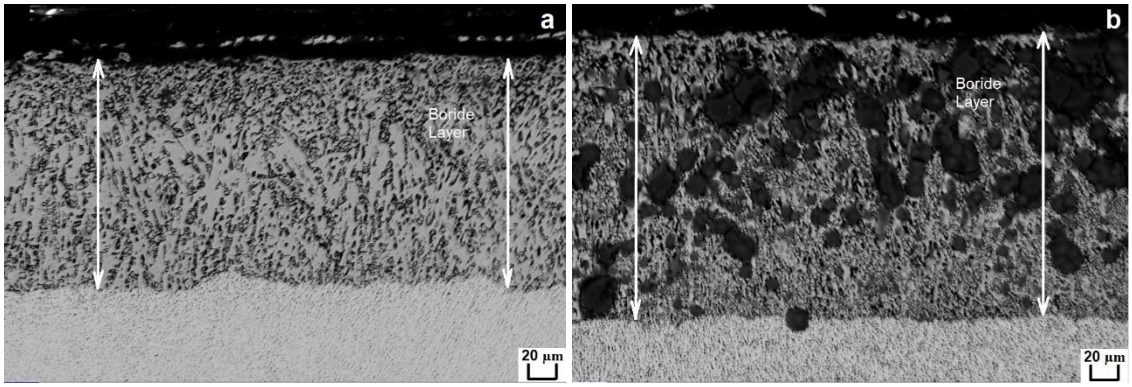

Figure 2. SEM analysis images of borided at 900 °C of 90% Cr-10% Co alloy (a) 1.5 h, (b) 4,5 h

Boron layers formed on the substrate of Cr-Co alloys, depending on the increasing temperature and time after the boriding process, sawtooth-like morphology. Due to Co element's high melting temperature of the Co element, it is seen that the powders do not fully adhere to each other in the microstructure and therefore form a partially porous structure. On the other hand, there has been an increase in boron layer thicknesses. Boriding layer thickness on the surface, depending on the chemical composition of the substrates, boriding time and temperature of the 90% Cr-10% Co alloy vary between 32,24 to 143.84 µm in Figure 2a and 2b. Changes occurred in the morphology of the saw tooth due to the increase in the boring time. This indicates that oxidation occurs in the building, even if only partially.

3.2. XRD Analysis

Figures 3a and 3a show XRD phase values at 900 °C temperatures, 1.5-4.5 hours on the surface of borided 90% Cr-10% Co alloy. XRD samples indicated that the boride layers consisted of Chromium and Cobalt borides. XRD results showed that boride layers formed in Cr-Co alloys contain CrB, Cr_2B, and Cr_2Co phases. In Cr-Co alloy, CrB phase is more dominant than other phases. XRD results reveal that boride layers formed in Cr-Co alloys cover the CrB, Cr_2B, and Cr_2Co phases. With the increase in boriding temperature and duration, CrB phases became more dominant. Boride layers, consisting mainly of intermetallic phases, result from the diffusion of boron atoms to the Cr-Co alloys substrate for certain boriding process factors.

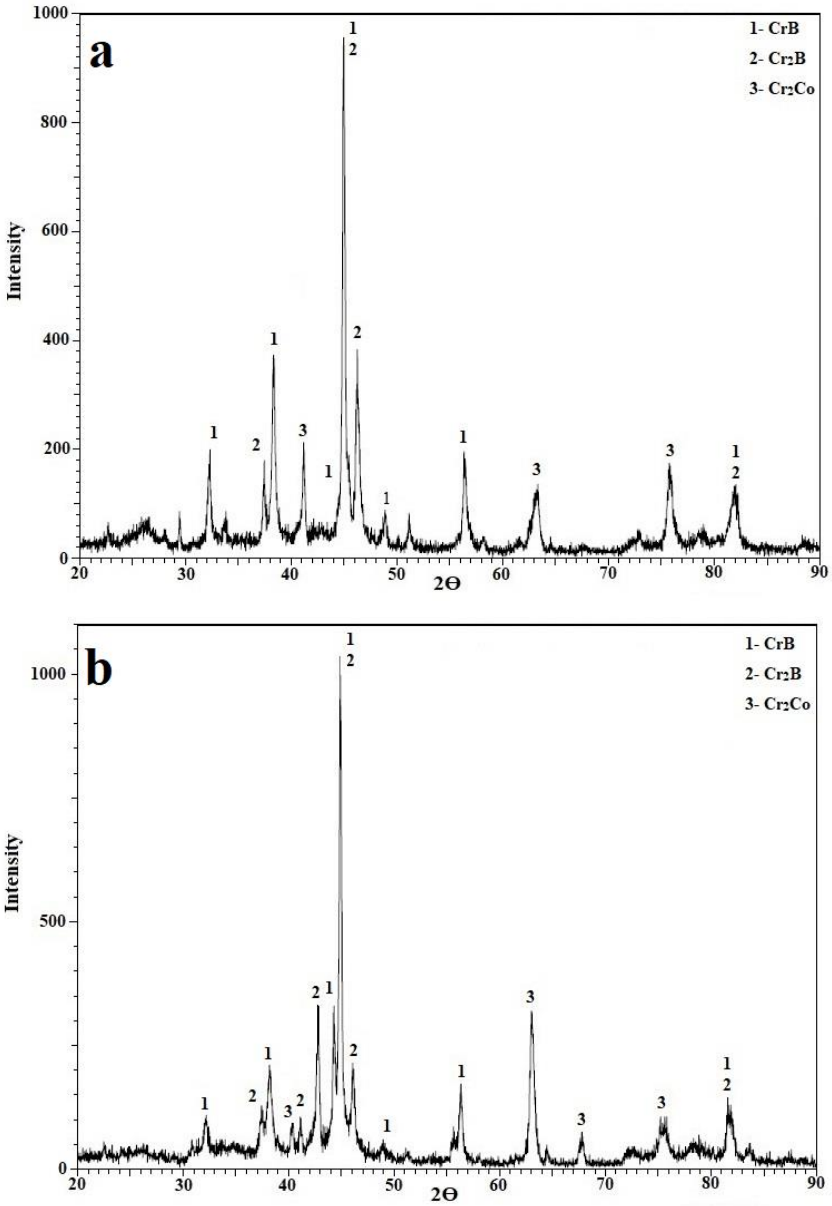

Figure 3. XRD analysis images of borided at 900 °C of 90% Cr-10% Co alloy (a) 1.5 h, (b) 4,5 h

3.3. Surface Roughness and Density

As a result of the surface roughness measurement, Ra values were found between 0.25-0.58 μm for Cr-Co alloy. After the density test, it was obtained as 6.82 gr/cm^3 for alloy.

While the roughness values increased between the surface roughness and density, the density values decreased. The surface roughness decreases, and the density increases due to the high boriding temperature on the surface and the boride layers filling these pores. It is seen that if the surface roughness values of boron coatings are low, the surface roughness values after coating increase, and if the surface roughness value of the substrate material before the coating is high, it is seen to decrease after coating.

4. Conclusions and Recommendations

The results obtained after the tests and analyzes of the Co-Cr alloy after boriding are given below:

- The highest boron layer thickness after boriding was found to be 143.84 μm after 4.5 hours.
- XRD analysis was performed as metallographic analysis. As a result of the analysis, CrB, Cr_2B and Cr_2Co phase structures were obtained.
- The density value of Co-Cr alloys measured after sintering was found to be 6.82 gr/cm^3.
- As a result of the hardness test performed after sintering, a value of 194 $HV_{0.05}$ was found.
- As a result of the microhardness test performed after boriding, the hardness values of 1752 $HV_{0.05}$ and 1865 $HV_{0.05}$ were measured in the samples, respectively.
- In the boriding method, boride layers became evident in parallel with the temperature and time, and there was a corresponding increase in the layer thickness. 900 °C was determined as the best boriding temperature according to the results.
- Higher boron layer thickness and microhardness value may occur by setting 1000 or 1100 °C as boriding temperature.

5. Acknowledge

This study was supported by Afyon Kocatepe University BAPK 17.MYO.05. Many thanks to the Scientific Research Projects Commission for their support.

References

[1] X. Dong, N. Li, Y. Zhou et al. “Grain boundary character and stress corrosion cracking behavior of Co-Cr alloy fabricated by selective laser melting”, *Journal of Materials Science & Technology*, vol. 93, 244-253, 2021.

[2] A. Amanov, “Effect of post-additive manufacturing surface modification temperature on the tribological and tribocorrosion properties of Co-Cr-Mo alloy for biomedical applications”, *Surface and Coatings Technology*, vol. 421, 127378, 2021.

[3] T. Aldhohrah, J Yang, J. Guo et al., “Ion release and biocompatibility of Co-Cr alloy fabricated by selective laser melting from recycled Co-Cr powder: An in vitro study”, *The Journal of Prosthetic Dentistry*, In Press, 2021.

[4] Y. Han, F. Liu, K. Zhang, et al. “A study on tribological properties of textured Co-Cr-Mo alloy for artificial hip joints”, *International Journal of Refractory Metals and Hard Materials*, vol. 95, 105463, 2021.

[5] A. Gabriella C. Presotto, J. M. Cordeiro, et al. “Feasibility of 3D printed Co–Cr alloy for dental prostheses applications”, *Journal of Alloys and Compounds*, vol. 862, 158171, 2021.

[6] Q. Hu, Y. Liu, Y. Pan, et al. “Assessments of ionic release and biocompatibility of Co-Cr and CP-Ti produced by three different manufacturing techniques”, *Materials Today Communications*, vol. 30, 103100, 2022.

[7] Y. Zhou, Q. Sun, X. Dong, et al. "Microstructure evolution and mechanical properties improvement of selective laser melted Co-Cr biomedical alloys during subsequent heat treatments", *Journal of Alloys and Compounds*, vol. 840, 155664, 2020.

[8] I. Gunes, I. Yıldız, "Rate of Growth of Boride Layers on Stainless Steels", *Oxidation Communication*, vol. 38(4/A), 2189-2198, 2015.

[9] I. Campos-Silva, D. Bravo-Bárcenas, H. Cimenoglu, et al. "The boriding process in CoCrMo alloy: Fracture toughness in cobalt boride coatings", *Surface and Coatings Technology*, vol. 260, 362-368, 2014.

[10] I. Yıldız, I. Gunes, "%3,0 Mg içeren Borlanmış Co-Mg Alaşımının Yüzey Özelliklerinin İncelenmesi", *El-Cezerî Journal of Science and Engineering,* vol: 6 (3), 533-542, 2019.

[11] M. A. Doñu-Ruiz, N. López-Perrusquia, A. Renteria-Salcedo, et al., "Tribocorrosion behavior of boride coating on CoCrMo alloy produced by thermochemical process in 0.35% NaCl solution", *Surface and Coatings Technology*, vol. 425,127698, 2021.

[12] R. C. Morón, A. M. Delgado-Brito, I. Campos-Silva, "Scratch resistance of cobalt boride layer subjected to a diffusion annealing process", *Materials Letters*, vol. 309, 131352, 2022.

[13] I. Gunes, I. Yıldız, "Investigation of Adhesion and Tribological Behavior of Borided AISI 310 Stainless Steel", *Revista Materia*, vol. 21, 61-71, 2016.

[14] R. Gupta, K. C. Hari Kumar, M. J. N. V. Prasad, et al. "Compositionally graded nano-sized borides in a directionally solidified nickel-base superalloy", *Scripta Materialia,* vol. 201, 113981, 2021

[15] I. Gunes, A. G. Celik, "Surface Characterization of Borided S220 Rebar", *Journal of Characterization*, vol. 1(2), 66-70, 2021.

[16] J. Hou, M. Zhang, H. Yang, et al. "Surface strengthening in Al0.25CoCrFeNi high-entropy alloy by boronizing", *Materials Letters*, vol. 238, 258-260, 2019.

[17] I. Turkmen, E. Yalamac, M. Keddam, "Investigation of tribological behaviour and diffusion model of Fe_2B layer formed by pack-boriding on SAE 1020 steel", *Surface and Coatings Technology*, vol. 377, 124888, 2019.

[18] I. Yildiz, A. G. Celik and I. Gunes, "Characterization and Diffusion Kinetics of borided Ni–Mg Alloys", *Protection of Metals and Physical Chemistry of Surfaces*, vol. 56(5), 1015–1022, 2020.

JOURNAL of CHARACTERIZATION

https://jcharacterization.com
https://jcharacterization.org

Journal of Characterization
Cilt 1, Özel Sayı, pp. 42-53, Aralık 2021

ISSN: 2757-9166
Derleme Makale

Tersine Mühendisliğin Makine Mühendisliği Alanındaki Uygulamaları Üzerine Bir Derleme

Ahmet Hasçelik[1*]

[1*] Afyon Kocatepe Üniversitesi, İscehisar Meslek Yüksekokulu, Makine ve Metal Teknolojileri Bölümü, Afyon, Türkiye, (ORCID: 0000-0002-4615-0640), ahascelik@aku.edu.tr

(İlk Geliş Tarihi 24.12.2021 ve Kabul Tarihi 31.12.2021)

(DOI: 10.29228/JCHAR.55624)

ATIF: Tersine Mühendisliğin Makine Mühendisliği Alanındaki Uygulamaları Üzerine Bir Derleme. *Journal of Characterization*, (1), Özel sayı, 42-53, 2021.

Öz

Tersine mühendislik, bir parçanın üretim sürecini geriye doğru gerçekleştirme işlemidir. Tersine mühendisliğin amacı, mevcut bir bilgisayar destekli tasarım (BDT) modeli olmadan, üç boyutlu (3B) model oluşturmaktır. Tersine mühendislik, üreticinin herhangi bir ürünle ilgili eksik dokümantasyona sahip olduğu durumlarda başvurduğu bir süreçtir. Mevcut bir üründen, BDT modelinin elde edilmesi için gerekli bir aşamadır. Bu çalışmada tersine mühendislik aşamaları anlatılmış ve makine mühendisliği alanındaki uygulamalarından bahsedilmiştir. Literatürdeki çalışmalar incelenmiş ve bu alandaki çalışmalar derlenmiştir. Bu alanda sıklıkla karşılaşılan birkaç tersine mühendislik işlemi ile ilgili detaylı bilgi verilmiştir. Çalışmada genel olarak tersine mühendislik sürecinin anlaşılması hedeflenmiş ve özellikle makine mühendisliği alanında, hangi durumlarda tersine mühendislik işlemine başvurulduğunun tespiti üzerinde durulmuştur. Böylece tersine mühendislik sürecinin makine sektöründe oldukça pratik ve verimli bir seçenek olduğu vurgulanmıştır.

Anahtar Kelimeler: Tersine Mühendislik; Makine Mühendisliği; Bilgisayar Destekli Tasarım; Hızlı Prototipleme; Optik Tarama; Üç Boyutlu Model.

A Review on the Applications of Reverse Enginnering in the Mechanical Enginnering

Abstract

Reverse engineering is the process of performing the manufacturing process of a part backwards. The goal of reverse engineering is to create a three-dimensional (3D) model without an existing computer aided design (CAD) model. Reverse engineering is a process that a manufacturer resorts to when they have missing documentation for any product. It is a necessary step to obtain a CAD model from an existing product. In this study, reverse engineering stages are explained and its applications in the field of mechanical engineering are mentioned. Studies in the literature were examined and compiled. Detailed information is given about a few reverse engineering processes that are frequently encountered in this field. The aim of this study is to understand the reverse engineering process in general and. especially in the field

of mechanical engineering, it has been focused on the determination of the situations in which reverse engineering is applied. Thus, it is emphasized that the reverse engineering process is a very practical and efficient option in the machinery industry.

Keywords: Reverse Engineering; Mechanical Engineering; Computer Aided Design; Rapid Prototyping; Optical Scanning; Three Dimensional Model.

1. Giriş

Mühendislik, insanlığın ihtiyaçları doğrultusunda, tasarlanan bir yapı, sistem ya da ürünün, matematik ve fen bilimlerine ilişkin bilgiler kullanılarak üretimini ve akabinde devamlılığını sağlayan, zaman ve verimi artırmaya yönelik değerlendirmeler yaparak bunları uygulamaya döken bir bilimdir. Mühendisliği en geniş kapsamda, ileriye dönük (forward) mühendislik ve geriye dönük (reverse) mühendislik olarak ikiye ayırabiliriz [1].

İleriye dönük mühendislik kavramı, geniş anlamdaki mühendislik uygulamaları süreçlerini kapsar. Örneğin makine mühendisliği alanında bir ürün imalatı sürecini inceleyecek olursak; bu süreç, öncelikle fikir olarak ihtiyaç doğrultusunda bir ürün tasarımı ile başlar, malzeme seçiminden sonra gerekli mühendislik hesaplamaları yapılır ve tasarım süreci tamamlanır. Tasarım süreci; teknik veriler, çizimler ve model üretimi gibi aşamaları kapsar. Kullanılacak üretim yöntemi seçildikten sonra uygulamaya geçilir. Bazı durumlarda, klasik mühendislik işlemindeki bu süreçlerden birkaçı eksik olabilir. Örneğin üreticide, mevcut ürünü seri üretimle çoğaltmak için gerekli teknik resim veya tasarım modeli olmayabilir [2]. Buna benzer durumlarda ürünün kendisinden hareket ederek üretim sürecini geriye doğru gerçekleştirme işlemi yapılır. Böylece ürünün başlangıç aşamasındaki teknik bilgileri elde edilir. Bu şekilde geriye giderek, ürünün başlangıçtaki bilgisayar destekli tasarım modelini elde etme işlemine Tersine Mühendislik (Reverse Engineering) denir [1], [3].

Tersine mühendislik ihtiyacı; üreticinin uzun zamandır üretmediği bir parçayı yeniden üretmek istemesi, orijinal tasarımın yeterli veriye sahip olmaması, mevcut bir ürün üzerinde revizyon yapılmak istenmesi, rakip ürünlerin analiz edilmesi, ürün performansını artıracak yeni yollar aranması, orijinal bilgisayar destekli tasarım modelinin yeterli olmaması, yedek parça temin etmekte meydana gelebilecek sıkıntılar ya da eski üretim işlemlerinin günümüz teknolojisi ile güncellenerek daha ucuza mal edilmek istenmesi gibi durumlarda ortaya çıkabilir [4], [7].

Tersine mühendisliğin amacı, mevcut bir BDT modeli olmadan, 3b model oluşturmaktır [14]. Bu modelin oluşturulması için birkaç aşama gereklidir. Şekil 1'de, tersine mühendislik süreci ile ilgili temel bir diyagram gösterilmiştir.

Şekil 1. Tersine mühendislikte izlenilen yol.

Şekil ve özellik bakımından farklı nesnelerin 3b modelinin oluşturulması için kullanılan makine görüş sistemleri, verilerin toplanması amacıyla görüntü verileri üzerinde çalışır. Verileri toplama işlemi; lazer radar, lazer tarama teknikleri ve nokta detektörleri ile gerçekleştirilir. Tarama işlemi boyunca yüzey üzerinde hareket eden sayısal tarama sustası, nokta bulutu matrisini oluşturur. Sayısallaştırma işlemi olarak da tanımlanan bu kısımda kullanılan cihazlar iki ana grup altında incelenebilir (Şekil 2) [1], [9].

Temas ederek (Problu) ölçüm yapan cihazlarda, ölçüm kolunun üzerinde bir küre mevcuttur. Bu küre, iş parçasının yüzeyine temas ettirilerek, iş parçasının geometrik ve boyutsal verileri üç boyutlu (x,y,z) olarak elde edilir ve bilgisayar ortamına aktarılır. Ölçüm alınabilmesi için probun yüzeye değme zorunluluğunun bulunması, karmaşık şekle sahip iş parçalarının taranmasında dezavantaj teşkil eder [7]. Temaslı yöntemleri, koordinat ölçüm makineleri (CMM) ve dokunmatik sensöre sahip robotik kollar olarak iki dalda sınıflandırabiliriz. CMM'ler ölçüm yüzeyi üzerindeki belirli bir yolu takip ederek yüksek hassasiyette veri toplayabilirler. Robotik kollar ise, üzerine entegre edilen dokunmatik algılayıcılar sayesinde temas ettiği yüzeylerden hassas veriler alabilecek şekilde programlanabilirler (Şekil 2) [1].

Temassız yöntemlerden biri olan manyetik yöntemde, yüzeye temas eden manyetik alan teknolojisi ile veri toplanır. Akustik yöntemde ise yüzeyden yansıyan ses dalgalarından faydalanılarak veri toplanmaktadır. Optik yöntemler, hızlı veri toplama kapasitesine sahip olmasından dolayı, temaslı yöntemlere göre kıyasla daha sık tercih edilirler. Optik yöntemleri; lazer üçgenleme, uçuş zamanı, interferometre, yapısal ışıklandırma ve stereo analizleri olarak beş ana kategoriye ayırabiliriz (Şekil 2) [1].

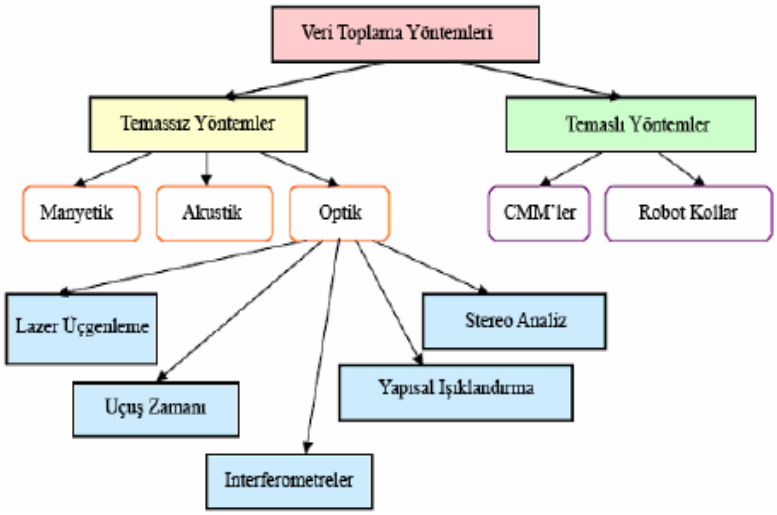

Şekil 2. Tersine mühendislik temel süreç diyagramı [13].

Temassız sistemlerde ölçüm bir lazer hüzmesi kullanılarak ya da topometrik (kameralı) tarama yaparak gerçekleştirilir (Şekil 3). Lazer hüzmesi ile gerçekleştirilen ölçüm, iş parçasının ölçüm yapılmak istenilen bölgelerine gönderilen lazer ışınının kaynaktan gidiş ve dönüş zamanının, ışık hızıyla çarpılması sonucu otomatik olarak hesaplanır. Bu şekilde koordinatlar belirlenir. Lazer ışınının geri dönmesinin söz konusu olamayacağı karmaşık şekle sahip iş parçalarının taranmasındaki güçlüklerden dolayı, bu biçimdeki iş parçaları için önerilen bir yöntem değildir. Topometrik ölçümde ise, iş parçasının yaklaşık 70-100 cm kadar ön tarafına tutulan tarama kafası sayesinde parçanın kenar oluşumlarının izdüşümlerinin yansıması sağlanır. Bu ölçümler kaydedilerek, üç boyutlu koordinatlar hesaplanır [5], [8].

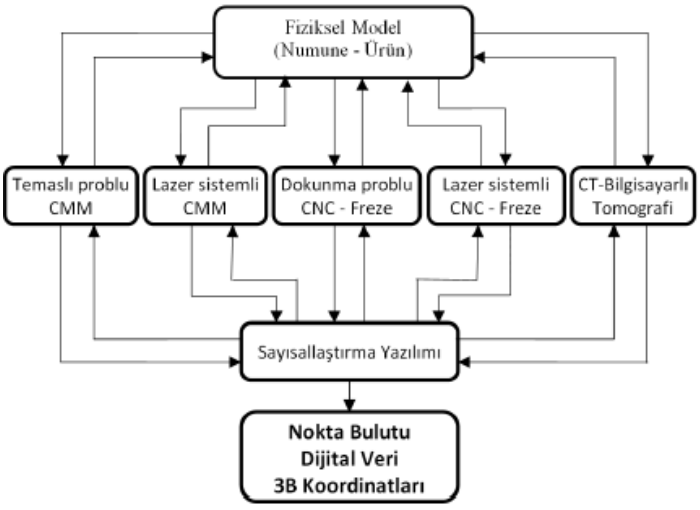

Şekil 3. Ölçüm teknikleri şeması [18].

Temaslı ve temassız veri toplama yöntemlerinde ana hedef, üç boyutlu koordinat sisteminde bir nesnenin sınırlarını belirleyen bir nokta bulutu elde etmektir. Nokta bulutu formatı uygun yazılımlar kullanılarak bilgisayar destekli tasarım ve üretim (BDT/BDÜ) süreçlerine uygun formata (stereolithography-stl) dönüştürülür. Böylelikle nesnenin 3b modeli bilgisayar ortamına aktarılarak model üzerinde istenilen değişiklikler yapılabilir [10], [11]. Model son halini aldıktan sonra, 3b modelden fiziksel yapılar elde edilmesini sağlayan hızlı prototipleme (rapid prototyping) teknolojisi ile üç boyutlu yazıcı kullanılarak üretime geçilebilir. Şekil 4'de tersine mühendislik işlem basamaklarıgösterilmiştir [6].

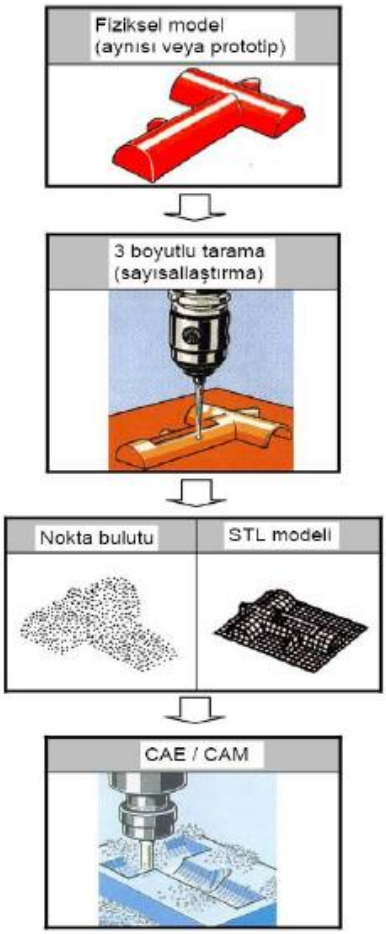

Şekil 4. Tersine mühendislik süreci işlem basamakları [13,18]

Bu çalışmanın amacı, tersine mühendislik yaklaşımı ile ilgili bilgi vermek, sürecin nasıl işlediğini anlatmak ve makine mühendisliği ile tersine mühendislik arasındaki ilişkiyi irdelemektir. Tersine mühendisliğin makine sektöründeki uygulamalarının nasıl yapıldığı açıklanarak, hangi durumlarda tersine mühendisliğe ihtiyaç duyulduğunun anlaşılması amaçlanmıştır.

2.Makine ve Malzeme Sektöründe Tersine Mühendislik Çalışmaları

Tersine mühendisliğin makine mühendisliği alanındaki uygulamaları genellikle parçalarının onarımı üzerine olmaktadır. Deforme olmuş makine elemanları ya da kalıplar, tersine mühendislik teknolojisi kullanılarak yeniden üretilebilmektedir. Ayrıca geliştirilmek istenilen ürünlerin tersine mühendislik uygulamaları ile yeniden BDT modeli elde edilip, ürün revize edilmektedir. Tersine mühendisliğin makine alanındaki bir başka kullanımı ise, seri üretimi yapılmak istenilen bir ürünün BDT modelinin elde edilmesinin amaçlanmasıdır. Üretim aşamasında geriye gidilerek elde edilen BDT modeli, bilgisayar

destekli üretim (BDÜ) teknolojisi ile yeniden üretilebilmektedir. Literatürde bu amaçlara benzer şekilde birçok tersine mühendislik uygulaması mevcuttur.

Berbercuma [15], türbin çarkını, tersine mühendislik uygulaması ile optik tarayıcıda sayısallaştırıp, nokta bulutu formatında oluşan veriyi 3b BDT formatına çevirmiştir. Paulic vd. [16], sac kesme kalıbı üretim sürecini tersine mühendislik ile geriye giderek yeniden incelemişler ve elde ettikleri nokta bulutu verilerini 3b BDT verileri ile karşılaştırmışlardır. Budak vd. [17], karmaşık şekle sahip parçaları kolayca modelleyebilen bir yazılım geliştirmişlerdir. Sokoviç ve Kopac [18], BDT modeli mevcut olmayan ürünlerde tersine mühendislik yöntemlerinin faydalarını incelemişlerdir. Ayyıldız [7], hasarlı kalıp parçalarının tamiri ve üretimi için tersine mühendislik yaklaşımını ele almıştır. Tam ve Chan [19], tersine mühendislik yaklaşımı ile termoform kalıp tasarlamışlardır. Ayrıca, düz ve helis dişli çarklar tersine mühendislik ile BDT modellerinden yola çıkarak tanımlanmıştır [20], [21]. Matta vd. [22], BDT/BDÜ/CAM, hızlı prototipleme ve imalat sistemleri ile ilgili gerçekleştirilen çalışmaları kapsamlı bir şekilde sunmuşlardır. Çetinel [1]'in tersine mühendislik yaklaşımı ise, bir nesnenin 3D modelini oluşturabilmek için fotogrametri yöntemini kullanmayı içermektedir. Salamoun ve Suchy [12], alttan kesmeye maruz kalan ve kalmayan düz ve helis dişli çark yarıçaplarının hesaplanması ve sınır noktalarının belirlenmesi için bir algoritma geliştirmişlerdir. Aziz [23], yaptığı çalışmada, adım, helis açısı diş sayısı ve kalınlığı gibi temel geometrik parametrelerden diş profili oluşturmak ve dişli çarkların üzerindeki bütün noktaları tespit ederek SEM modellerini oluşturmak için yöntemler sunmuştur. Brauer [24], çalışmasında konik evolvent dişli çarkı, üç farklı evolvent dişli ile matematiksel tanımlamıştır. Yang [25], çalışmasında asimetrik helis dişli çarklarının matematiksel modelini, bilgisayar destekli sonlu eleman gerilme analizleri ve alttan kesme analizleri yaparak gerçekleştirmiştir. Rosic [26], evolvent düz dişli çarkların tasarımı için bilgisayar destekli kinematik bir model oluşturarak dişli çarkların optimum ölçülerde imal etmek ve basma/çekme analizlerini yapmak için yardımcı bir yaklaşım geliştirmiştir. Liu vd. [27], hızlı prototipleme ve tersine mühendisliği birleştirmiş ve yeni bir yöntem geliştirmişlerdir. Unigraphics platformu bünyesinde C++ ile geliştirdikleri bu yöntemde, nokta bulutunu iki boyut kesit alarak modelleyip dilimlere ayırmışlardır. İki boyutlu BDT modeli, hızlı prototipleme için dilimlere ayrılmış ve yüzey modelini STL dosyasına çevirmeye gerek duymadan hızlı prototipleme makinesine göndermişlerdir. Kim vd. [28], tersine mühendisliğe yardımcı olabilecek serbest yüzeyli parçaların geometrik özelliklerini tespit edebilen bir sayısallaştırma cihazı tasarlamışlardır. Sayısallaştırma cihazının kullanabillirliğini deneysel olarak kanıtlamışlardır. Galantucci vd. [29], hızlı prototipleme ile tersine mühendislik arasındaki bağlantıya odaklanarak üçgensel ağ örme ve hacimsel yaklaşım işlemi ile bir yöntem geliştirmişlerdir. Mavromihales vd. [30], kiriş havalandırma kanatlarını tersine mühendislik kullanarak yeniden imal etmişlerdir. Chen vd. [33], türbin kanatlarının üç boyutlu geometrik tasarımını yapmak amacıyla tek bir yüzeyde, türbin kanadının modellenmesi ve yüzey sayısallaştırma işlemlerini birleştirmişlerdir. İskender vd. [36] gelişmiş çizilme direncini tespit etmişler ve yüzey modifikasyonunu incelemişlerdir.

3. Tersine Mühendislik Çalışmalarında Kullanılan Yöntem

Tersine mühendisliğin makine sektöründeki ihtiyaçlar doğrultusunda kullanılması ile ilgili literatürde mevcut olan Ayyıldız [7] ve Şahin vd. [34] nin yaptığı çalışmalar detaylı olarak ele alınacaktır. Böylece tersine mühendisliğin hangi durumlarda nasıl uygulandığı ve aşamalarının ne olduğunun daha detaylı incelenmesi amaçlanmaktadır. Tersine mühendislikte bir tasarım modeli oluşturmak için öncelikle taranacak model belirlenir. Modelin geometrik özelliklerine uygun tarayıcıyla ölçüm işlemi gerçekleştirildikten sonra BDT modeli elde edilir [31], [32].

Ayyıldız [7], çalışmasında, hasarlı kalıp elemanlarının tamiri amacıyla tersine mühendislik yaklaşımını ele almıştır. Hasarlı kalıp elemanından tarama aleti kullanılarak nokta bulutu formatı oluşturulur ve BDT formatına çevrilir. Gerekli düzenlemeler yapıldıktan sonra BDT modeli haline getirilen ürün bilgisayar destekli üretim/imalat uygulamalarında kolaylıkla kullanılabilir. Şekil 5'de hasarlı kalıp elemanının tamiri için geliştirilen sistemin akış şeması verilmiştir [7], [8].

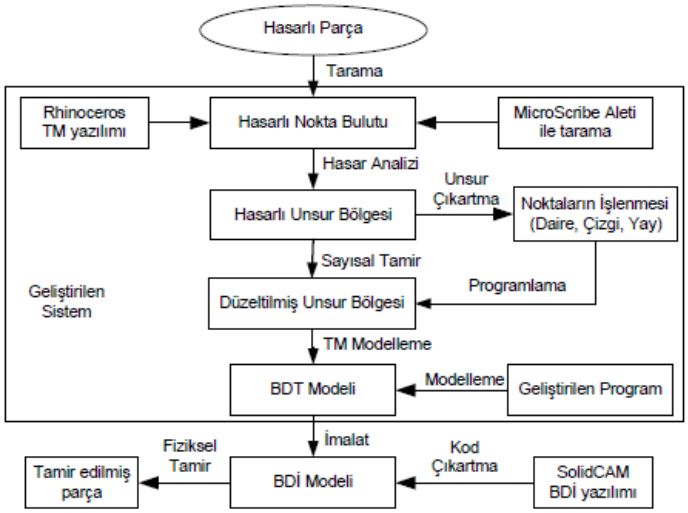

Şekil 5. Hasarlı kalıp elemanının tamiri için geliştirilen sistemin akış şeması [7].

Ayyıldız'ın [7], bu çalışmasında geliştirdiği program Visual Basic programlama dilinde yazılmıştır. BDT sistemi olarak ise Solidworks ve Rhinoceroes paket programları kullanılmıştır. Visual Basic programlama dilinden Solidworks ve Rhinoceros programlarıyla harekete geçerek bu programların eş zamanlı çalışması sağlanmıştır. Şekil 6'da Rhinoceros programıyla eşzamanlı çalışan Solidworks penceresinin genel bir görünümü verilmiştir [7], [8].

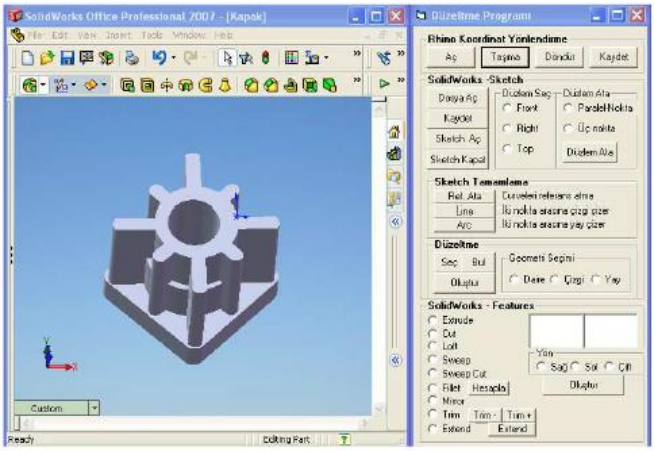

Şekil 6. Rhinoceros programı ile eşzamanlı çalışan Solidworks için örnek arayüz [7].

Geliştirilen sistem, hasarlı bir kalıp elemanı (kalıp lokması) üzerinde uygulama yapılarak açıklanmıştır (Şekil 7).

Şekil 7. Hasarlı kalıp elemanı [7].

Hasarlı parça düz bir zemin üzerine sabitlendikten sonra MicroScribe üç boyutlu tarama cihazı yardımıyla nokta bulutu verisi alınmıştır. Parçanın koordinatları Rhinoceros programı ile alınıp hasarlı parça üzerinden boyut bilgisi elde edilmiştir (Şekil 8).

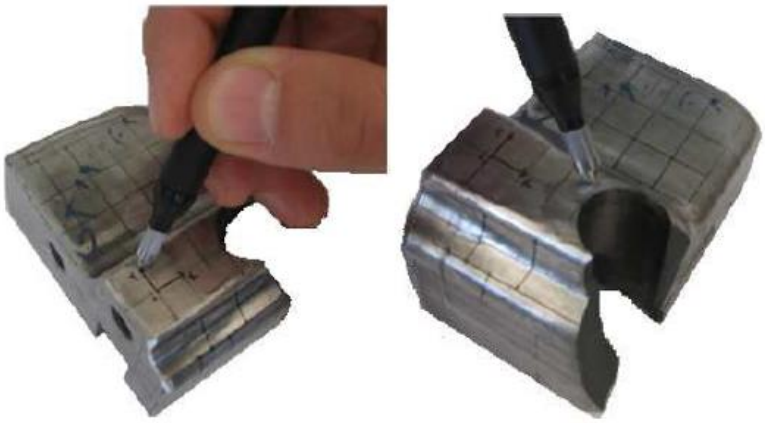

Şekil 8. Parça üzerinden orijin alma ve boyut bilgisi elde etme [7].

Rhinoceros BDT programında parçadan elde edilen boyut bilgisi, nokta bulutu olarak gösterilmiştir (Şekil 9).

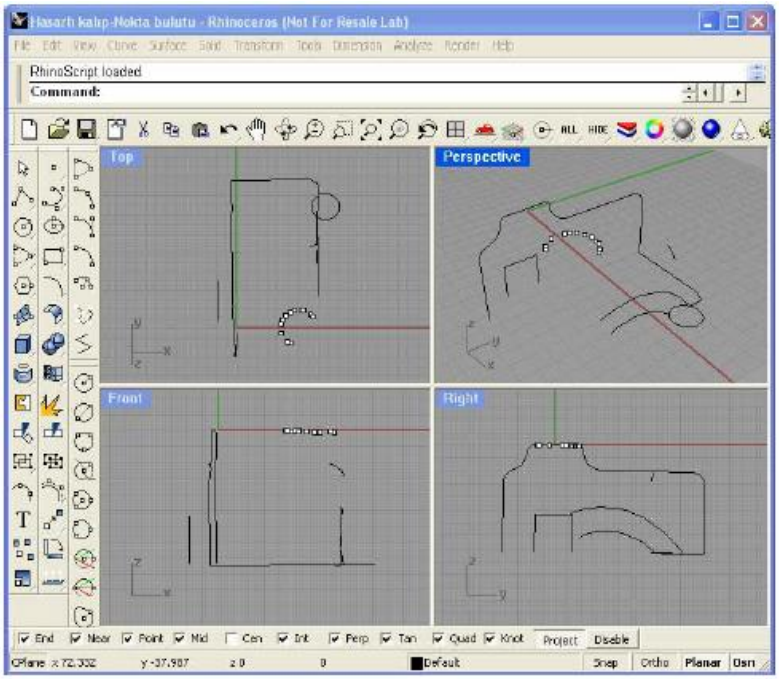

Şekil 9. Rhinoceros BDT programındaki nokta bulutu görüntüsü [7].

Nokta bulutu verisinde orijinin tanıtılmasında oluşabilecek hatalardan dolayı taşıma ve döndürme gibi düzenleme işlemleri gereklidir. Bu düzenlemelerinden ardından kaydedilen nokta bulutu verisi, IGES dosyası olarak Solidworks programına aktarılır. Çizimle ilgili bir dizi düzeltme işleminin ardından hasarlı kalıp elemanının BDÜ verisi son halini alır (Şekil 10).

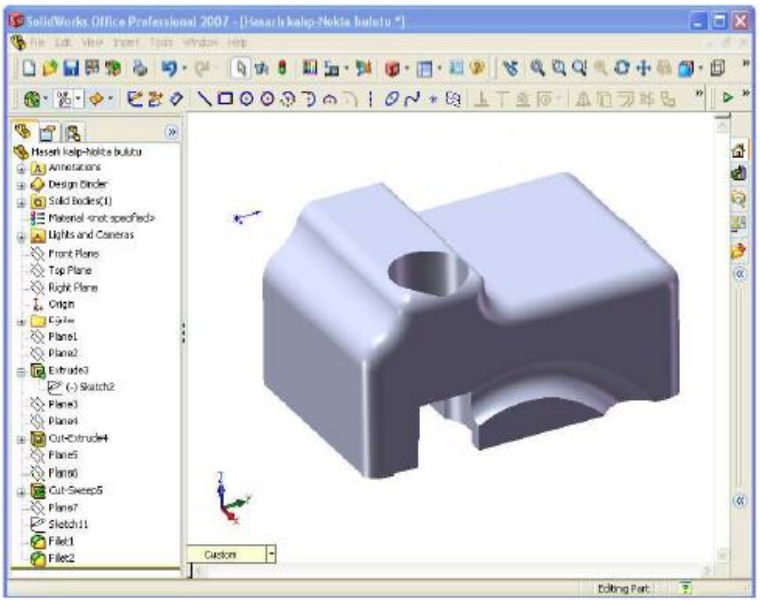

Şekil 10. Hasarlı kalıp elemanının onarımı yapılmış modeli [7].

Hasarlı kalıp elemanının BDT/BDÜ dönüşümü yapılarak G ve M kodları çıkarılır ve uygun talaşlı imalat yöntemiyle ya da hızlı prototipleme ile üretimine geçilir. Böylelikle hasarlı bir kalıp elemanı tersine mühendislik işlemi ile yeniden üretilip kullanılabilir hale getirilmiştir.

Bir başka çalışmada ise; şanzıman mekanizmasında kullanılan deforme olmuş diş profiline sahip bir helis dişlinin, tadilatı yapmak üzere geliştirilen üç boyutlu modelinin tersine mühendislik yaklaşımı ile elde edilmesi anlatılmaktadır. Çalışmada hasarlı dişliye ait veriler üç boyutlu tarayıcı kullanılarak taranmıştır. Tarama işlemi AICON Smart Scan marka tarayıcı ile yapılmıştır (Şekil 11) [34].

Şekil 11. Tarama işleminden görüntüler [34].

Parça 15-20° döndürülerek görüntü almaya devam edilmiş ve bu şekilde toplam 20 adet görüntü alınmıştır. Tarama işlemi tamamlandıktan sonra tarayıcının kör noktasında kalan boşluklar doldurulmuş ve görüntü STL formatında kaydedilmiştir. Hasarlı diş profili modelinin oluşturulmasında Geomagic Design X yazılımı kullanılmıştır. Bu yazılım içine alınan nokta bulutu verisinde 230077 adet nokta sayısı mevcuttur (Şekil 12a). Modelleme yapılabilmesi için nokta bulutu verisinden ağ modeli elde edilmiştir (Şekil 12b) [34], [35].

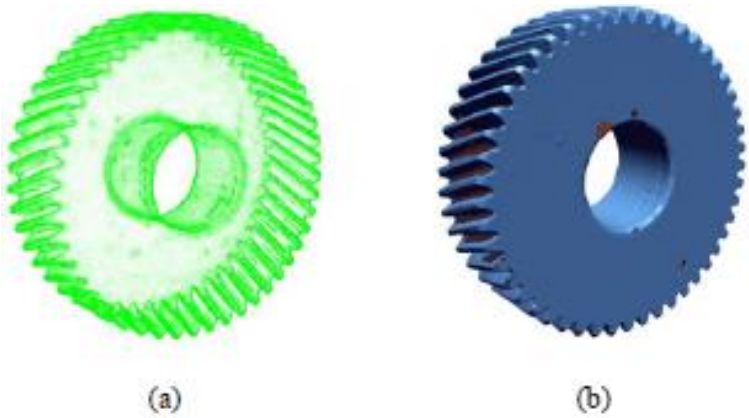

Şekil 12. Hasarlı dişli: (a) nokta bulutu verisi, (b) ağ modeli [34].

Elde edilen üç boyutlu diş profilinde sapma miktarının minimize edilmesi oldukça önemlidir. Sapma analizi yapılarak parça boyutu, çalışma hassasiyeti ve bölgesel kararlılık değişkenleri dikkate alınır. Bütün bu düzenlemelerden sonra hasarlı diş profilinin üç boyutlu modeli elde edilir ve imalat aşamasına geçilir (Şekil 13) [34].

Şekil 13. (a) Hasarlı diş profili, (b) Onarılmış diş profili [34].

Üç boyutlu modeli oluşturulan heliş dişlinin üretilmesi için hızlı prototipleme yapılmıştır. 3Dison Pro marka yazıcı kullanılmıştır. (Şekil 14) [34].

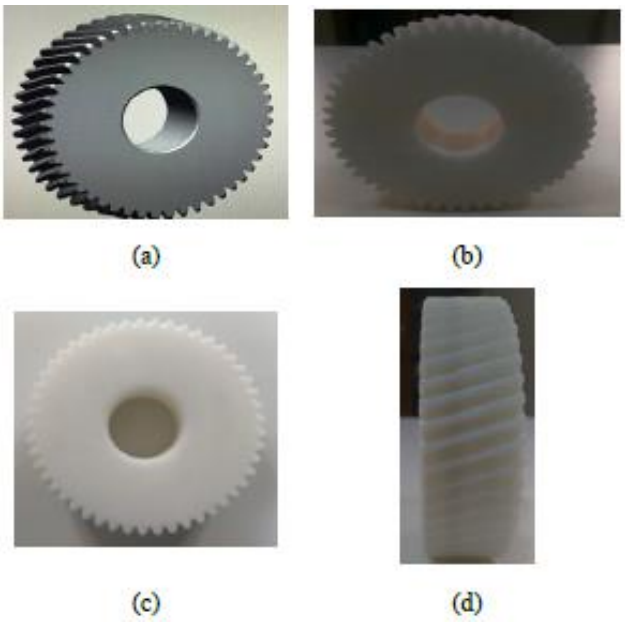

Şekil 14. BDT Modeli oluşturulan dişli ve dişili çıktıları [34].

4. İrdelenen Çalışma Sayısı

Bu derleme çalışmasında, tersine mühendislik ile ilgili literatürde mevcut olan birçok çalışma incelenmiştir. Çalışma kapsamında araştırma ve derleme makaleleri, yüksek lisans ve doktora tez çalışmaları gibi akademik çalışmaların yanında bu alanda hazırlanan proje, sunum ve raporlara da ulaşılmaya çalışılmıştır. Araştırma kapsamında tersine mühendislik ve uygulamaları ile ilgili, araştırma makaleleri, derlemeler, sunumlar, yüksek lisans ve doktora tezleri olmak üzere toplam 40 kadar çalışma incelenmiştir. Bu derlemede faydalanılan çalışmaların dağılımları Çizelge-1 de sayısal olarak ifade edilmiştir.

Çizelge 1. Tersine Mühendislik ile ilgili incelenen toplam çalışma sayısı.

Çalışmanın tipi	Sayı	%
Doktora tezi	2	5
Yüksek lisans tezi	7	17,5
Araştırma makalesi	20	50
Derleme makalesi	4	10
Proje	1	2,5
Rapor	1	2,5
Sunum	1	2,5
Diğerleri	4	10
Toplam	40	100

Tersine mühendislik yazılımının kullanımı, teknolojinin de gelişmesiyle her geçen gün artmaktadır. Dolayısıyla literatürde bu konuyla ilgili birçok çalışma mevcuttur. Bu çalışmada sadece tersine mühendisliğin makine mühendisliği alanındaki uygulamaları incelenmiş, tersine mühendislik süreci ile ilgili bilgi verilmiş ve hangi durumlarda tersine mühendislik işlemine ihtiyaç duyulduğu açıklanmıştır.

5. Sonuçlar ve Tartışma

Bu derleme kapsamında Tersine mühendisliğin, Makine mühendisliği alanında uygulamaları incelenmiş, tersine mühendisliğin aşamaları hakkında detaylı bilgi verilmiştir. Tersine mühendislikte temel amaç, mevcut üründen yola çıkarak BDT modelinin elde edilmesidir. BDT modeli elde edilen ürün, yeniden kolaylıkla üretilebilmektedir. Makine sektöründe tersine mühendislik ihtiyacı genellikle, deforme olmuş bir malzemenin tadilatında ya da geliştirilmek / yeniden üretilmek istenilen eksik dokümantasyona sahip bir malzemenin üretiminde ortaya çıkmaktadır. Buna benzer durumlarda literatürde de görüldüğü üzere, tersine mühendislik süreci oldukça tercih edilen verimli bir yoldur.

Kaynaklar

[1] M. Çetinel, “Tersine mühendislik ile üç boyutlu cisimlerden grafik tasarım için veri eldesi”, Yüksek Lisans Tezi, Yıldız Teknik Üniversitesi Fen Bilimleri Enstitüsü, İstanbul, 124, 2008.

[2] A. Önçağ, H. Tosun, “İzmir universiade oyunları maskot heykelinin tersine mühendislik yöntemleri ile dijitalleştirilmesi ve küçük ölçekli olarak üç boyutlu yazıcı ile imalatı,” *Soma Meslek Yüksekokulu Teknik Bilimler Dergisi*, 2(26), 1-10, 2018.

[3] E. Günpınar, “Tersine mühendislik yoluyla üç boyutlu geometrik modelin oluşturulması ve gemi yapım endüstrisindeki bazı uygulamaları”, *Dokuz Eylül Üniversitesi Mühendislik Fakültesi Fen ve Mühendislik Dergisi*, 18(54), 624-639, 2016.

[4] F. İşbilir, B. Çelik, A. Özsan, M. Kaynak, "Tersine mühendislik temelli araç üst yapı tasarım, analiz ve üretiminin incelenmesi", *Sürdürülebilir Mühendislik Uygulamaları ve Teknolojik Gelişmeler Dergisi*, 1(2), 72-79, 2018.

[5] A. Önçağ, Ç. Tekcan, H. Özden, "Mekanik parçaların tersine mühendislik ile modellenmesinin değerlendirilmesi ve bir uygulama. Pamukkale Üniversitesi Mühendislik Bilimleri Dergisi, **24(1)**, 43-49, 2018.

[6] H. Demir, "Cad datası olmayan parçaların tersine mühendislik metodu ile cad datalarının oluşturulması", Yüksek Lisans Tezi, Fırat Üniversitesi Fen Bilimleri Enstitüsü, Elazığ, 97, 2018.

[7] M. Ayyıldız, "Hasarlı makine elemanlarının tersine mühendislikle ile tasarım ve imalat için yenilenmesi", Yüksek Lisans Tezi, Karabük Üniversitesi Fen Bilimleri Enstitüsü, Karabük, 106, 2009.

[8] M. Ayyıldız, C. Göloğlu, C., "Hasarlı kalıp elemanlarının tamiri için tersine mühendislik destekli bir çerçeve çalışması", 5. Uluslararası İleri Teknolojiler Sempozyumu, Iats, Karabük, Mayıs 13-15, 1437-1441, 2009.

[9] J. P. Kruth and A. Kerstens "Reverse engineering modeling of-free-form surfaces from point cloud subject to boundary conditions", *Journal of Materials Processing Technology*, 76, 120-127, 1998.

[10] K. Nitish, H. Kumar, J. S. Khurmi, "Experimental Investigation of Process Parameters for Rapid Prototyping Technique (Selective Laser Sintering) to Enhance the Part Quality of Prototype by Taguchi Method", *Procedia Technology*, vol. 23, Pages 352-360, 2016.

[11] Y. Jun, V. Raja, S. Park, "Geometric Feature Recognition for Reverse Engineering using Neural Networks", *International Journal of Advanced Manufacturing Technology*, 17, 462-470, 2001.

[12] C. Salamoun, M. Suchy, "Computation of helical or spur gear fillets," *Mechanism and Machine Theory* 8(3), 305-322, 1973.

[13] N. Sherry, "Reverse engineering of automotive parts applying laser scanning and structured light techniques" The University of Tennessee, Knoxville, 2005.

[14] T. Türkücü, H. Börklü, "Tersine mühendislik yaklaşımına dayalı yeni bir imalat için tasarım işlem modeli", *Gazi Üniversitesi Fen Bilimleri Dergisi* Part C: Tasarım ve Teknoloji, 6(1), 91-104, 2018.

[15] G. Berbercuma, "Üç boyutlu tarayıcılar ile veri toplanması ve CAD ortamına değişik formatlarda aktarılması", T.C. Gebze Yüksek Teknoloji Enstitüsü, Mühendislik ve Fen Bilimleri Enstitüsü, Yüksek Lisans Tezi, Gebze, 258, 2006.

[16] M. Paulic, T. Irgolic, J. Balic, F. Cus, A. Cupar, T. Brajlih, I. Drstvensek, "Reverse Engineering of Parts with Optical Scanning and Addictive Manufacturing" 24th DAAAM International Symposium on Intelligent Manufacturing and Automation. *ScienceDirect, Procedia Engineering*, 69, 795-803, 2014.

[17] I. Budak, J. Hodolic, M. Sokovic, "Development of a programme system for datapoint pre-processing in Reverse Engineering", *Journal of Materials Processing Technology* 162-163, 730-735, 2005.

[18] M. Sokovic and J. Kopac, RE (reverse engineering) as necessary phase by, journal of materials processing technology, Faculty of Mechanical Engineering, University of Ljubljana, Slovenia, 398–403, 2006.

[19] K. W. Tam, K.W. Chan, "Thermoforming mould design using a reverse engineering approach", *Robotics and Computer-Integrated Manufacturing* 23, 305–314, 2009.

[20] M. Ayyıldız, A. Çiçek, "Düz Dişli Tasarımında Bir Tersine Mühendislik Uygulaması", *Sakarya University Journal of Science*, 14(1), 39-44, 2010.

[21] A. Çiçek, "Dişlilerin uzman sistem tabanlı tanımlanması ve detaylı boyutlarının çıkarılması", *Gazi Üniversitesi Mühendislik ve Mimarlık Fakültesi Dergisi,* 23(3), 709-717, 2008.

[22] A. K. Matta, D. R. Raju, K. N. S. Suman, "The Integration of CAD/CAM and Rapid Prototyping in Product Development", *A Review, Materialstoday: Proceedings*, 2, 3438-3445, 2015.

[23] E. S. Aziz, "Knowledge-Based Geometry Generation for Spur and Helical Gears." *Concurrent Engineering,* 10(3), 251-261, 2002.

[24] J. Brauer, "A general finite element model of ınvolute gears," *Finite Elements in Analysis and Design,* 40, 1857–1872, 2004.

[25] S. C. Yang, "Mathematical Model of a Helical gear with asymmetric ınvolute teeth and ıts analysis", *International Journal Advanced Manufacturing Technology*, 26, 448-456, 2005.

[26] B. Rosic*,* "Design and simulation of meshing of ınternal ınvolute spur gears with pinion cutters", Facta Universitatis Series: Mechanical Engineering, 1(9), 1193-1198, 2002.

[27] G. Liu, Y. Wong, Y. Zhang, H. Loh, "Modelling cloud data for prototype manufacturing," *Journal of Materials Processing Technology*, 138, 53-57, 2003.

[28] S. Kim, Y. Choi, J. Oh, "Reverse engineering: high speed digitization of free-form surfaces by phase-shifting grating projection moire topography," *International Journal of Machine Tools & Manufacture*, 39, 389-401, 1999.

[29] L. Galantucci, G. Percoco, U. Dal Maso, "A volumetric approach for STL generation from 3D scanned products", *Journal of materials processing technology*, 204, 403-411, 2008.

[30] M. Mavromihales, J. Mason, W. Weston, "A case of reverse engineering fort he manufacture of wide chord fan blades (WCFB) used in Rolls Royce aero engines", *Journal of Materials Processing Technology*, 134: 179-286, 2003.

[31] C. Moenning, N. Dodgson, "A new point cloud simplification algorithm", Presented at 3rd IASTED International Conference on Visualization, Imaging and Image Processing, Spain, 1-6, 2003.

[32] J. K. Ruan, Y. L. Ke, S. Q. Fan, H. Y. Dong, "Research on rapid repairing techniques for auto panel dies", *Journal of Materials Processing Technology*, 187-188: 69-72, 2007.

[33] L. Chen, G. Lin, "Reverse engineering in the design of turbine blades- a case study in applying the MAMD", Robotics and Computer Integrated Manufacturing, 16, 161-167, 2000.

[34] İ. Şahin, T. Şahin, H. Gökçe, O. Eren, "Hasarlı dişlilerin tersine mühendislik yaklaşımıyla yeniden oluşturulması", *Düzce Bilim ve Teknoloji Dergisi*, 5, 485-495, 2017.

[35] P. Ratnadeep, A. Sam "A new Steiner patch based file format for Additive Manufacturing processes" *Computer-Aided Design*, Volume 63, Pages 86-100, 2015.

[36] Ş. İskender, S. Işmar, A. Evcin "Surface modification of PC and PMMA sheet for enhanhed scratch resistance", *Journal of Characterization",* 1(3) 131-136, 2021.

JOURNAL of CHARACTERIZATION

https://jcharacterization.com
https://jcharacterization.org

Journal of Characterization
Vol 1, Special Issue, 54-61, December, 2021

ISSN: 2757-9166
Research Article

Characterization of Portland Cement Clinker by Image Processing Technique

Abdul Vahap Korkmaz[1*],

[1*] Afyon Kocatepe University, İscehisar vocational school, Departmant of Construction, Afyonkarahisar, Turkey, (ORCID: 0000-0001-8691-1937), avkorkmaz@aku.edu.tr

(Received date: 25.12.2021 and Accepted date: 31.12.2021)

(**DOI: 10.29228/JCHAR.55634**)

REFERENCES: Korkmaz, A. V., Characterization of Portland Cement Clinker by Image Processing Technique, *Journal of Characterization*, (1) Special Issue, 54-61, 2021

Abstract

With the developing technology, devices that can fully control the quality of cement and clinker in cement production have been produced. These devices can give accurate results in a short time and with minimum error margins, with all necessary analyzes and phase compositions. Although these methods are very useful for cement factories in practice, they cannot fully reveal some parameters such as crystal structure and morphology of clinker phases, size distribution and clinker porosity. In microscopic studies, the formation, size, distribution and amount of clinker phases in the examined cross-sectional area can be determined. In this study, optical microscope examination and image processing techniques were used to determine the clinker characteristics. Raw meal was formed by mixing limestone and clay from cement raw materials in certain proportions. Then, clinker was obtained as a result of burning the raw meal at approximately 1400 ^{o}C. In addition to performing rapid phase analysis using image processing programs, information about the crystal properties of the phases was obtained. The size, number, average equivalent diameter, distribution of clinker phases and porosities can also be examined with the help of image processing programs. According to the result of the image processing method, Portland cement clinker with easy burning properties, high alite and low belite content was obtained.

Keywords: Optical microscope, Clinker, Characterization, Quality, Alite, Belite

Portland Çimento Klinkerinin Görüntü İşleme Tekniği ile Karakterizasyonu

Öz

Gelişen teknoloji ile çimento üretiminde çimento ve klinker kalitesini tam olarak kontrol edebilen yeni cihazlar üretilmiştir. Bu cihazlar, gerekli tüm analizler ve faz kompozisyonları ile kısa sürede ve minimum hata payı ile doğru sonuçlar verebilmektedir. Bu yöntemler pratikte çimento fabrikaları için çok faydalı olmasına rağmen, klinker fazlarının kristal yapısı ve morfolojisi, boyut dağılımı ve klinker gözenekliliği gibi bazı parametreleri tam olarak ortaya koyamamaktadır. Mikroskobik çalışmalarda incelenen kesit alanındaki klinker fazlarının oluşumu, boyutu, dağılımı ve miktarı belirlenebilir. Bu çalışmada, klinker özelliklerini belirlemek için optik mikroskop incelemesi ve görüntü işleme teknikleri kullanılmıştır. Çimento hammaddelerinden kireçtaşı ve kiltaşı belirli oranlarda karıştırılarak farin hazırlanmıştır. Daha sonra farinin yaklaşık 1400 ^{o}C' de pişirilmesi sonucu klinker ürünü elde edilmiştir. Optik mikroskop tekniği ve görüntü işleme programları kullanılarak faz analizinin hızlı yapılmasının yanı sıra fazların kristal özellikleri hakkında bilgiler elde edilmiştir. Görüntü işleme programları yardımıyla boyut, ortalama eşdeğer çap, klinker fazlarının dağılımı ve gözenekler de incelenebilmiştir. Görüntü işleme yönteminin sonucuna

göre kolay pişme özelliklerine sahip, yüksek alit ve düşük belit içeriğine sahip Portland çimentosu klinkeri elde edilmiştir.

Anahtar Kelimeler: Optik mikroskop, Klinker, Karakterizasyon, Kalite, Alit, Belit
.

1. Introduction

The first meaning that comes to mind for engineers and scientists is the use of light or optical microscopy to study the microstructure of materials. The first microstructure study dates back to 1880. It is frequently used by materials scientists in the study of metallic materials and is called metallography. It is the basic instrument used in the microstructural investigation of metals, ceramics and polymers [1].

Many destructive and non-destructive methods are traditionally applied in the quality control of cementitious materials, especially concrete. These methods are very useful in terms of giving an idea about the general quality of the concrete and are widely used. However, classical methods may be insufficient in many cases to obtain information about the internal structures of cementitious materials, and different approaches may need to be preferred in order to obtain the desired data. Some of the most important of these techniques are macroscopy and complementary methods related to microscopy [2].

In microscopic studies, the formation, size, distribution, and amount of clinker phases in the examined cross-sectional area can be determined. It is not possible to distinguish unetched clinker phases in clinker bright sections. By etching (eg 1% HNO_3 solution in ethyl alcohol) silicate crystals become evident. Each clinker phase becomes distinct with different etching chemicals. Besides etching with different chemical solutions, clinkers can be processed by titration and steam diffusion to reveal different phases. At the same time, optical microscope examinations give information about porosity, size and shape of pores, sintering conditions. However, in order to obtain a statistically significant result, data must be obtained from a large number of points. This can only be possible by using image processing programs. By using image processing programs, besides performing rapid phase analysis, information about the crystal properties of the phases can also be obtained [3].

In this study, phase determination calculations of typical Portland cement clinker will be made under the optical microscope and the results will be compared with the phase determinations calculated with the Bogue formula. In literature studies, phase determinations of clinkers produced at industrial scale were investigated under optical microscope [4]. In this study, a new clinker was produced from clay and limestone material from raw material quarries under laboratory conditions. Phase determinations of clinker produced under laboratory conditions were determined by optical microscope and image processing technique. In this way, the phase determinations of the clinker produced under laboratory conditions and the production process of the clinker produced at industrial scale will be controlled and process errors will be minimized.

2. Material and Method

2.1. Material

In the study, fireability analysis was carried out on 1 limestone and claystone samples. The chemical and mineralogical compositions of limestone and clay samples were determined. Burnability test was carried out on the raw meal sample prepared in line with the analysis results obtained from the raw material samples. Within the scope of the analysis, one clinker sample was produced under laboratory conditions. Chemical, mineralogical, and microscopic analyzes of the obtained clinker sample were made and its fireability properties were determined.

2.2. Method

X-ray diffraction (XRD) analysis of the raw material samples were conducted using Bruker Brand D 8 Advance model X-ray diffraction (XRD) instrument with Cu Kα rays ($\lambda = 1.54$ Å). The chemical analyses were determined using ARL-8680+ Model X-ray spectrophotometer device according to TS EN 196-2 Turkish Standard.

2.2.1. Optical Polarized Microscope Method

Clinker granules are cut with a diamond saw to obtain a cross section. Clinker granules are fixed by embedding in polyester. The surfaces of the clinker frozen in polyester are sanded. With the help of aluminum paste, the sanded surface is polished. The cross-sectional surface is colored by being exposed to hydrofluoric acid vapor [5].

Figure 1. Diamond saw method (a) Surface sanding method (b).

2.2.2. The Method of Determining the Color Distribution of Phases and Porosity in Optical Microscope Examinations

The prepared clinker bright section samples were etched using 1% HNO3 solution in ethyl alcohol. With the etching process, the colors and geometries of the alite and axitic phases became clear. When etching in nitric acid solution, alite and alite phases become evident, and the intermediate phases emerge as a whole, but the distribution of the interphases among themselves cannot be clearly determined by nitric acid etching. For this reason, etching with different chemicals is required in order to distinguish between C3A and C4AF intermediate phases [6]. Coloring and optical microscope imaging works of the clinker cross-sectional surface are given in Fig. 2.

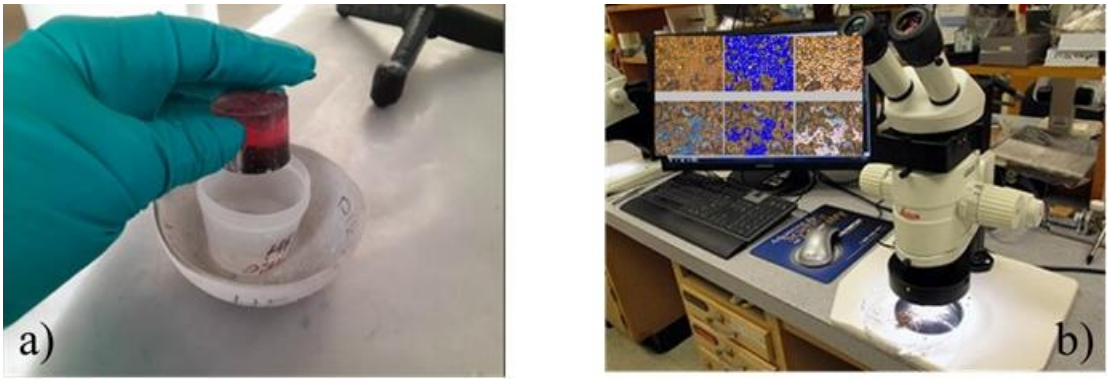

Figure 2. Section surface coloring process (a) Optical microscopic imaging process (b)

A section was taken from the clinker granules of different sizes and appearances, whose polished sections were prepared, and their surfaces were etched by contacting with HF acid vapor. As a result of etching, each clinker phase has its own color [(alite (C3S) brown, belite (C2S) blue, liquid phase (C3A + C4AF) dark gray + white part on the ground and free lime white)]. Allite (C3S), belite (C2S) and liquid phase (C3A+C4AF) ratios were found by dot counting method in the polarized microscope device. It is a more robust and reliable method than the Bogue formula [7].

3. Results and Discussion

3.1. Chemical analysis

Chemical analyzes of raw material samples were made using TS EN 196-2, Flame Photometer, UV Spectrophotometer, XRF and ICP-OES method and the results are given in the table below. In order to learn the chemical contents of the raw materials, the oxide ratios were determined in the XRF device. The silicate modules and aluminum modules of the cement raw materials were calculated by using their chemical contents (Table 1).

Table 1. Chemical analysis of raw material samples

Chemical component	Clay stone	Limestone
	%	%
Loss of igniton	6.24	43.68
SiO_2	65.83	0.24
Al_2O_3	11.44	0.07
Fe_2O_3	4.98	0.05
CaO	4.01	55.45
MgO	1.88	0.49
SO_3	0.05	<0.01
Na_2O	2.60	<0.01
K_2O	1.46	<0.01
TiO_2	0.65	-
P_2O_5	0.12	-
Cr_2O_3	0.03	-
Mn_2O_3	0.09	-
SİM	4.01	2.00
ALM	2.30	1.40

It is seen that the chemical contents of limestone and claystone raw materials are suitable for cement production and can be used for cement production (Table 1).

3.1. Mineralogical Analysis

As a result of the evaluation of the peak intensities, it can be said that the claystone unit has a high grade in terms of quartz, muscovite and cola. It is known that quartz, calcite, albite are minerals that make firing difficult and muscovite, chlorite and montmorillonite group clay minerals have positive effects on burning (Fig. 3).

Mineralogical analysis was performed for the cement limestone sample taken from the quarry using a high resolution X-Ray Diffractometer. As a result of the XRD analysis of the limestone sample used in the experiments, it was determined that its component was calcite (CaCO3) mineral, and no other mineral was found (Figure 4.1). In the limestone quarry where the sample was taken, siliceous structures are found in very small amounts, especially in the metamorphosed and altered veins. In the results of chemical analysis (XRF), siliceous structures within the limestone veins do not exceed 5% (Fig. 4).

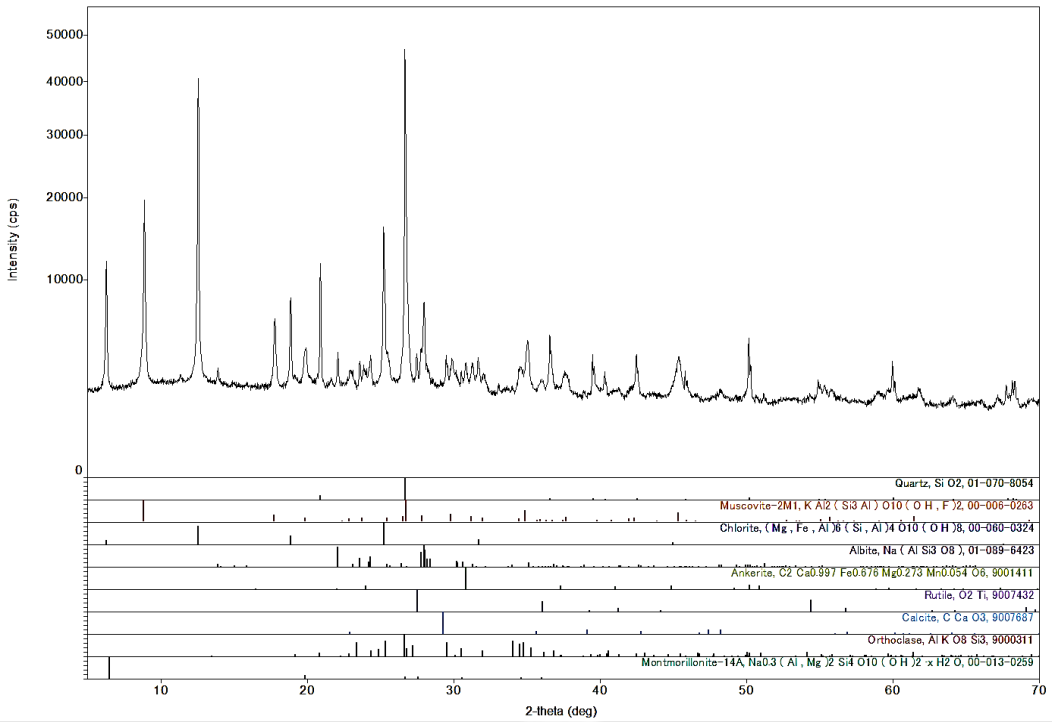

Figure 3. Claystone XRD image

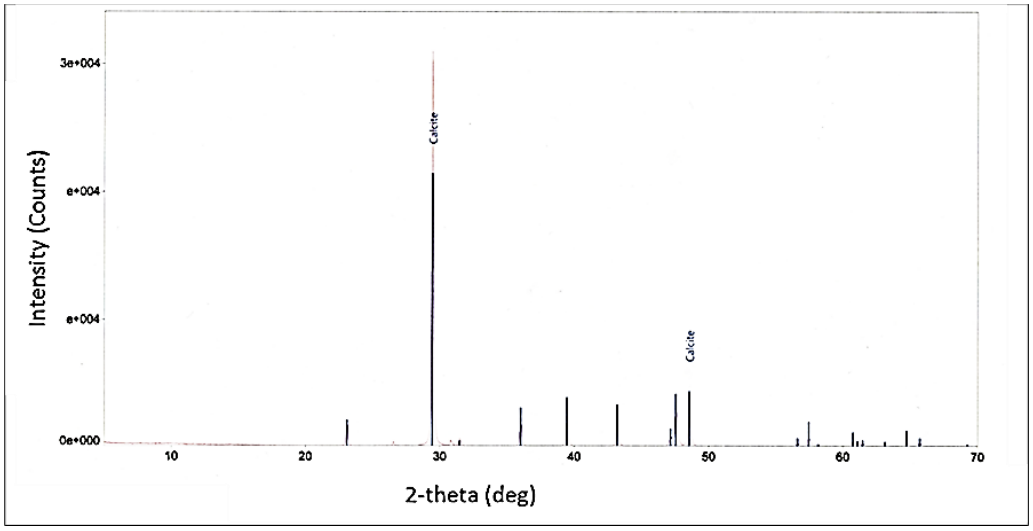

Figure 4. Limestone XRD image

3.2. Clinkerization

Free CaO ratios were measured at each temperature by subjecting the raw meal sample to programmed heating at temperatures of 1200-1300-1350-1400 and 1450°C. The results are given in Table 2.

Table 2. Variation of Free CaO values with temperature in raw meal sample during clinkerization

(%) Free Lime	1200 °C	1300 °C	1350 °C	1400 °C	1450 °C
Clinkerization	14.51	4.45	4.42	2.66	1.60

Mineralogical analysis of the obtained clinkerization sample was made and it was observed that basic clinker phases were formed. The fact that the Free CaO values are 1.60 in the clinker formed at 1450°C indicates that the prepared raw meal has an easy burning character (S.CaO: less than 2.00). The mineralogical results of the metastasis sample used also confirm the easy-firing property of raw meal.

The chemical properties and the calculated modules and phase percentages of the clinker sample produced at 1450°C are given in Table 3.

Table 3 Chemical analysis of clinker sample obtained after clinkerization (1450 °C)

Chemical components	%
Loss of igniton	0.42
SiO_2	20.19
Al_2O_3	6.88
Fe_2O_3	2.86
CaO	65.11
MgO	1.63
SO_3	0.01
K_2O	1.28
Free Lime	1.60
LSF	97.90
SİM	2.07
ALM	2.41
C_3S	54.80
C_2S	16.55
C_3A	13.39
C_4AF	8.70
Liquid Phase	29.64

3.3. Microscopic Analysis Results

The phase amount was determined by point counting method with the help of polarized light microscope. For the aforementioned process, two different granules of the clinker sample obtained as a result of the firing process were placed in polyester and fixed by freezing. The phase amounts determined for the clinker sample are given in Table 4.

Table 4. Determination of Clinker Sample Phase Amount with Microscope

Clinker phases	%
Alite - C_3S	51.68
Belite - C_2S	17.31
C3A+C4AF+Free CaO+ Alkaline Sulphate)	31.01

In order to produce good quality cement clinker, the firing of the clinker provides the formation of a large amount of alite on the other hand. It is necessary to keep the growth and coarsening of the crystals under control. Thus, for a certain raw material mixture, it is necessary to optimize the kiln regime that will minimize the crystal size and ensure the formation of the appropriate composition [8]. The image of the produced clinkers is shown in figure 5.

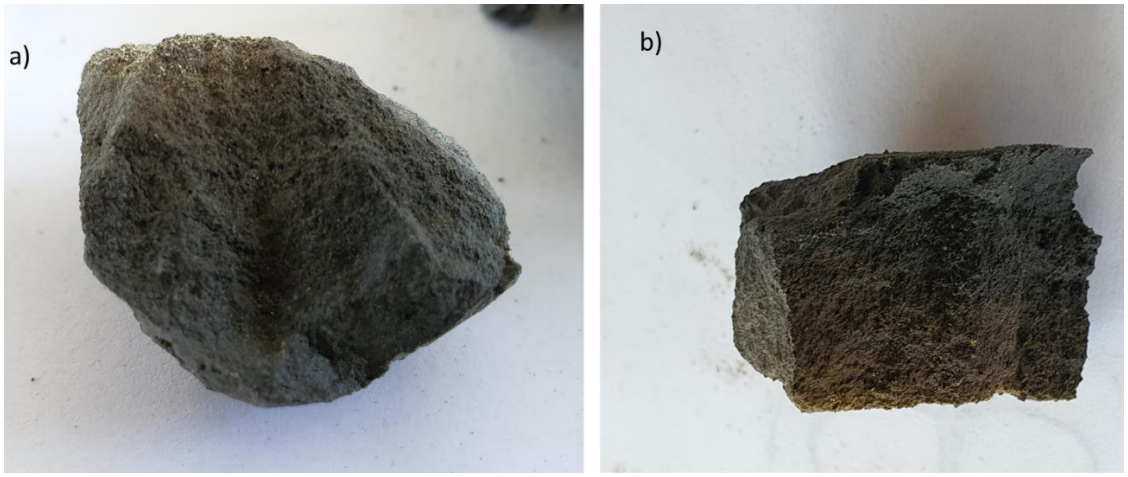

Figure 5. exterior view (a) and cut interior view of clinker (b)

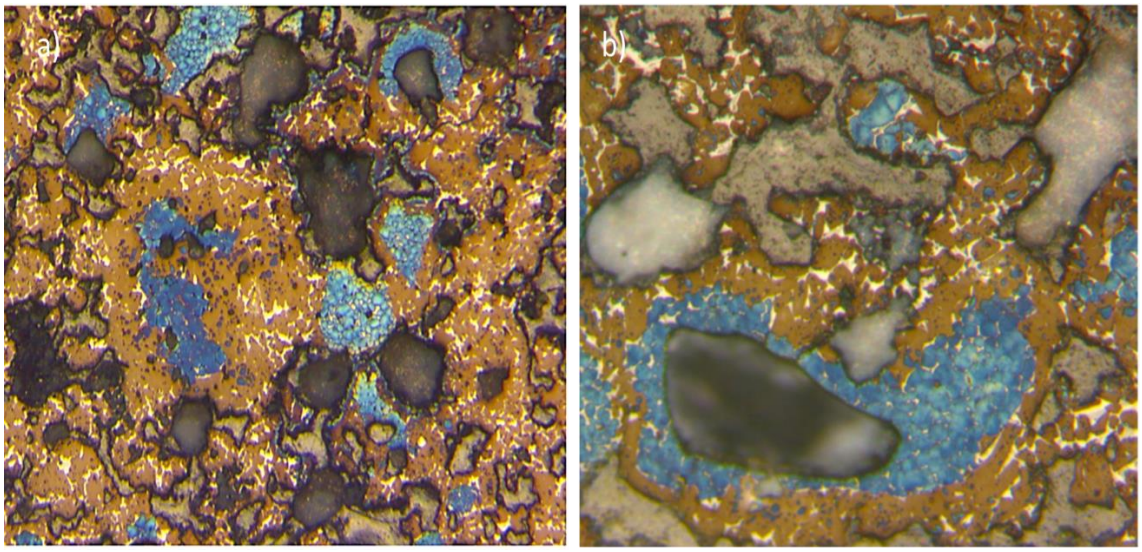

Figure 7. Clinker optical microscope phase images (Brown: alite; blue: belite)

Blue crystals are alite, brown-orange crystals are alite. In the clinker sample, partly cuminated belite crystals were encountered. Homogeneous phase distribution is desired in clinker samples. However, this situation can be achieved if raw material homogenization is done well, and it is unlikely that such a situation will occur in a clinker produced in a laboratory environment. In addition, the clustered structure shows free lime crystals. The amount of free lime is not very high in the clinker sample. In general, the clinker sample shows good burning.

When we look at the clinker phase distribution in general, it is seen that the alite mineral is more dense and the belite mineral is less (Fig. 7a). The intense alite phase has a positive effect on Grindability [9,10]. It facilitates grinding and reduces energy consumption. Belite minerals are found in clusters in some regions, and in most of them they are dispersed among the alites. This situation requires coarse-grained minerals in the clay stone raw mixture and requires finer grinding in order to fully homogenize it (Fig. 7b). When the crystal sizes of the clinker granules were examined, it was observed that the alite and belite crystals were of variable size (5-40 microns) in general. Large sized alite and belite crystals were also observed in some granules in the clinker. For this reason, the burning ability can be increased with the improvements to be made in the process [11, 12].

4. Conclusions and Recommendations

When the limestone sample was examined from a mineralogical point of view, the presence of calcite, which causes difficulty in firing, was found in its composition. When the mineralogical analysis result of the clay sample is evaluated in terms of fireability, it is known that quartz, calcite and albite detected in the structure of the clay sample make firing difficult, and the clay minerals montmorillonite, muscovite and chlorite affect firing positively.

The fact that the Free CaO values are 1.60 in the clinker formed at 1450°C indicates that the prepared raw meal has an easy burning character (S.CaO: less than 2.00). Mineralogical results of the claystone sample used also confirm the easy-burning feature of raw meal.

When the clinker produced is examined in terms of quality parameters, it is observed that it has a relatively lower quality than the optimum quality (C_3S < 60.0 %). The amount of liquid phase (29.64) in the clinker shows a height (around 27 optimum) due to low SIM and high ALM modulus values, depending on the raw material characteristics. In the use of this raw meal, it is important to pay attention to the liquid phase in terms of belt formation. It is thought that the clinker quality and the amount of liquid phase will be positively affected in the clinker that is formed by bringing SIM and ALM to the optimum point (additional use of correcting agents, such as iron ore and sand).

References

[1]. Bartın, malzeme karakterizasyonu 2 .pdf. Nov. 30, 2021.[Online]. Available: https://cdn.bartin.edu.tr/metalurji/d7ee7cd9-f063-4669-8e1c-393503ed6ffb/malzemekarakterizasyonunu2 [Accessed December. 12, 2021].

[2]. Çopuroğlu, ‘’Çimentolu Malzemelerin Karakterizasyonunda Mikroskop Kullanımı.2014

[3]. Felekoğlu, B., Güllü, D. ‘‘Klinker incelemelerinde optik mikroskop ve görüntü işleme tekniklerinin kullanılması’’, İMO *Teknik Dergi, 3761*(3770), 247, 2006.

[4]. Çimsa, 2021. Çimento Klinker Fazları ve Öğütme Parametreleri Arasındaki İlişkiler, Dec. 20, 2021.[Online].Available: https://www.cimsa.com.tr/ca/docs/4FE58AA58E3A4B7B85FA9E4EE011A8/F36E64383F844B33BA6595F24D191855.pdf, [Accessed December. 20, 2021]. https://www.cimsa.com.tr/ca/docs/71DDECEE521E470BA4ADA95A091840/F4EE24A8802D44DAADAA006C3C1AE784.pdf [Accessed December. 11, 2021].

[5]. Korkmaz, A. V., & Hacıfazlıoğlu, H, ‘‘Çimento Üretiminde Kil Taşına Alternatif Bir Hammadde: Meta Şist’’, Bilimsel *Madencilik Dergisi*, *58*(2), 95-110.

[6]. D. Güllü, ‘‘Çimento Klinker Fazlarının Mikro Yapısı ve Öğütme Parametreleri Arasındaki İlişkilerin Araştırılması’’, Yüksek lisans tezi, Dokuz Eylül Üniversitesi Fen Bilimleri Enstitüsü, İzmir, 2006.

[7]. Altun, A., Ölmez, N., ‘‘Çimento Klinkerinin Öğütülebilirliği ve İç Yapısı Üzerine Karşılaştırmalı Araştırmalar’’, *Cevher Hazırlama Dergisi*, 1-5, 2001.

[8]. Çimsa, 2017. Çimento Kalite Kontrol Parametreleri ve Beton Üzerindeki Etkileri, Dec. 20, 2021.[Online].Available: https://www.cimsa.com.tr/ca/docs/4FE58AA58E3A4B7B85FA9E4EE011A8/F36E64383F844B33BA6595F24D191855.pdf, [Accessed December. 20, 2021].

[9]. A. Korkmaz, “Avaılabılıty Of Metachıst As An Alternatıve To Clay Raw Materıal In Cement Productıon,” D. S. thesis, University of İstanbul, İstanbul, IL, 2017.

[10]. Saxena, S. K., Kumar, M., Chundawat, D. S., Singh, N. B, ‘‘ Utilization of wollastonite in cement manufacturing’’, *Materials Today: Proceedings*, *29*, 733-737.2020.

[11]. Lai, H., Lv, S., Lai, Z., Liu, L., Lu, Z. ‘‘Utilization of oil-based mud drilling cuttings wastes from shale gas extraction for cement clinker production’’, *Environmental Science and Pollution Research*, *27*(26), 33075-33084, 2020.

[12]. Gu, K., Chen, B., ‘‘Research on the incorporation of untreated flue gas desulfurization gypsum into magnesium oxysulfate cement’’, *Journ*

JOURNAL of CHARACTERIZATION

https://jcharacterization.com
https://jcharacterization.org

Journal of Characterization
Vol 1, Special Issue, 62-69, December 2021

ISSN: 2757-9166
Research Article

Dry Grinding of Bentonite by Stirred Media Mill

Hakan Çiftçi[1*], Melih Özçatal[2]

[1*] Afyon Kocatepe University, Faculty of Engineering, Department of Mining Engineering, Afyonkarahisar, Turkey, (ORCID: 0000-0001-7910-7350), hakanciftci86@gmail.com
[2] Afyon Kocatepe University, Faculty of Technology, Department of Metallurgical and Materials Engineering, Afyonkarahisar, Turkey, (ORCID: 0000-0002-0831-9038), mozcatal@aku.edu.tr

(Received date: 28.12.2021 and Accepted date: 30.12.2021)

(**DOI: 10.29228/JCHAR.55663**)

REFERENCES: Hakan, Ç., Melih, Ö., Dry grinding of bentonite by stirred media mill, *Journal of Characterization*, (1), Special Issue, 62-69, 2021.

Abstract

In this study, a pin-type vertical stirred media mill was used to perform the dry grinding of bentonite. Grinding time and stirring speed were investigated for effect on the particle size distribution and energy consumption (E_c), while ball charge and bentonite charge were kept constant as 60% and 40%, respectively. It was observed that raw bentonites could be ultra-fine dry ground using vertical stirred media mills for the potential dry uses of bentonites. The experimental results revealed that a ground bentonite product having a d_{80} value of about 10 µm was obtained with 128.1 kWh/ton energy consumption. Optimum operational parameters were selected as 60% ball charge, 40% bentonite charge, 600 rpm stirring speed, and 20 min grinding time.

Keywords: Bentonite, Montmorillonite, Grinding, Stirred media mill.

Bentonitin Karıştırmalı Ortam Değirmeni ile Kuru Öğütülmesi

Öz

Bu çalışmada bentonitin kuru öğütülmesi için pim tipi dikey karıştırma ortamlı değirmen kullanıldı. Tane boyutu dağılımına ve enerji tüketimine (Ec) etkisi için öğütme süresi ve karıştırma hızı araştırılırken bilye ve bentonit şarj oranı sırasıyla %60 ve %40 olarak sabit tutuldu. Bentonitlerin potansiyel kuru kullanımları için ham bentonitlerin dikey karıştırmalı öğütücüler kullanılarak ultra ince kuru öğütülebildiği gözlemlendi. Deneysel sonuçlar, 128.1 kWh/ton enerji tüketimi ile yaklaşık 10 µm d_{80} değerine sahip öğütülmüş bentonit ürününün elde edildiğini ortaya koydu. Optimum çalışma parametreleri %60 bilye şarjı, %40 bentonit şarjı, 600 rpm karıştırma hızı ve 20 dk öğütme süresi olarak seçildi.

Anahtar Kelimeler: : Bentonit, Montmorillonit, Öğütme, Karıştırmalı ortam değirmeni.

1. Introduction

Bentonite, a type of clay ore, mainly contains smectite minerals (montmorillonite, saponite, nontronite, hectorite). Smectite minerals occur by the decomposition of the volcanic tuffs, ashes, and lavas. Montmorillonite, the most abundant smectite mineral in bentonite ores, is aqueous aluminum silicate and has a layered crystalline structure with the general chemical formula of $(Na, Ca)_{0.33}(Al, Mg)_2(Si_4O_{10})(OH)_2*nH_2O$. Bentonites have superior properties such as high cation exchange capacity, large surface area, high swelling capacity, plasticity, good mechanical properties, and chemical stability [1–5]. Therefore, bentonites are used in various applications such as adsorption, pharmaceutical and cosmetic industry, drilling mud, food, paper, paint, and ceramics [1, 6–8].

Recently, great attention has been paid to the fine grinding of clay minerals by planetary or stirred ball mills. Because the physical properties of clay minerals (especially structural and textural) are developed for new application areas by this way [9]. Colloidal dispersions for various applications, food protective materials, drug delivery systems, paint, paper, cosmetic, and dry bentonite beneficiation can be shown for the new application uses of fine ground bentonites. There are many studies performed to investigate the operating parameters that affect the grinding performance of stirred media mills [10-14]. However, to our best knowledge, there are few studies on dry grinding of the bentonite by vertical stirred media mill. Dry grinding is a necessary application in some areas, especially in dry beneficiation of clay minerals by sieving, aero cyclones, and dynamic separators.

This study focused on the dry grinding of sodium bentonite using a pin-type vertical stirred media mill. Operational parameters such as grinding time and stirring speed were investigated. Particle size distribution of the ground material and energy consumption of grinding application analyzes were also performed to determine optimum grinding conditions. A product having a d_{80} value of about 10 µm was aimed to obtain for potential uses in the cosmetic, chemistry, and pharmaceutic industries.

2. Material and Method

2.1. Materials

Bentonite sample was obtained from Karben Bentonite Cooperation located in Reşadiye Tokat, Turkey. Yttrium stabilized zirconium oxide balls (3 mm and 5 mm) were used as grinding media.

2.2. Methods

2.2.1. Characterization Studies

The bentonite sample was dried at 55ºC for 24 h and then ground using a laboratory scaled ring mill before all characterization analysis. The chemical composition of the sample was analyzed by Rigaku ZSX Primus II XRF (x-ray fluorescence) device. X-ray diffraction (XRD) pattern was scanned with Cu-Ka radiation (40 kV, λ: 1.54184 Å) using a Shimadzu XRD-6000 device to determine mineralogical components. The sample was scanned at the angular range of 2-40° with 0.02°/step scan speed. LEO 1430 VP scanning electron microscope (SEM) was used to examine the morphology of the bentonite sample. Particle size distributions were determined by the Malvern Master-sizer 2000 instrument using dry analysis apparatus.

2.2.2. Grinding Studies

Grinding studies were performed using a laboratory scaled vertical stirred media mill (Figure 1) with a pin-type stirrer. The effective volume of the mill chamber was 1.0 L. The grinding chamber was equipped with a water jacket for cooling. Yttrium stabilized zirconium oxide balls (3 mm: 598 g, 5 mm: 1967 g, total volume: 530 mL) were used as grinding media. The volume of the grinding media and the bentonite sample was kept constant as 530 mL (60%) and 350 mL (40%), respectively, for all grinding experiments.

Figure 1. Pin-type vertical stirred media mill used for the grinding experiments.

The grinding experiment was performed as a batch process. First, the raw bentonite sample dried at 50ºC for 24 h and then crushed under 1 mm using a roll mill. 350 mL of pre-ground bentonite sample (-300 µm) and 530 mL grinding media were placed into the mill chamber. The circulation of the cooling water and then stirring of the pin type stirrer was started. After a certain time, stirring was stopped, and the ground sample was separated from the balls using a 1 mm sieve. The energy consumption of each grinding experiment was measured using an electricity meter connected to the mill. Operational parameters used in the grinding tests are summarized in Table 1.

Table 1. Operational parameters of the grinding experiments.

Experiment No	Stirring speed (rpm)	Grinding time (min)	Ball charge (%)	Material charge (%)
1	500	5	60	40
2	500	10		
3	500	20		
4	500	30		
5	500	40		
6	600	20		
7	700	20		
8	800	20		

3. Results and Discussion

3.1. Characterization of the bentonite

The chemical analysis (XRF) results (Table 2) showed that the bentonite sample had high percentages of silicon and aluminum oxides (81.3 wt.% in total), indicating the probability of a clay mineral. $(Na_2O+K_2O)/(CaO+MgO)$ ratio was determined to be 0.69. A value high than 0.33 is attributed to the Na-smectites [2].

Smectite minerals (montmorillonite, etc.) usually exhibit a morphology that resembles a honeycomb, cornflake, leafy, and rosette-like appearance [2, 15]. SEM micrograph (Figure 2) revealed that the bentonite sample used in this study consisted of smooth-surfaced grain aggregates and had a leaf layer morphology with curved edges.

Table 2. Chemical composition of the bentonite sample.

Component	SiO_2	Al_2O_3	Fe_2O_3	MgO	Na_2O	CaO	K_2O	LOI
Content, wt.%	62.23	19.06	3.63	2.70	2.61	2.05	0.65	6.30

LOI: loss on ignition.

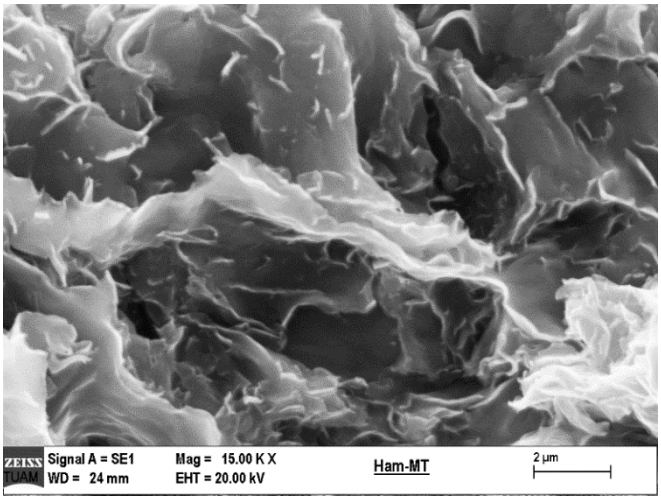

Figure 2. SEM micrograph of the bentonite sample.

The XRD pattern of the bentonite sample is given in Figure 3. The sample mostly consisted of montmorillonite minerals and non-clay minerals such as feldspar, calcite, opal (C-T), quartz, mica, and clinoptilolite (zeolite). Characteristic reflection at 2θ: 7.07° with the d_{001} basal spacing of 12.4 Å confirmed that the bentonite sample contains a high amount of Na^+-rich montmorillonite [16] which was in good agreement with XRF analysis (Table 2). Furthermore, the d_{060} value (1.5 Å) showed that the sample was composed of dioctahedral montmorillonites [17].

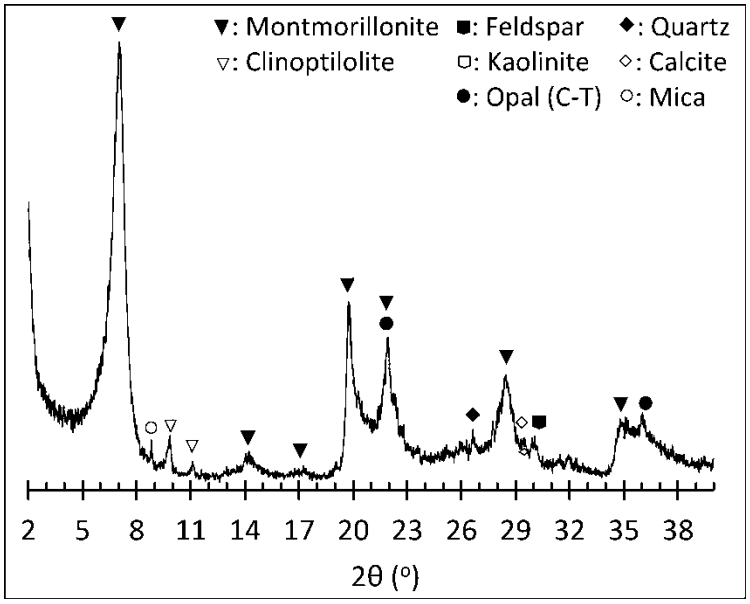

Figure 3. XRD pattern of the bentonite sample.

3.2. Grinding of the bentonite

3.2.1 Effect of the Grinding Time

Time-dependent grinding experiments were performed at a stirring speed of 500 rpm. The effects of grinding times of 5, 10, 20, 30, and 40 minutes on the particle size distribution and energy consumption (E_c) were investigated. The effect of the grinding time on the particle size distribution of the bentonite and E_c was given in Figure 4 and Table 2. As clearly seen in Figure 4, grinding time had a significant effect on the particle size and so energy consumption. An increase in the grinding time decreased the product size and simultaneously increased the Ec. It has been proven once again that the energy consumption (E_C) in the mill has a linear relationship with the grinding time. When the mill reaches meta-steady state dynamics, the power consumption of the mill becomes constant [18]. Similar results were also reported by other studies [14, 19-21].

Table 2. The d_{50} and d_{90} sizes of the products change depending on the grinding time.

	5 min	10 min	20 min	30 min	40 min
d_{50}	25.2	18.5	6.1	4.7	3.9
d_{80}	69.0	69.0	22.0	15.2	10.0

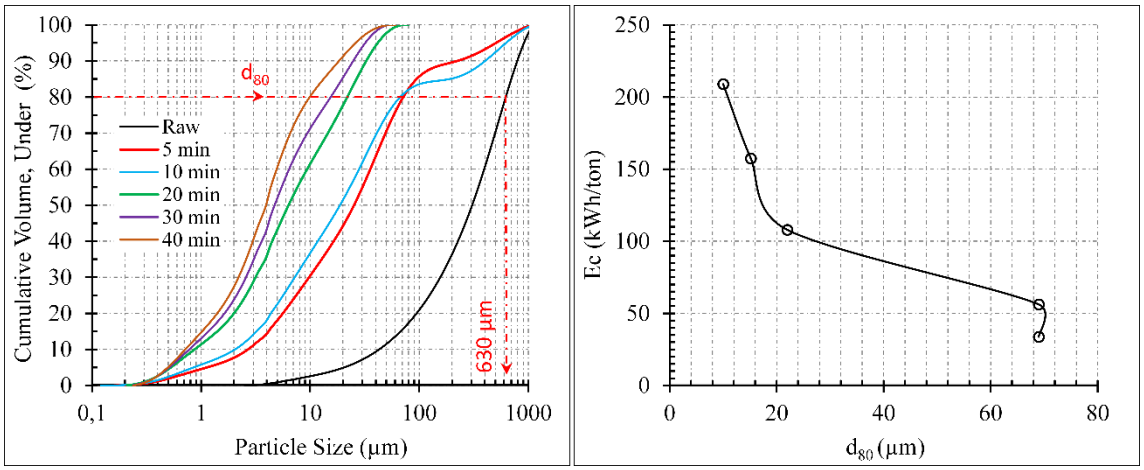

Figure 4. Effect of the grinding time on the particle size distribution and the energy consumption (E_c).

Energy consumption in the mill as a function of the particle size (d_{80}) of the ground bentonite products (Figure 4) revealed that E_c increased as particle size was more reduced by higher grinding times. The results displayed that increase in the grinding time from 5 min to 40 min decreased the product size (d_{80}) from 69.0 to 10.0 µm, whereas E_c was increased significantly from 33.7 to 209 kWh/t. The optimum grinding time was selected to be 20 min for the ongoing grinding experiment as a function of stirring speed.

3.2.2 Effect of the Stirring Speed

The stirring speed creates a high energy strength environment in the grinding chamber, increasing the probability of the grinding media impact and attrition of the particles. As the stirring speed increases, the stress intensity inside the mill chamber also increases, which seriously affects the interaction between the grinding media and the material to be ground [18, 22-23]. Grinding experiments were performed as a function of stirring speed (400, 500, 600, 700, 800 rpm) while grinding time was kept constant as 30 min. The effect of the stirring speed on the particle size distribution of the bentonite and E_c was given in Figure 5. The results displayed that increase in the stirring speed from 500 rpm to 800 rpm decreased the product size (d_{80}) from 22.0 to 8.0 µm, whereas E_c was increased significantly from 107.9 to 168.5 kWh/t**.** Increasing the mixing speed increases the stress intensities and eventually grinding speed due to the high

probability of particle collisions with the grinding media. Furthermore, as the mixing speed increases, the grinding media reaches higher kinetic energy, which is transferred to the particles, making breakage easier.

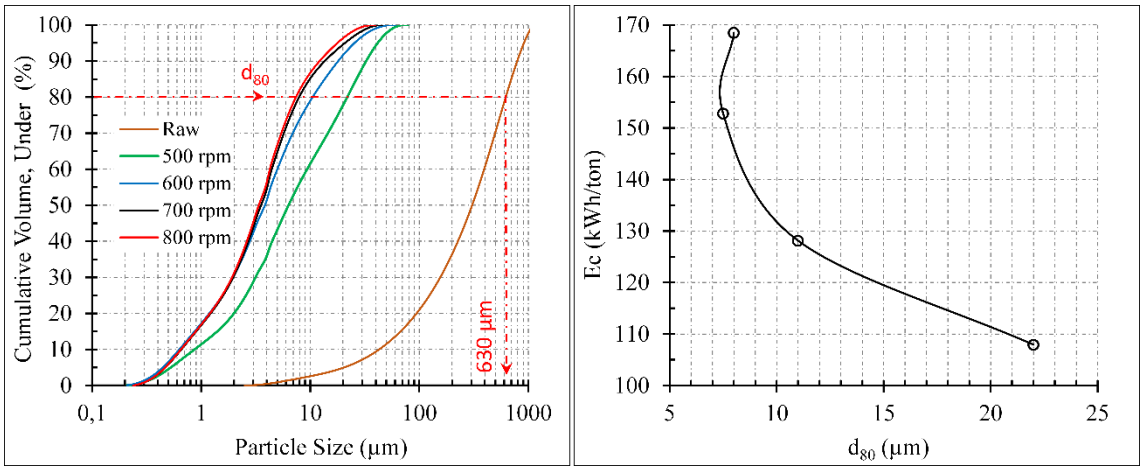

Figure 5. Effect of the grinding time on the particle size distribution and the energy consumption (E_c).

The increase in grinding performance with the increase in stirring speed is a condition that is effective up to a certain stirring speed. Even if the mixing speed increases after a certain speed, the grinding performance decreases as the grain size reduction rate will be meager. Figure 5 and Table 3 revealed that the grinding performance was decreased when the stirring speed was increased to 800 rpm**.** Therefore, optimum operational parameters were selected as 60% ball charge, 40% bentonite charge, 600 rpm stirring speed, and 20 min grinding time to obtain a product having a d_{80} value of about 10 µm.

Table 3. The d_{50} and d_{90} sizes of the products change depending on the stirring speed.

	500 rpm	600 rpm	700 rpm	800 rpm
d_{50}	6.1	3.6	3.5	3.3
d_{80}	22.0	11.0	7.5	8.0

4. Conclusion

Dry grinding experiments of the raw bentonite sample using a pin-type vertical stirred media mill were successfully performed. Characterization studies revealed that the bentonite sample mostly consists of Na^+ rich montmorillonite. Grinding time and stirring speed were investigated as two operational parameters while material and ball charge were kept constant. It was concluded that bentonites could be dry ground to ultrafine particle sizes using stirred media mills for the potential dry uses. A ground bentonite product having a d_{80} value of about 10 µm was obtained with 128.1 kWh/ton energy consumption using selected operational parameters, which are 60% ball charge, 40% bentonite charge, 600 rpm stirring speed, and 20 min grinding time.

5. Acknowledge

This study was financially supported by Scientific Research Projects Coordination Unit of Afyon Kocatepe University under project number 21.KARIER.01.

References

[1] H. Çiftçi, "An introduction to montmorillonite purification", In: Montmorillonite clay, Eds. F. Uddin, London, IntechOpen, pp. 1-7, 2021.

[2] H. Çiftçi, B. Ersoy, and A. Evcin, "Purification of Turkish Bentonites and Investigation of the Contact Angle, Surface Free Energy and Zeta Potential Profiles of Organo-Bentonites as a Function of CTAB Concentration," *Clays and Clay Minerals*, vol. 68 no. 3, pp. 250-261, 2020.

[3] J. H. Yang, J. H. Lee, H. J. Ryu, A. A. Elzatahry, Z. A. Alothman, and J. H. Choy, "Drug-clay nanohybrids as sustained delivery systems," *Applied Clay Science*, vol. 130, pp. 20-32, 2016.

[4] J. Nones, H. G. Riella, A. G. Trentin, and J. Nones, "Effects of bentonite on different cell types: A brief review," *Applied Clay Science*, vol. 105-106, pp. 225-230, 2015.

[5] S. Jain, and M. Datta, "Oral extended release of dexamethasone: Montmorillonite-PLGA nanocomposites as a delivery vehicle," *Applied Clay Science*, vol. 104, pp. 182-188, 2015.

[6] S. Jayrajsinh, G. Shankar, M. Pharm, Y. K. Agrawal, and L. Bakre, "Montmorillonite nanoclay as a multifaceted drug-delivery carrier: A review," *Journal of Drug Delivery Science and Technology*, vol. 39, pp. 200-209, 2017.

[7] S. E. Elmore, N. Mitchell, T. Mays, K. Brown, A. Marroquin-Cardona, A. Romoser, and T. D. Phillips, "Common African cooking processes do not affect the aflatoxin binding efficacy of refined calcium montmorillonite clay," *Food control*, vol. 37, pp. 27-32, 2014.

[8] V. Summa, and F. Tateto, "Clay minerals as adsorbents of aflatoxin M1 from contaminated milk and effects on milk quality," *Applied Clay Science*, vol. 88, pp. 92-99, 2014.

[9] W.K. Mekhamer, "Stability changes of Saudi bentonite suspension due to mechanical grinding", *Journal of Saudi Chemical Society*, vol. 15, pp. 361-366, 2011.

[10] O. A. Orumwense, and E. Forssberg, "Superfine and ultrafine grinding, A literature survey, *J. Mineral Processing and Extractive Metall Rev*, vol. 11, pp. 107-127, 1992.

[11] J. Lichter, and G. Davey, "Selection and sizing of ultrafine and stirred grinding mills," *Advances in Comminution*. Colorado, Society for Mining, Metallurgy and Exploration, 2006.

[12] K. Ohenoja, M. Illikainen, and J. Niinimäki, "Effect of operational parameters and stress energies on the particle size distribution of TiO_2 pigment in stirred media milling," *Powder Technology,* vol. 234, pp. 91–96, 2013.

[13] A. Jankovic, "Variables affecting the fine grinding of minerals using stirred mills," *Minerals Engineering*, vol. 16, pp. 337-345, 2003.

[14] O. Y. Toraman, and D. Katırcıoglu, "Study on the effect of process parameters in stirred ball mill," *Advanced Powder Technology*, vol. 22, pp. 26-30, 2011.

[15] W. D. Keller, and R. C. Reynolds, A. Inoue, "Morphology of clay minerals in the smectite-to-illite conversion series by scanning electron microscopy," *Clays and Clay Minerals,* vol. 34, pp. 187-197, 1986.

[16] G. Brown, and G. W. Brindley, "X-ray diffraction procedures for clay mineral identification," in: G. W. Brindley, G. Brown (Eds.), Crystal Structures of Clay Minerals and their X-ray Identification, Monograph 5 (pp. 305–360), London, Mineralogical Society, 1980.

[17] R. E. Grim, "Clay Mineralogy. International series in the earth and planetary sciences," pp. 596, New York, Mc Graw-Hill Book Co. Inc., 1968.

[18] T. Santosh, K. Rahul Soni, C. Eswaraiah, D. S. Rao, and R. Venugopal, "Optimization of stirred mill parameters for fine grinding of PGE bearing chromite ore," *Particulate Science and Technology*," vol. 39, no. 6, Jul., pp. 663-675, 2020. DOI: 10.1080/02726351.2020.1795016

[19] C. Eswaraiah, N. Venkat, B. K. Mishra, and R. Holmes, "A comparative study on a vertical stirred mill agitator design for fine grinding." *Separation Science and Technology*, vol. 50, pp. 39-48, 2015. doi:10.1080/01496395.2015.1065888.

[20] O. Y. Toraman, "Dry fine grinding of calcite powder by stirred mill," *Particulate Science and Technology*, vol. 31 no. 3, pp. 205-209, 2013. *doi:10.1080/02726351.2012.694135.*

[21] H. Hacıfazlıoğlu, and A.V. Korkmaz, "Performance comparison of stirred media mill and ball (BOND) mill in bauxite grinding," *Particulate Science and Technology*, vol. 38, no. 4, pp. 404-408, 2020. DOI: 10.1080/02726351.2018.1547342

[22] O. Altun, H. Benzer, and U. Enderle, "Effects of operating parameters on the efficiency of dry stirred milling," *Minerals Engineering*, vol. 43-44, pp. 58-66, 2013. doi:10.1016/j.mineng.2012.08.003

[23] M. Hasan, S. Palaniandy, M. Hilden, and M. Powell, "Calculating breakage parameters of a batch vertical stirred mill," *Minerals Engineering,* vol. 111, pp. 229-237, 2017. doi:10.1016/j.mineng.2017.06.024.